12-14-2013

Multilevel Design Optimization Under Uncertainty with Application to Product-Material Systems

Saber DorMohammadi

Multilevel design optimization under uncertainty

with application to product-material systems

By

Saber DorMohammadi

A Dissertation
Submitted to the Faculty of
Mississippi State University
in Partial Fulfillment of the Requirements
for the Degree of Doctor of Philosophy
in Computational Engineering
in the Bagley College of Engineering

Mississippi State, Mississippi

December 2013

Multilevel design optimization under uncertainty

with application to product-material systems

By

Saber DorMohammadi

Approved:

Masoud Rais-Rohani
(Director of Dissertation)

Christopher D. Eamon
(Committee Member)

Tomasz Haupt
(Committee Member)

Douglas J. Bammann
(Committee Member)

Seth F. Oppenheimer
(Committee Member)

Roger L. King
(Graduate Coordinator)

Achille Messac
Dean
Bagley College of Engineering

Name: Saber DorMohammadi

Date of Degree: December 14, 2013

Institution: Mississippi State University

Major Field: Computational Engineering

Major Professor: Masoud Rais-Rohani

Title of Study: Multilevel design optimization under uncertainty with application to product-material systems

Pages in Study: 172

Candidate for Degree of Doctor of Philosophy

The main objective of this research is to develop a computational design tool for multilevel optimization of product-material systems under uncertainty. To accomplish this goal, an exponential penalty function (EPF) formulation based on method of multipliers is developed for solving multilevel optimization problems within the framework of Analytical Target Cascading (ATC). The original all-at-once constrained optimization problem is decomposed into a hierarchical system with consistency constraints enforcing the target-response coupling in the connected elements. The objective function is combined with the consistency constraints in each element to formulate an augmented Lagrangian with EPF. The EPF formulation is implemented using double-loop (EPF I) and single-loop (EPF II) coordination strategies and two penalty-parameter-updating schemes. The computational characteristics of the proposed approaches are investigated using different nonlinear convex and non-convex optimization problems.

An efficient reliability-based design optimization method, Single Loop Single Vector (SLSV), is integrated with Augmented Lagrangian (AL) formulation of ATC for

solution of hierarchical multilevel optimization problems under uncertainty. In the proposed SLSV+AL approach, the uncertainties are propagated by matching the required moments of connecting responses/targets and linking variables present in the decomposed system. The accuracy and computational efficiency of SLSV+AL are demonstrated through the solution of different benchmark problems and comparison of results with those from other optimization methods.

Finally, the developed computational design optimization tool is used for design optimization of hybrid multiscale composite sandwich plates with/without uncertainty. Both carbon nanofiber (CNF) waviness and CNF-matrix interphase properties are included in the model. By decomposing the sandwich plate, structural and material designs are combined and treated as a multilevel optimization problem. The application problem considers the minimum-weight design of an in-plane loaded sandwich plate with a honeycomb core and laminated composite face sheets that are reinforced by both conventional continuous fibers and CNF-enhanced polymer matrix. Besides global buckling, shear crimping, intracell buckling, and face sheet wrinkling are also treated as design constraints.

DEDICATION

To my loving and supportive wife, Marta

To my always encouraging, ever faithful parents

ACKNOWLEDGEMENTS

I would like to express the deepest appreciation to my advisor Professor Masoud Rais-Rohani for his attitude and excellent guidance, support and the substance of a genius during my graduate studies. I would like to appreciate him for all of his exceptional insight in the design optimization and giving me the chance to work with Vanderplaats Research & Development, Inc in a unique opportunity, as an intern student.

I would like to express my gratitude to Professor Douglas Bammann, from whom I learned a lot in his lectures in different aspects of large deformation, inelasticity and continuum mechanics. I would like to thank Dr. Christopher D. Eamon, who helped me a lot in the field of reliability-based design optimization during my research. I would like to express my gratitude to Dr. Tomasz Haupt who introduced me computational design framework and cyber infrastructures. I would like to thank Professor Seth Oppenheimer to serve as my committee member.

I would like to thank my friend and colleague, Dr. Mohammad Rouhi, for their invaluable assistance with the nano-enhanced polymer composite structures simulation. I have had a unique opportunity to work with a very highly talented engineering group at Vanderplaats Research & Development, Inc in Novi Michigan. I would like to express my appreciation to Mr. Juan Pablo Leiva COO for his everlasting faith on me and challenging me with the most difficult problems.

I would like to give my heartfelt appreciation to my parents, who brought me up with their love and encouragement me to pursue advanced degrees abroad. I offer sincere thanks to my dear wife, who has accompanied me with her love, patience, helping and encouragement.

The financial support provided by the National Science Foundation under Award Number (CMMI-0826547) is greatly appreciated.

TABLE OF CONTENTS

LIST OF TABLES

LIST OF FIGURES

CHAPTER I

INTRODUCTION

Multilevel Design Optimization

The design of complex engineered systems may be decomposed into two or more subsystems with each tied to a different discipline or part of the system with smaller set of design variables, separate objective functions and design constraints. The decomposed system can be expanded to include several *levels* with each containing multiple *elements*. The multilevel architecture offers autonomy to each element to optimize a separate objective function subject to element-specific set of constraints based on information provided by the lower-level elements and design targets imposed by the connecting upper-level element. By reducing dimensionality of each element optimization problem, the system becomes more manageable as each element represents only a fraction of the total set.

In mathematical programming problems, the decomposition is based on functionality of objective and constraint functions, which results in a set of smaller problems. In multidisciplinary (MDO) design problems, decomposition partitioning can be done as object- or discipline-based (Kim 2001). For example, the structure consists of two or more members that can be decomposed into structural and material subsystems, then each member can be treated as a separate element.

In the field of structural optimization, early works in multilevel decomposition and optimization of hierarchical systems can be traced to those of (Kirsch 1975) and (Sobieszczanski-Sobieski 1974). (Kirsch 1975) used model coordination and goal coordination methods to formulate a general multilevel decomposition whereas (Sobieszczanski-Sobieski 1982) developed multilevel optimization by linear decomposition (MOLD) with applications to two- and three-level systems (Sobieszczanski-Sobieski et al. 1985) (Sobieszczanski-Sobieski et al. 1987). (Haftka 1984), (Thareja and Haftka 1986), and (Renaud and Gabriele 1989) explored various options to offset the numerical difficulties occasionally encountered in MOLD. As an alternative to MOLD, (Vanderplaats et al. 1990) developed a reformulated decomposition method by including all variables and constraints at the system level and using a sequential linearization method.

More modern approaches include that of (Michelena et al. 1999) who introduced analytical target cascading (ATC) for sequential optimization of hierarchical systems. The main premise of ATC is the use of level-by-level cascading whereby the upper-level design targets are propagated down to lower-level elements while outputs of individual elements are transferred upward as inputs to higher-level elements. A coordination strategy is used to ensure that the separately optimized subsystems satisfy the optimality conditions at the system level (Michelena et al. 2003). In the initial formulation of ATC (Kim et al. 2000), (Kim 2001), (Kim et al. 2002), deviation tolerances were defined for the responses as well as the linking (or shared design) variables. The goal was the minimization of the deviation tolerances subject to system design constraints and deviation constraints that coordinate subsystem responses and subsystem linking variables. The commonly used ATC formulations (Tzevelekos et al. 2003), (Michalek and Papalambros 2005a), and (Michalek and Papalambros 2005b) are based on quadratic penalty functions. The quadratic penalty functions minimize the consistency constraints (equality or inequality) to force targets and responses to match. Ideally, these consistency constraints have to be relaxed, allowing inconsistencies between targets and responses that are gradually eliminated in the iterative solution process. In proposing the separable ordinary Lagrangian function, (Lassiter et al. 2005) considered a large-scale convex nonlinear programming problem and decomposed it according to the scheme of ATC. They also developed a Lagrangian duality-based coordination approach in which the solutions of the resulting subproblems converge to the solution of the original problem. By combining the classical Lagrangian Duality (LD) and the Augmented Lagrangian Duality (ALD), (Blouin et al. 2005) provided a simple method for decomposition without imposing restrictive conditions to alleviate the difficulty of convexity requirement. They updated two parameters that have the same role as the weight factors. The modified Lagrangian dual formulation and coordination for ATC (Kim et al. 2006) enhances the formulation and coordination proposed earlier in the literature, with a guideline to set the step size for sub-gradient optimization when solving the Lagrangian dual problem. (Tosserams et al. 2006) proposed and investigated ATC problem relaxation with an augmented Lagrangian penalty (ALP) function using the method of multipliers (AL) and the alternating direction method of multipliers (AL-AD). By means of the augmented Lagrangian function relaxation, ill-conditioning is reduced for the ATC problem of the inner loop because accurate solutions can be obtained for smaller weight factors. This formulation was later adopted by (Li et al. 2008) who used Diagonal Quadratic

Approximation (DQA) for parallelization of ATC. Similarly, (Wang et al. 2010) also applied this formulation but used three different methods for updating in the outer loop. A new convergent strategy for ATC (Chan 2008), (Han 2008), (Han and Papalambros 2010) coordinates interactions among subproblems using sequential linearizations. The linearity of subproblems is maintained using infinity norms to measure deviations between targets and responses. Since all subsystems are linear, they can be solved with high efficiency.

It is important to note that in all of the efforts cited above the design optimization problem is treated as deterministic with no uncertainty. More recently, (Kokkolaras et al. 2006) formally introduced the issues of uncertainty and risk into the design optimization of hierarchically decomposed multilevel systems by developing a probabilistic version of ATC methodology. We believe this is a very powerful methodology and intend to adopt it in this research with some enhancements as will be noted later in the dissertation.

Reliability-Based Design Optimization

In design optimization of structural systems, uncertainty is commonly introduced as random variability in controllable and/or uncontrollable parameters (e.g., loading, material properties, geometry, boundary condition). The mathematical representation and propagation of uncertainty help quantify variability in responses that depend on such random variables. Probability theory is one of the most common approaches for uncertainty quantification. Reliability-based design optimization (RBDO) is a combination of probabilistic modeling and mathematical design optimization.

There are two generic ways of formulating and solving an RBDO problem. In the double-loop structure methods, a nested optimization problem or sub-optimization problem is required to estimate the reliability index or the most probable point (MPP) of failure. Reliability index approach (RIA) (Nikolaidis and Burdisso 1988;Enevoldsen and Sørensen 1994) and performance measure approach (PMA) (Tu et al. 1999) are based on reliability analysis.

The computational cost of the double-loop approaches can be prohibitive when the problem involves computationally expensive function evaluations or a large number of probabilistic constraints. As a result, many approximate RBDO methods have been presented to convert the double-loop structure to single or serial loop to improve computational efficiency. The approximate methods include but are not limited to the traditional approximation method (TAM), single-loop single-vector (SLSV), safety-factor approach (SFA), and sequential optimization and reliability assessment (SORA).

Grandhi and Wang (1998) computed the structural reliability with a two-point adaptive non-linear approximation while using FORM for reaching the constraint boundary. Kirjner-Neto et al. (1998) implemented outer approximations algorithms to minimize the initial cost of a structure considering the reliability requirement. Yu et al. (1997) proposed a mixed design approach in which a FORM-based RBDO is performed only if the probability of the failure of the deterministic optimum solution is acceptable. Koch and Kodiyalam (1999) proposed a variable-complexity technique in which the accuracy of FORM solutions and the efficiency of Mean-Value First-Order Reliability Method (MVFORM) are put together for more efficient RBDO. Lee and Kwak (1995) suggested using the Neumann expansion technique to reduce the computational cost of obtaining the MPP. Papadrakakis and Lagaros (2002) examined the combination of neural networks and evolution strategies using Monte Carlo simulation (MCS) method exploiting the importance sampling technique to estimate both deterministic and probabilistic constraints. Kharmanda et al. (2002) developed a technique to combine the design and random variables into a single albeit more complex Hybrid Design Space (HDS) for a simultaneous (single-loop) solution of the reliability and optimisation problems. The proposed HDS-based method is shown to be much more computationally efficient when compared with the traditional double-loop procedure. Mohsine et al. (2004) proposed a modification to the HDS-based method called the Improved Hybrid Method (IHM) by minimizing the standard deviations as optimization variables, and showed more minimized objective function can be obtained than HDS method. Kharmanda et al. (2004) introduced a new methodology called the Safety Factor (SF) approach based on the sensitivity study of the limit state function for the reliability evaluation at a reduced computational cost. The SF approach was later applied to problems involving highly non-linear and non-normal random variables (Kharmanda and Olhoff, 2007). Choi et al. (2001) introduced a general Design Potential Concept (DPC) for RBDO with smooth and non-smooth probabilistic constraints. The second-order reliability method (SORM) and the extreme case probability analysis are used to obtain the design potential surfaces in the unified system space. They also provided the extension of DPC for extreme cases, for instance the structures with very small probability of failure. Youn and Choi (2004a) compared three different approaches, the approximate moment, reliability index, and performance measure, to evaluate probabilistic constraints in RBDO and suggest that the PMA is more efficient than the other two approaches while providing more accurate and stable solutions for non-linear limit-state functions. Yang and Gu (2004) found that the Single-Loop-Single-Vector

(SLSV) approach of Chen et al. (1997) provides the best solution in terms of accuracy and efficiency compared to traditional approximation method (TAM), safety-factor approach (SFA) of Wu and Wang (1998) and Wu et al. (2001), and sequential optimization and reliability assessment (SORA) of Du and Chen (2002). Wang and Kodiyalam (2002) proposed a single-level approach for probabilistic and robust design with non-normal distributions. This is the same as SLSV and the normal tail transformation is used to find the equivalent means and standard deviations for non-normally distributed variables. It is shown that the single-level approach is very efficient and robust. Zou and Mahadevan (2006) proposed a decoupled approach to solve an RBDO problem by using direct reliability analysis which allows the use of simulation-based methods for highly nonlinear reliability constraints. The reliability analysis is performed only for the potentially active reliability constraints which improves the efficiency of the proposed approach. Agarwal et al. (2007) have replaced the inverse FORM in PMA by its first-order KKT necessary optimality conditions at the upper-level optimization problem and show that the new approach provides improved robustness and better convergence characteristics as compared to a unilevel variant given by Kuschel and Rackwitz (2000).

Design Optimization of Hierarchically Decomposed Multilevel Systems under Uncertainty

Kokkolaras et al. (2006) formally introduced the notion of uncertainty and risk into the design optimization of hierarchically decomposed multilevel systems by developing a probabilistic version of ATC methodology, which they refer to as PATC. They assume that standard deviations of random variables are available only at the bottom level of the hierarchy, and use a bottom-up coordination strategy that requires uncertainty propagation. The objective function in each element is expressed in terms of deviation from target values cascaded down from the corresponding element immediately above it. To reduce error in uncertainty propagation, they use the advanced mean value (AMV) method (Wu et al. 1990) in evaluating the probability of violating a design constraint under the presence of uncertainty. Recently, Liu et al. (2006) suggested a more general formulation of PATC whereby the interrelated random variables may be described by general probabilistic characteristics. In this research, the general framework of ATC methodology is adopted with several enhancements to prior approaches (e.g., Kokkolaras et al. 2006) as noted later in this section. As for uncertainty propagation and associated constraints, the current approaches in PATC address the consistency of the first two statistical moments (i.e., mean and variance) of random linking variables and shared random responses, while using AMV method for probabilistic design optimization in each element.

In the current research, we propose a more efficient formulation of the augmented Lagrangian based on exponential method of multipliers, which is then integrated with an efficient method for probabilistic design optimization. Moreover, with development and availability of process integration software, different simulation codes are integrated into a computational design tool.

The goal of this research is to develop a computational design tool that is capable of optimizing hierarchically decomposed multiscale product-material systems under uncertainty. To achieve this goal, the following activities are pursued:

Activity 1 – Explore capabilities of current ATC formulations; this activity is focused on an empirical investigation of the numerical behavior of ATC in solving multilevel optimization of hierarchical systems based on the Augmented Lagrangian Penalty formulation and four different solution strategies. It also includes examination of the solution accuracy and efficiency depending on how a problem is decomposed, and establishing general guidelines on the role of coordination strategy and influence of selected parameters on the solution of the ATC problem.

Activity 2 – Propose a new ATC formulation and solution strategy; this activity is aimed at developing a more efficient approach for solving multilevel optimization problems based on the exponential method of multipliers within the framework of ATC. In each element, the consistency constraints are combined with the objective function to formulate an augmented Lagrangian with an exponential penalty function.

Activity 3 – Develop a new approach for probabilistic ATC; this activity explores different approaches for solving a probabilistic design optimization problem. More specifically, it examines the use of efficient single loop single vector approach for reliability-based design optimization with normal and non-normal distributions and its integration with Augmented Lagrangian (AL) formulation of ATC for solution of hierarchical multilevel optimization problems under uncertainty.

Activity 4 – Develop a computational framework for coupled hierarchical material-product simulations; this activity focuses primarily on development of a prototype design tool that can solve problems involving multiple simulation software and codes. The application of this tool is demonstrated in design optimization of a product-material system using all-at-once and ATC approaches.

Activity 5 – Apply the developed approaches to analytical and engineering design problems; multiple analytical problems with different number of design variables, design constraints, and decomposition models are solved as part of this activity. In addition, the application of deterministic and probabilistic ATC for multilevel optimization of a product-material system is investigated.

The primary contribution of this research is the development of exponential penalty function in ATC framework and its integration with an efficient reliability-based design optimization approach to improve the computational efficiency of probabilistic ATC. The secondary accomplishments are the development of the computational design tool that can implement the proposed formulation and solution techniques and its application to multilevel optimization of product-material systems under uncertainty.

The remaining portion of this dissertation is organized as follows: Chapter 2 discusses the numerical behavior of ATC using augmented-Lagrangian penalty function with four different coordination strategies. Chapter 3 provides details of the integration of reliability-based design optimization method in ATC framework. Chapter 4 presents new approach in ATC using exponential method of multipliers. Chapter 5 gives details of the design optimization of a material-product system. The optimization of the material-product system in Chapter 5 under uncertainty is described in Chapter 6. Chapter 7 discusses the computational design framework developed for material-product simulation and optimization. Chapter 8 summarizes the research findings and suggests some insights for future work.

CHAPTER II

COMPARISON OF ALTERNATIVE STRATEGIES FOR MULTILEVEL OPTIMIZATION OF HIERARCHICAL SYSTEMS

Analytical target cascading (ATC) (Michelena et al. 1999; Kim et al. 2003) was developed for systems such as that shown in figure 2.1. In the initial formulation of ATC (Kim et al. 2000, 2001, 2002, 2003), deviation tolerances are defined for the responses and targets as well as the linking (or shared design) variables. The multilevel optimization problem is solved while minimizing the deviation tolerances and satisfying the design constraints.

ATC solution has been shown to converge to a point that satisfies the necessary optimality conditions of the original design optimization problem (Michelena et al. 2003). Using a formulation of ATC with similarities to that in (Kim et al. 2000), the inequality constraints on deviation tolerances were brought into the objective function to form an augmented objective function; this formulation included the addition of weight factors to the deviation tolerances. The scaled tolerance formulation (Kim et al. 2000) was used by Tzevelekos et al. (2003) to investigate the numerical behavior of the ATC methodology and the local convergence properties of different coordination strategies. They examined the effects of linking variables, subproblem solution accuracy, and the number of significant digits on numerical stability.

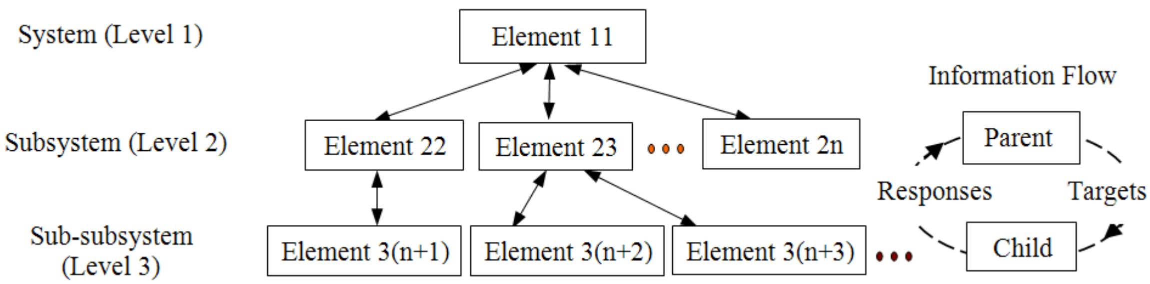

Figure 2.1 An illustrative model of a hierarchically decomposed multilevel system

The commonly used ATC formulations are based on quadratic penalty (QP) functions (Tzevelekos et al. 2003), (Michalek and Papalambros 2005a), (Michalek and Papalambros 2005b), (Tosserams 2004). Numerical experiments with these formulations show significant computational effort to obtain accurate solutions. The QP functions minimize the consistency constraints (equality or inequality) to force targets and responses to match. Ideally, these consistency constraints have to be relaxed, allowing inconsistencies between targets and responses that are gradually eliminated in the iterative solution process. For the QP function, in general, large weight factors are required to find accurate solutions (Bertsekas 1999). Due to lack of a mathematical relationship between weight factors and solution accuracy, the weight factors are given arbitrarily large values that may cause computational difficulties (Michalek and Papalambros 2005,2005a; Tosserams 2004).

An iterative method was presented by Michalek and Papalambros (2005) for finding the minimal penalty weight factors that provide converged solutions within user-specified inconsistency tolerances, and its effectiveness was demonstrated through several examples. This method contains an inner and an outer loop. The inner loop solves the decomposed ATC problem with a coordination scheme. The outer loop updates the penalty weight factors based on information obtained from the inner loop. The iterative method calculates the Lagrange multipliers and derivatives of the response function to update the weight factors.

In the separable ordinary Lagrangian (OL) approach, a large-scale convex nonlinear programming problem is formulated and decomposed using the ATC (Lassiter et al. 2005). By combining the classical Lagrangian duality and the augmented Lagrangian duality, a simple method was proposed in (Blouin et al. 2005) for decomposition without imposing restrictive conditions to alleviate the difficulty of convexity requirement. The modified Lagrangian dual formulation and coordination enhances the ATC performance (Kim et al. 2006) over those proposed earlier in the literature. ATC problem relaxation with an augmented Lagrangian penalty (ALP) function using the method of multipliers (AL) and the alternating direction method of multipliers (AL-AD) was proposed and investigated by Tosserams et al. (2006). By means of the ALP relaxation, ill-conditioning is reduced in the inner loop because accurate solutions can be obtained for smaller weight factors. This formulation was later adopted in (Li et al. 2008) that used Diagonal Quadratic Approximation (DQA) and Truncated DQA (TDQA) for parallelization of ATC. Similarly, the ALP formulation was also applied in (Wang et al. 2010), but three different updating methods were used in the outer loop.

In this chapter, the (ALP) function using the method of multipliers with four different coordination strategies (i.e., AL, AL-AD, DQA, and TDQA) is used to study the numerical behavior of ATC. Moreover, the role of two penalty parameters that can have large influence on solution accuracy and computational cost is investigated. The effects of the penalty parameter updating coefficient in the outer loop and the initial guessed values for the decision variables to start the multilevel optimization process are examined by solving three example problems.

Overview of ATC

For a decomposed system with N levels and M elements, as shown in figure 2.2, the subscripts ij denote the jth element in the ith level (Tosserams et al. 2006).

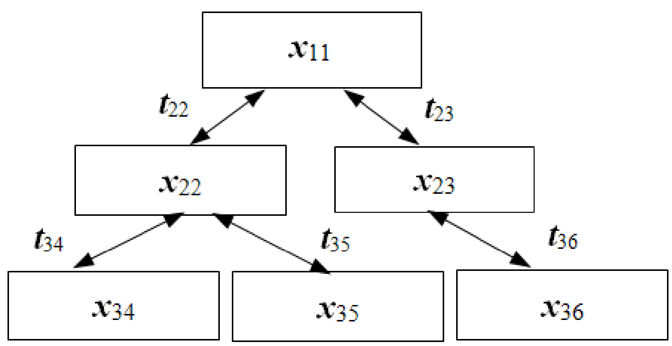

Figure 2.2 Variable allocation in a hierarchical system

The vector of local variables is denoted by $\boldsymbol{x}_{ij}$ with $\boldsymbol{t}_{ij}$ as the vector of target variables shared by element ij and its parent at level $i-1$; E_i is the set of elements at level i (e.g., $E_3 = \{4,5,6\}$ in figure 2.2); $D_{ij} = \left\{k_1, \dots, k_{D_{ij}}\right\}$ is the set of children of element ij (e.g., $D_{22} = \{4,5\}$); f_{ij} is the local objective; $\boldsymbol{g}_{ij}$ is the vector of local inequality constraints; and $\boldsymbol{h}_{ij}$ is the vector of local equality constraints. Hence, an all-in-one (AIO) problem of such a system is defined as

$$\min_{\boldsymbol{x}_{ij},\boldsymbol{t}_{ij}} \sum_{i=1}^{N} \sum_{j\,\in\,E_i} f_{ij}\left(\boldsymbol{x}_{ij}, \boldsymbol{t}_{ij}, \boldsymbol{t}_{(i+1)k_1}, \dots, \boldsymbol{t}_{(i+1)k_{D_{ij}}}\right)$$

$$\text{s.t.} \quad \boldsymbol{g}_{ij}\left(\boldsymbol{x}_{ij}, \boldsymbol{t}_{ij}, \boldsymbol{t}_{(i+1)k_1}, \dots, \boldsymbol{t}_{(i+1)k_{D_{ij}}}\right) \le 0 \tag{2.1}$$

$$\boldsymbol{h}_{ij}\left(\boldsymbol{x}_{ij}, \boldsymbol{t}_{ij}, \boldsymbol{t}_{(i+1)k_1}, \dots, \boldsymbol{t}_{(i+1)k_{D_{ij}}}\right) = 0$$

$$\forall j \in \mathrm{E}_i, i = 1, \dots, N$$

In the ATC formulation adopted from Tosserams et al. (2006), response copies $\boldsymbol{r}_{ij}$ are introduced to make the objective function and constraints separable, which leads to the addition of consistency constraints expressed as $\boldsymbol{c}_{ij} = \boldsymbol{t}_{ij} - \boldsymbol{r}_{ij} = 0$, where $\boldsymbol{c}_{ij}$ is a measure of inconsistency between the targets and the corresponding responses in element ij. Moreover, the objective function is augmented by the addition of a penalty term π that leads to the relaxed form of the AIO problem formulated as

$$\min_{\overline{\boldsymbol{x}}_{11},\dots,\overline{\boldsymbol{x}}_{NM}} \sum_{i=1}^{N} \sum_{j\,\in\,E_i} f_{ij}\left(\overline{\boldsymbol{x}}_{ij}\right) + \pi\left(\boldsymbol{c}_{ij}\right)$$

$$s.t. \quad \boldsymbol{g}_{ij}\left(\overline{\boldsymbol{x}}_{ij}\right) \le 0$$

$$\boldsymbol{h}_{ij}\left(\overline{\boldsymbol{x}}_{ij}\right) = 0 \tag{2.2}$$

$$\boldsymbol{c}_{ij} = \boldsymbol{t}_{ij} - \boldsymbol{r}_{ij} = 0$$

$$\text{with } \overline{\boldsymbol{x}}_{ij} = \left[\boldsymbol{x}_{ij}, \boldsymbol{r}_{ij}, \boldsymbol{t}_{ij}, \boldsymbol{t}_{(i+1)k_1}, \dots, \boldsymbol{t}_{(i+1)k_{D_{ij}}}\right]$$

$$\forall j \in E_i, i = 1, \dots, N$$

where $\boldsymbol{c} = [\boldsymbol{c}_{22}, \dots, \boldsymbol{c}_{NM}]$ in the hierarchy.

It is now possible to decompose the relaxed AIO problem in equation (2.2) into separate subproblems (e.g., P_{ij} for element ij) involving only a subset of decision variables $\overline{\boldsymbol{x}}_{ij}$ given by

$$\begin{aligned} &min_{\overline{\boldsymbol{x}}_{ij}} f_{ij}(\overline{\boldsymbol{x}}_{ij}) + \pi(\boldsymbol{c}_{ij}) \\ &s.t.\ \ \boldsymbol{g}_{ij}(\overline{\boldsymbol{x}}_{ij}) \leq 0 \\ &\boldsymbol{h}_{ij}(\overline{\boldsymbol{x}}_{ij}) = 0 \end{aligned} \tag{2.3}$$

$$\text{with } \overline{\boldsymbol{x}}_{ij} = \left[\boldsymbol{x}_{ij}, \boldsymbol{r}_{ij}, \boldsymbol{t}_{(i+1)k_1}, \dots, \boldsymbol{t}_{(i+1)k_{D_{ij}}}\right]$$

In QP, OL, and ALP, the penalty term takes the form

$$\pi_Q(\boldsymbol{c}_{ij}) = \left\|\boldsymbol{w}_{ij} \circ \boldsymbol{c}_{ij}\right\|_2^2 \tag{2.4}$$

$$\pi_L(\boldsymbol{c}_{ij}) = \boldsymbol{\lambda}_{ij}^T \boldsymbol{c}_{ij} \tag{2.5}$$

$$\pi_{AL}(\boldsymbol{c}_{ij}) = \boldsymbol{\lambda}_{ij}^T \boldsymbol{c}_{ij} + \left\|\boldsymbol{w}_{ij} \circ \boldsymbol{c}_{ij}\right\|_2^2 \tag{2.6}$$

The ALP method contains two loops. In the inner loop, the decomposed ATC problem is solved for fixed penalty parameters (**λ** and **w)** whereas in the outer loop, an algorithm is applied to update both **λ** and **w** as

$$\boldsymbol{\lambda}^{(k+1)} = \boldsymbol{\lambda}^{(k)} + 2\, \boldsymbol{w}^{(k)} \circ \boldsymbol{w}^{(k)} \circ \boldsymbol{c}^{(k)} \tag{2.7}$$

$$\boldsymbol{w}^{(k+1)} = \beta \boldsymbol{w}^{(k)} \tag{2.8}$$

where the penalty parameter updating coefficient β is required to be ≥ 1 for convex objective functions (Tosserams et al. 2006).

The double-loop approach in AL avoids setting arbitrarily large weight factors that can often cause ill-conditioning in the solution. The weight factors are updated using the information obtained from the inner loop. Whereas the inner loop is very computationally expensive, the outer loop is very inexpensive. It has been shown in the literature that the AL method can significantly reduce the computational cost of solving a problem with ATC without loss of accuracy.

Alternative Coordination Strategies

For the ALP formulation, the four alternative coordination strategies are described by the algorithms outlined in figures 2.3 and 2.4.

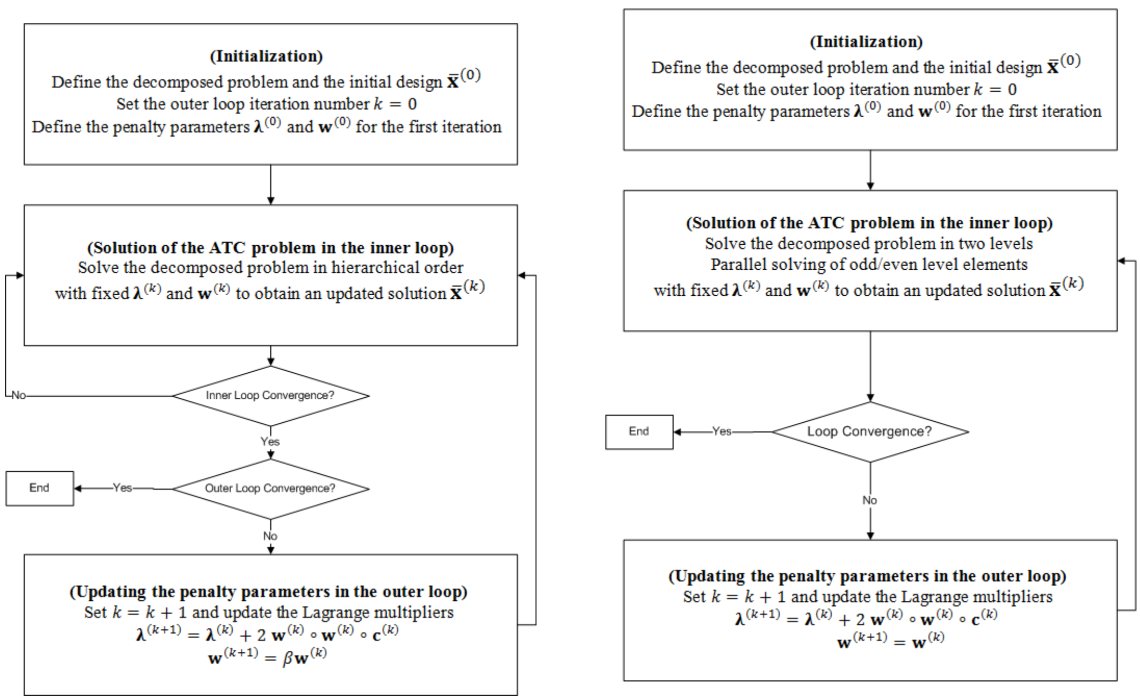

(a) (b)

Figure 2.3 Flowcharts of (a) AL and (b) AL-AD algorithms

For AL and AL-AD in figure 2.3, the outer-loop convergence criterion is satisfied when the reduction of inconsistencies in two successive solutions is sufficiently small (i.e., $\left\|\mathbf{c}^{(k)} - \mathbf{c}^{(k-1)}\right\| < \tau$, where k denotes the outer loop counter and τ is a user-defined termination tolerance). The inner loop convergence criterion is reached when the difference in the objective function values in two consecutive inner loop iterations is less than $\tau_{ATC} = \tau/10$.

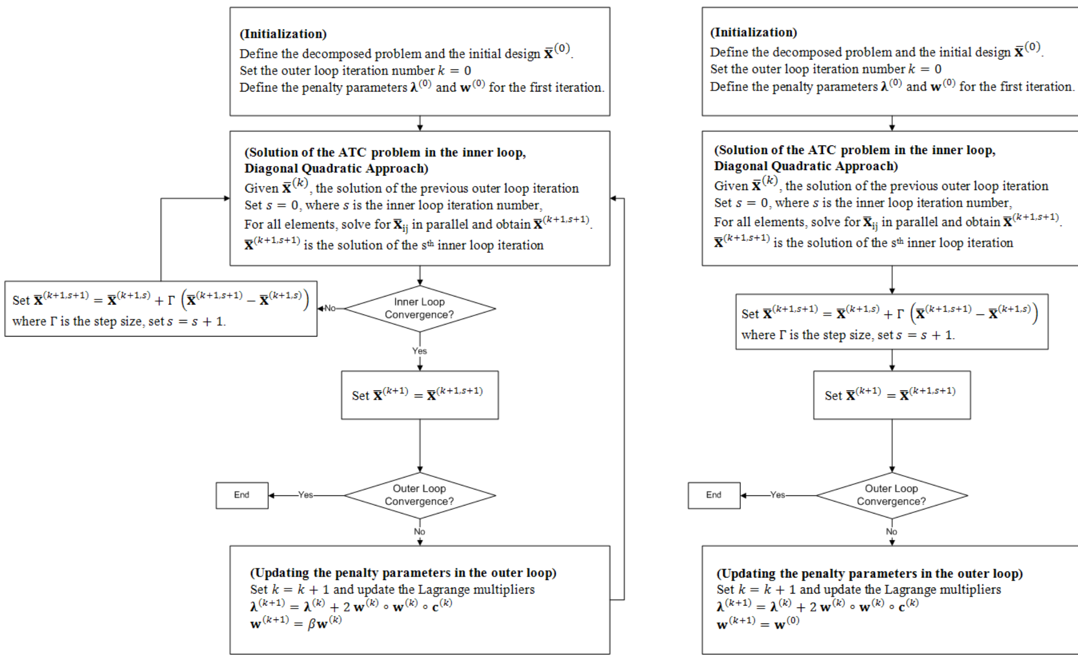

(a) (b)

Figure 2.4 Flowcharts of (a) DQA and (b) TDQA algorithms

In the DQA and TDQA algorithms in figure 2.4, the convergence criteria are defined as

$$max\left(\left\|\boldsymbol{t}^{(k+1,s+1)} - \boldsymbol{t}^{(k+1,s)}\right\|, \left\|\boldsymbol{r}^{(k+1,s+1)} - \boldsymbol{r}^{(k+1,s)}\right\|\right) \leq \sigma_{in} \tag{2.9}$$

$$max\left(\left\|\boldsymbol{t}^{(k+1)} - \boldsymbol{t}^{(k)}\right\|, \left\|\boldsymbol{r}^{(k+1)} - \boldsymbol{r}^{(k)}\right\|\right) \leq \sigma_{out} \tag{2.10}$$

where σ_{in} and σ_{out} are the inner and outer loop termination tolerances with $\sigma_{in} = \sigma_{out}/10$ and $\sigma_{out} = \tau$.

Illustrative Example Problems

The effect of β on the accuracy and computational cost has not been addressed in the literature. Although it has been mentioned that β can take a wide range of values, it is unclear what value must be chosen with respect to the desired levels of accuracy and computational cost as well as the selected ATC solution methodology and coordination strategy. Furthermore, since in ATC the initial values for response/target and linking variables are selected at random, it is unclear what effects these values would have on the ATC results.

To examine these effects, three different example problems are solved using the four different methods of ATC described in the previous section. For each method, the solution starts from different initial guessed values (IGV) that correspond to different randomly selected design points relative to the optimum point. The solution is repeated for 20 different values of β and every IGV.

Two performance metrics are considered: the computational cost that is captured by the number of function evaluations, and the error, which is defined as

$$e = \|\boldsymbol{x}^{*} - \boldsymbol{x}^{ATC}\|_{\infty} \tag{2.11}$$

where $\boldsymbol{x}^{*}$ is the exact optimum design point and $\boldsymbol{x}^{ATC}$ is the solution found by ATC. All of the ATC formulations cited were developed into separate MATLAB codes and used to solve the following example problems.

Problem 1

This is a 7-variable geometric programming problem with the AIO formulation expressed as

$$\min_{x_1,\ldots,x_7} f = x_1^2 + x_2^2 \tag{2.12}$$

$$s.t. \qquad g_1 = \frac{x_3^{-2}+x_4^2}{x_5^2} - 1 \le 0$$

$$g_2 = \frac{x_5^2+x_6^{-2}}{x_7^2} - 1 \le 0$$

$$h_1 = x_1^2 - x_3^2 - x_4^{-2} - x_5^2 = 0$$

$$h_2 = x_2^2 - x_5^2 - x_6^2 - x_7^2 = 0$$

$$x_1, x_2, \ldots, x_7 \ge 0$$

where the point of optimum is at $\boldsymbol{x}^* = [2.15, 2.06, 1.32, 0.76, 1.07, 1.0, 1.47]$ with all four constraints active.

This problem is decomposed into a two-level hierarchy (Tosserams 2004) with a single element at the top level and another element at the bottom level. Local variables in the top element are $x_1, x_3,$ and x_4 along with $f_1 = x_1^2$ as the objective function subject to the inequality constraint g_1 and equality constraint h_1. Variables $x_2, x_6,$ and x_7 are the local design variables for the bottom element with the objective function $f_2 = x_2^2$ and constraints g_2 and h_2. The response/target variable for the two elements is x_5. The initial values for the penalty parameters are defined as $\lambda^{(0)} = 0$ and $w^{(0)} = 1$. The starting design point is $\boldsymbol{x}^{(0)} = [3, 3, 3, 3, 3, 3, 3]$ for all the formulations. The ten initial guessed values (IGV), i.e., IGV #1, … #10 for x_5 are chosen as {0, 2, 4, 6, 8, 10, 20, 40, 70, 100}. For AL and DQA, β is given different values in the range of $\{1.1, 1.2, 1.3, \ldots, 3.0\}$, whereas for AL-AD and TDQA, $\beta = 1$. The IGV for x_5 and β are chosen arbitrarily to simply diversify the iterative solution process. The termination tolerance is chosen as $\tau = \{10^{-2}, 10^{-3}, 10^{-4}\}$.

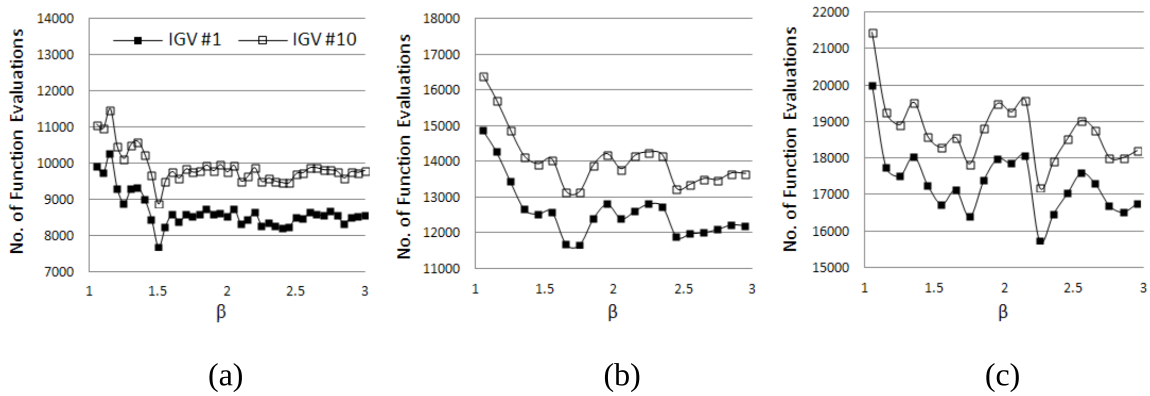

Figure 2.5 Cost trends for AL-based solution of Problem 1 using (a) $\tau = 10^{-2}$, (b) $\tau = 10^{-3}$, and (c) $\tau = 10^{-4}$

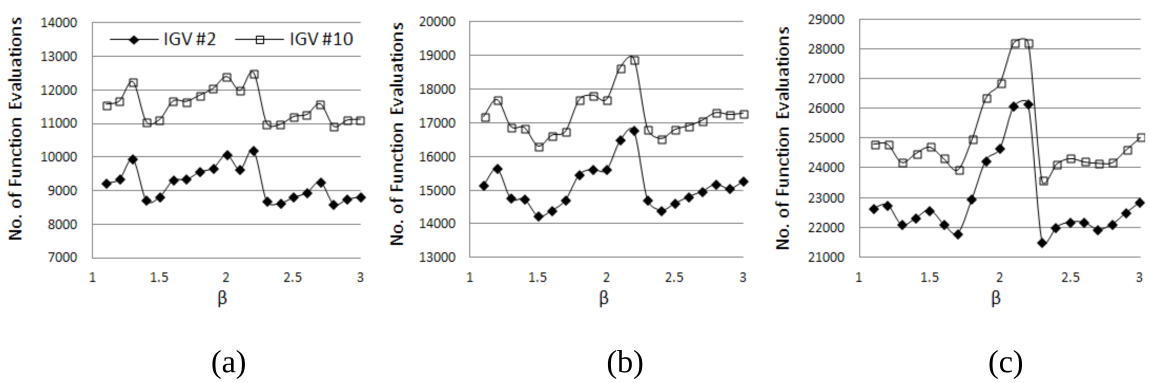

Figure 2.6 Cost trends for DQA-based solution of Problem 1 using (a) $\tau = 10^{-2}$, (b) $\tau = 10^{-3}$, and (c) $\tau = 10^{-4}$

Figures 2.5 and 2.6 show the plots of function evaluations number (cost) versus β for AL and DQA, respectively, using different IGV for x_5. These figures show that the cost is affected by the choice of β. The optimum β value to minimize cost depends on the termination tolerance used, but it appears to be near 1.5 or 2.3 for most cases. For different IGV, the relationship between cost and β is similar, but it is not necessarily monotonic. Due to this similarity, only the upper and lower bounds are shown for each case using the corresponding IGV numbers. It appears that the value of β also has an influence on the error, especially for larger tolerances as shown in figure 2.7.

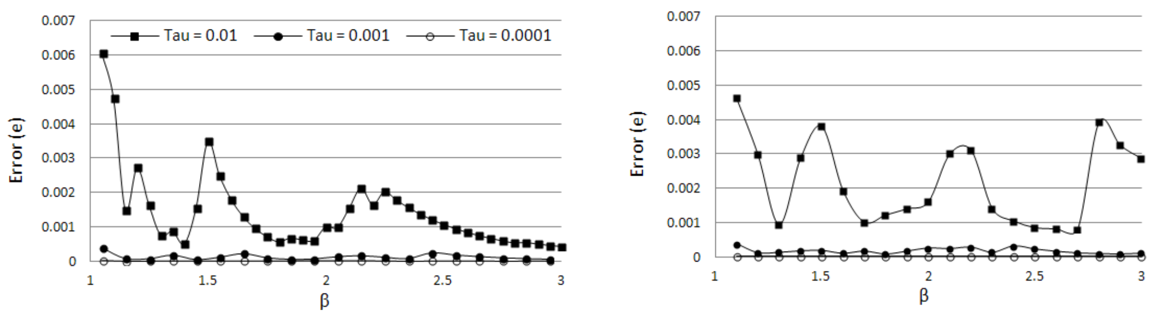

(a) (b)

Figure 2.7 Error trends for (a) AL and (b) DQA solutions of Problem 1 using x5 = 6 with $\tau = \{10^{-2}, 10^{-3}, 10^{-4}\}$

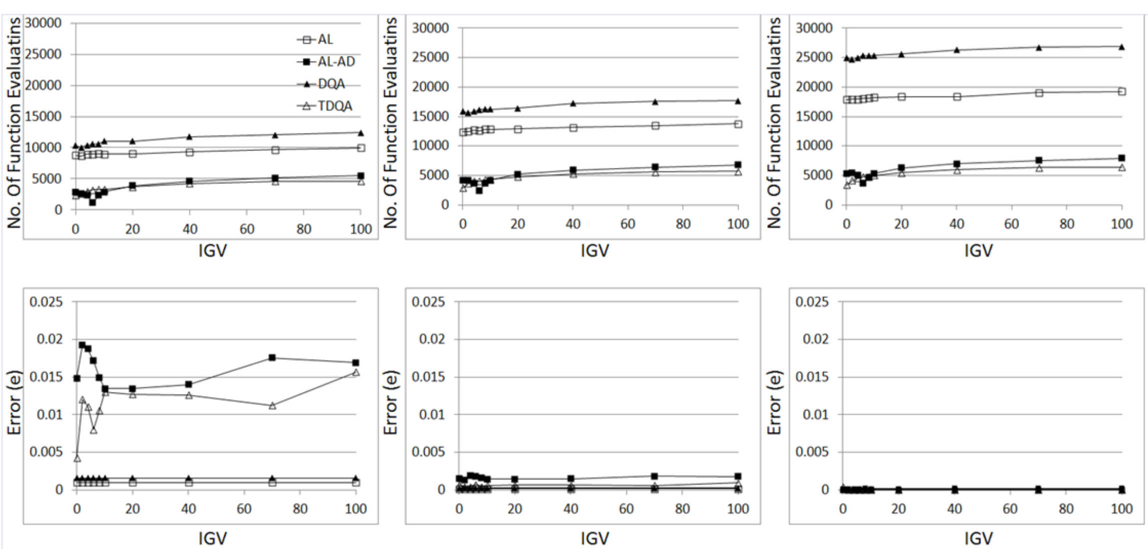

Figure 2.8 Cost and error trends from different solutions of Problem 1 using $\beta = 2$ for AL and DQA with (a) $\tau = 10^{-2}$, (b) $\tau = 10^{-3}$, and (c) $\tau = 10^{-4}$

The solution error trends for different IGV are identical; hence, the plot of error from equation (2.11) versus β is shown for only one case. Figure 2.8 is used to further highlight the effect of IGV on both function evaluations and error under different solution strategies and convergence tolerances. The plots are shown only for $\beta = 2$ case with three convergence tolerance values. The dependency of error on IGV for AL-AD and TDQA is very high at $\tau = 10^{-2}$, but minimal or nonexistent at $\tau = 10^{-3}$ and 10^{-4}. Thus, TDQA and AL-AD are much more dependent on IGV than DQA and AL. The efficiency of AL and DQA methods changes drastically with tighter termination tolerance, while solution error for AL and DQA does not change very much. Hence, for larger τ, AL and DQA are less costly, whereas for smaller τ, AL-AD and TDQA are more efficient.

Problem 2

This is a 14-variable geometric programming problem with the AIO formulation expressed as (Kim et al. 2001)

$$\min_{x_1, x_2, \ldots, x_{14}} \; f = x_1^2 + x_2^2 \tag{2.13}$$

$$s.t. \qquad g_1 = \frac{x_3^{-2} + x_4^2}{x_5^2} \leq 1$$

$$g_2 = \frac{x_5^2 + x_6^{-2}}{x_7^2} \leq 1$$

$$g_3 = \frac{x_8^2 + x_9^2}{x_{11}^2} \leq 1$$

$$g_4 = \frac{x_8^{-2} + x_{10}^2}{x_{11}^2} \leq 1$$

$$g_5 = \frac{x_{11}^2 + x_{12}^{-2}}{x_{13}^2} \leq 1$$

$$g_6 = \frac{x_{11}^2 + x_{12}^2}{x_{14}^2} \leq 1$$

$$h_1 = x_1^2 - (x_3^2 + x_4^{-2} + x_5^2) = 0$$

$$h_2 = x_2^2 - (x_5^2 + x_6^2 + x_7^2) = 0$$

$$h_3 = x_3^2 - (x_8^2 + x_9^{-2} + x_{10}^{-2} + x_{11}^2) = 0$$

$$h_4 = x_6^2 - (x_{11}^2 + x_{12}^2 + x_{13}^2 + x_{14}^2) = 0$$

$$x_1, x_2, \dots, x_{14} \geq 0$$

The global optimum is located at $x^* =$[2.84, 3.09, 2.36, 0.76, 0.87, 2.81, 0.94, 0.97, 0.87, 0.80, 1.30, 0.84, 1.76, 1.55] with $f^* = 17.6$ and all constraints active.

The decomposition model selected for this problem (Tosserams et al. 2006) has five elements in three levels: a top-level element (1) with two children (2 and 3) at level 2, each with one child (4 and 5, respectively) at the bottom level. Local variables in elements 2, 3, 4, and 5 are $\{x_4\}$, $\{x_7\}$, $\{x_8, x_9, x_{10}\}$, and $\{x_{12}, x_{13}, x_{14}\}$with design constraints being $\{g_1, h_1\}$, $\{g_2, h_2\}$, $\{g_3, g_4, h_3\}$, and $\{g_5, g_6, h_4\}$, respectively. The parameters $x_1, x_2, x_3,$ and x_6 are the responses/targets between elements 1-2, 1-3, 2-4, and 3-5, respectively, whereas x_5 and x_{11} are the linking variables between elements 2-3 and 4-5, respectively, both of which are coordinated in element 1.

The initial values for the penalty parameters in all the formulations are taken as $\boldsymbol{\lambda}^{(0)} = 0$ and $\mathbf{w}^{(0)} = 1$. The initial design point is $\boldsymbol{x}^{(0)} =$[5, 5, 2.76, 0.25, 1.26, 4.64, 1.39, 0.67, 0.76, 1.7, 2.26, 1.41, 2.71, 2.66] for all the formulations, which is the same as that used in the previous studies cited. The IGV for $x_1, x_2, x_3, x_5, x_6,$ and x_{11} are randomly selected in the design domain with a relative distance of $\{0, 2, 4, 6, 8, 10, 20, 40, 70, 100\}$ from the optimum point with the corresponding values shown in Table 2.1. These variables need to have predefined values to start the ATC solution sequence. For example in AL, it is necessary to guess values for response/linking variables x_1, x_2, x_5, and x_{11} from the lower level elements to solve element 1, response value for x_3 from element 4 to solve element 2 and response value for x_6 from element 5 to solve element 3. For AL and DQA, β ={1.1, 1.2, 1.3, …, 2.9, 3}, whereas for AL-AD and TDQA, $\beta = 1$. The termination tolerances were set to $\tau =$ {10^{-2}, 10^{-3}, 10^{-4}}. Computational cost in AL and DQA is affected by β values but it follows a non-monotonic manner. It has the minimum computational cost near $\beta = 2$ and it generally increases with higher β values as shown in figures 2.9 and 2.10.

Table 2.2 List of IGV for response/target and linking variables in Problem 2.

IGV	$[x_1, x_2, x_3, x_5, x_6, x_{11}]$
1	$[2.835, 3.090, 2.355, 0.870, 2.812, 1.301]$
2	$[2.979, 4.094, 1.417, 2.231, 2.886, 0.895]$
3	$[5.764, 2.848, 0.412, 1.748, 1.222, 0.777]$
4	$[0.125, 0.835, 3.382, 5.370, 1.457, 1.080]$
5	$[6.731, 3.675, 3.192, 7.602, 3.964, 2.437]$
6	$[7.444, 10.626, 2.843, 3.127, 6.366, 3.160]$
7	$[2.740, 4.545, 7.056, 18.179, 10.027, 5.410]$
8	$[1.582, 23.522, 19.805, 7.305, 8.027, 29.399]$
9	$[15.582, 53.774, 12.037, 6.821, 37.460, 29.94]$
10	$[0.141, 46.214, 8.356, 81.508, 19.002, 36.692]$

The plots in figure 2.11 show that error in both AL and DQA depends on the β value, especially with $\tau = 10^{-2}$, and this is very critical for the DQA method. The error in AL is nearly uniform for $\beta > 1.5$ while in DQA it has an ascending mode.

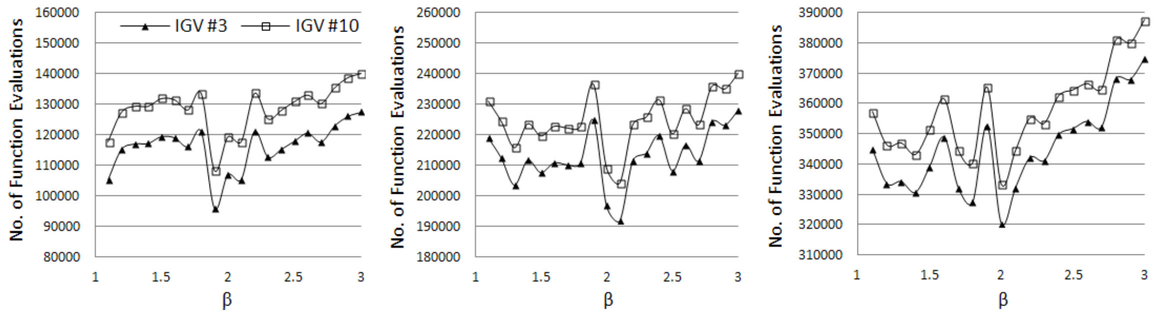

(a) (b) (c)

Figure 2.9 Cost trends for AL-based solution of Problem 2 using (a) $\tau = 10^{-2}$, (b) $\tau = 10^{-3}$, and (c) $\tau = 10^{-4}$

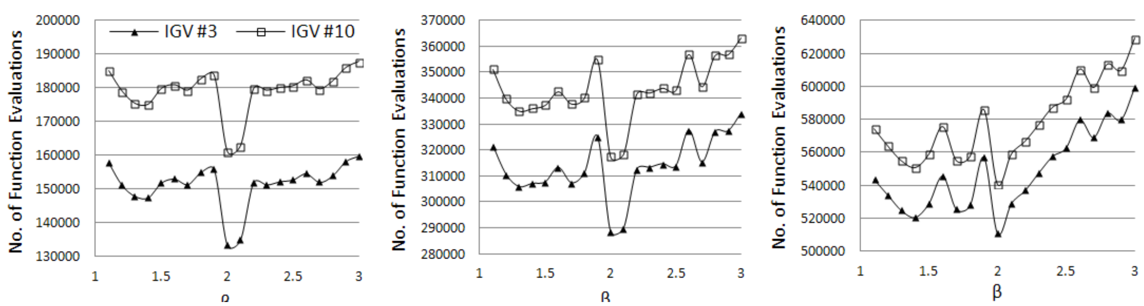

(a) (b) (c)

Figure 2.10 Cost trends for DQA-based solution of Problem 2 using (a) $\tau = 10^{-2}$, (b) $\tau = 10^{-3}$, and (c) $\tau = 10^{-4}$

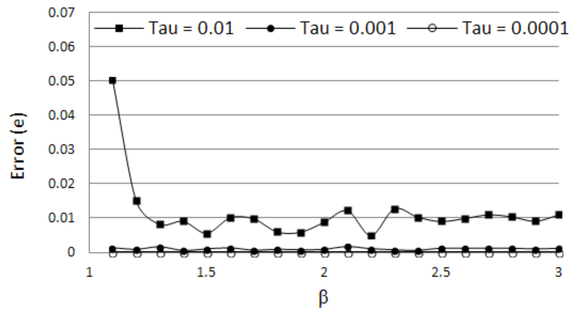

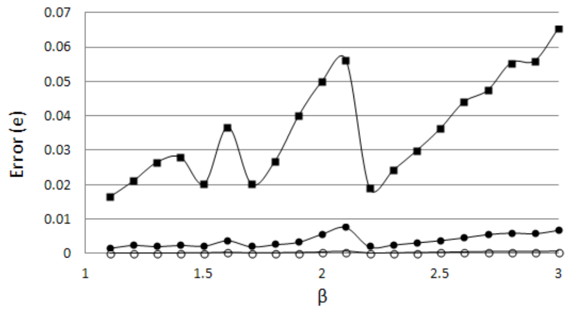

(a) (b)

Figure 2.11 Error trends for (a) AL and (b) DQA solutions of Problem 2 using IGV #4 with $\tau = \{10^{-2}, 10^{-3}, 10^{-4}\}$

Figure 2.12 indicates that the dependency of error on IGV for AL-AD and DQA is observable at $\tau = 10^{-2}$, diminishes slightly for TDQA at $\tau = 10^{-3}$, and vanishes at $\tau = 10^{-4}$. It can be concluded that TDQA and, to some extent, AL-AD are much more dependent on the IGV than DQA and AL. The computational costs of AL and DQA drastically change with tighter termination tolerance, while solution errors in AL and DQA do not change very much. In contrast to AL and DQA, the error in AL-AD and TDQA changes with different τ values while the computational costs are nearly similar. Hence, for larger τ, AL and DQA are better choices, whereas for tighter τ, AL-AD and TDQA are more efficient.

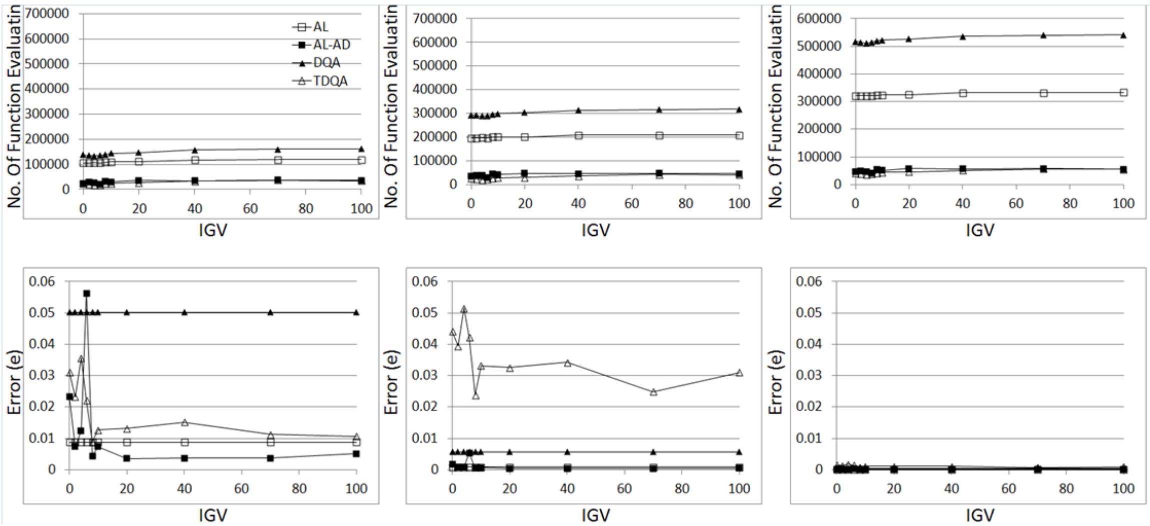

(a) (b) (c)

Figure 2.12 Cost and error trends from different solutions of Problem 2 using $\beta = 2$ for AL and DQA with (a) $\tau = 10^{-2}$, (b) $\tau = 10^{-3}$, and (c) $\tau = 10^{-4}$

Problem 3

This is a seven-variable geometric programming problem with only inequality constraints. The corresponding AIO problem is expressed as

$$\min f = (x_1 - 10)^2 + 5(x_2 - 12)^2 + x_3^4 + 3(x_4 - 11)^2 + 10x_5^6 + 7x_6^2 + x_7^4 - 4x_6x_7 - 10x_6 - 8x_7 \tag{2.14}$$

$$s.t. \quad g_1 = -127 + 2x_1^2 + 3x_2^4 + x_3 + 4x_4^2 + 5x_5 \leq 0$$

$$g_2 = -282 + 7x_1 + 3x_2 + 10x_3^2 + x_4 - x_5 \leq 0$$

$$g_3 = -196 + 23x_1 + x_2^2 + 6x_6^2 - 8x_7 \leq 0$$

$$g_4 = 4x_1^2 + x_2^2 - 3x_1x_2 + 2x_3^2 + 5x_6 - 11x_7 \leq 0$$

$$-10 \leq x_i \leq 10, i = 1, \ldots, 7$$

where $\boldsymbol{x}^{*}$ = [2.3305, 1.9513, -0.4775, 4.3657, -0.6245, 1.0371, 1.5942] is the unique optimal solution. The problem is decomposed into three elements in two levels: a top-level element with elements 2 and 3 at level 2. There is no local variable or constraint at the top level. Local variables of element 2 are x_4 and x_5 along with constraints g_1 and g_2. Local variables of element 3 are x_6 and x_7 with inequality constraints g_3 and g_4. There is no target variable in this decomposed structure. The linking variables x_1, x_2, and x_3 are shared between elements 2 and 3 and coordinated in element 1.

The starting design point is $\boldsymbol{x}^{(0)}$ = [0,0,0,0,0,0,0] for all the formulations. The IGV for $x_1, x_2,$ and x_3 are randomly selected in design domain at a distance nearly equal to $\{0, 2, 4, 6, 8, 10\}$ from the optimum point with the corresponding values shown in Table 2.2.

Table 2.3 List of IGV for linking variables in Problem 3.

IGV	$[x_1, x_2, x_3]$
1	$[2.3305, 1.9514, -0.4775]$
2	$[0.3635, 1.9144, -0.8961]$
3	$[-0.0929, 0.0739, 2.1134]$
4	$[5.0429, -2.6988, -3.2525]$
5	$[1.3226, 1.4993, 7.4720]$
6	$[8.1345, -3.6255, 5.3449]$

For AL and DQA, $\beta = \{1.1, 1.2, 1.3, \ldots, 2.9, 3\}$, whereas for AL-AD and TDQA, $\beta = 1$. The termination tolerances were set to $\tau = \{10^{-2}, 10^{-3}, 10^{-4}\}$.

Figures 2.13 and 2.14 show that the computational cost changes greatly with variations in β value and that the fluctuations are more pronounced for the smaller τ values. Figure 2.15 shows that error in AL is slightly dependent on β just for $\tau = 10^{-2}$ and it nearly disappears for $\tau = 10^{-3} and\ 10^{-4}$. The error in DQA is more dependent on β than AL.

Figure 2.16 indicates that the computational cost dependency on IGV is negligible; the changes in computational cost are lower than 5% for all the methods. The computational cost for AL and DQA, especially for DQA, changes significantly while the error is nearly identical for tighter tolerances. Also, dependency of the error on IGV in AL-AD and TDQA is observable at $\tau = 10^{-2}$ and vanishes for tighter tolerances.

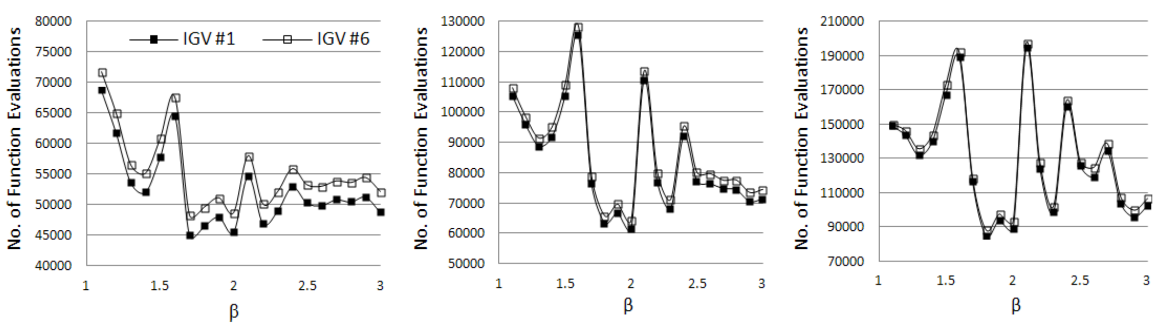

(a) (b) (c)

Figure 2.13 Cost trends for AL-based solution of Problem 3 using (a) $\tau = 10^{-2}$, (b) $\tau = 10^{-3}$, and (c) $\tau = 10^{-4}$

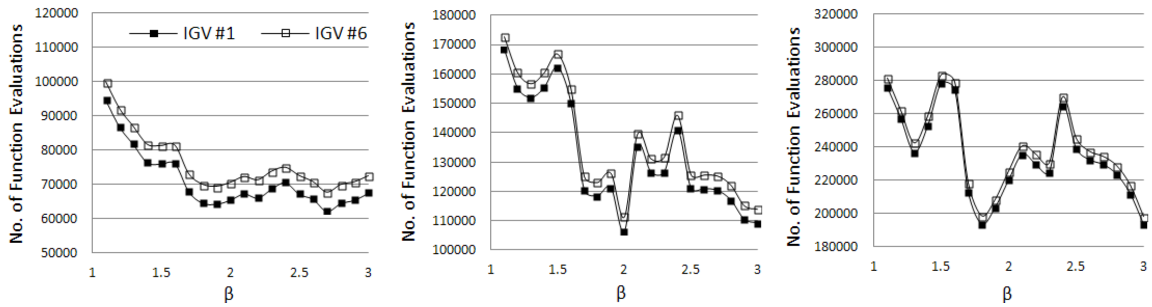

(a) (b) (c)

Figure 2.14 Cost trends for DQA-based solution of Problem 3 using (a) $\tau = 10^{-2}$, (b) $\tau = 10^{-3}$, and (c) $\tau = 10^{-4}$

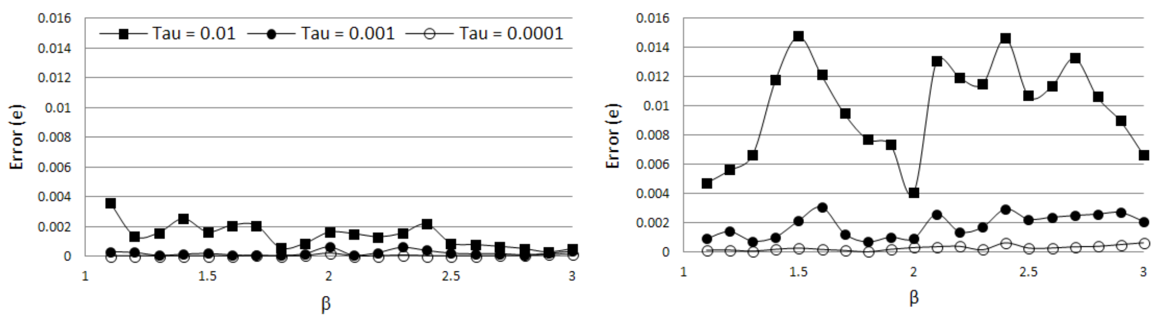

(a) (b)

Figure 2.15 Error trends for (a) AL and (b) DQA solutions of Problem 3 using IGV #3 with $\tau = \{10^{-2}, 10^{-3}, 10^{-4}\}$

Conclusion

The numerical behavior of the analytical target cascading (ATC) method was investigated for multilevel optimization of hierarchical systems based on different solution strategies. The strategies considered included Augmented Lagrangian with method of multipliers (AL), Augmented Lagrangian with Alternating Direction method of multipliers (AL-AD), Diagonal Quadratic Approximation (DQA), and Truncated

Diagonal Quadratic Approximation (TDQA). Three example problems were used to examine the effects of penalty parameter updating coefficient β and convergence tolerance τ on the computational cost and solution accuracy. In addition, the effect of initial guessed values (IGV) for the response/target and linking variables was also investigated.

The results showed that although the computational cost in the AL and DQA methods is influenced by the value of β, it does not follow a specific ascending/descending pattern. The computational cost dependency on β is generally higher with increasing the convergence tolerance. Although previous studies recommend $\beta > 1$ and $2 < \beta < 3$, the results found here indicate that $1 < \beta < 2$ is also acceptable and that no single value of β can be suggested to reduce the computational cost in all the ATC-based optimization problems and solution strategies. The results also showed that the relationship between the computational cost and β is not dependent on the IGV as best noted in the results of the DQA method.

In terms of solution accuracy, AL and DQA results depend on the β value irrespective of the selected IGV. With higher β values, better accuracy is obtained with AL while the behavior is different for DQA. The dependency of solution accuracy on β is reduced with tighter tolerance values. Comparison of the DQA and AL results indicate that AL is more stable in terms of accuracy whereas DQA needs to have a tighter tolerance to obtain reasonable accuracy, although a tighter tolerance causes significant changes in the computational cost. In the absence of optimum β for computational cost and accuracy, the AL method appears to be more reliable than DQA.

By moving the IGV farther away from the corresponding values at the point of optimum, all methods required more function calls, as expected. While the solution accuracy in AL and DQA was not influenced by the choice of IGV, the trend was quite the opposite for AL-AD and TDQA as they both had great dependency on IGV. The inner loop convergence requirement is more costly for AL and DQA than TDQA and AL-AD. Furthermore, the increase in computational cost for AL-AD and TDQA is much greater than AL and DQA when IGV is farther away from the optimum, but TDQA and AL-AD still show better performance. AL-AD and TDQA need tighter termination tolerances to have better accuracy.

In summary, the τ and β values have greater effect on AL and DQA solutions than the other two coordination strategies and they are not influenced by IGV. Hence, in using AL and DQA, appropriate values for these two parameters can enhance both solution accuracy and computational cost. In contrast, the computational cost and accuracy of AL-AD and TDQA are greatly dependent on the IGV.

CHAPTER III

RELIABILITY-BASED DESIGN OPTIMIZATION WITHIN ANALYTICAL TARGET CASCADING FRAMEWORK

The ATC formulation and coordination strategies have also been extended to design problems that include the presence and effects of uncertainties. There are, however, very few publications related to non-deterministic ATC formulations and applications. Liu et al. (2006) presented a particular probabilistic ATC (PATC) formulation that matches the first two moments of interrelated responses and linking variables whereas Kokkolaras et al. (2006) extended the deterministic ATC formulation using both probabilistic and interval analysis approaches. They considered representation of uncertain quantities as optimization variables with specific probability distributions, and propagated uncertainty through the decomposed system. In the area of reliability-based design optimization (RBDO), a large body of work is available. One of the principal challenges in RBDO is the evaluation of non-deterministic constraint functions that tend to be very computationally intensive, especially in presence of highly nonlinear limit state functions. Various approaches have been proposed to improve the computational efficiency of RBDO problems.

In this chapter, the SLSV approach (Chen et al. 1997) for RBDO is integrated with ALP formulation (Tosserams et al. 2006) of ATC for solution of multilevel hierarchical systems under uncertainty. The proposed SLSV+AL formulation matches the required moments of connecting responses/targets and linking variables. This method requires only a modest increase in computational cost over the deterministic ATC while the double-loop methods require significantly higher computational efforts. The RBDO with focus on SLSV and ALP methods along with SLSV+AL formulation are discussed. This is followed by the presentation of numerical example problems, associated results, and conclusions.

Reliability-Based Design Optimization

A general statement of the deterministic optimization can be typically presented as follows:

$$\min f(\boldsymbol{x}) \tag{3.1}$$

$$s.t. \quad g_j(\boldsymbol{x}) \leq 0, \;\; j = 1, \ldots, m$$

$$\boldsymbol{x}^L \leq \boldsymbol{x} \leq \boldsymbol{x}^U$$

where $f(\boldsymbol{x})$ is the objective function, $\boldsymbol{x}$ is the design vector, $g_j(\boldsymbol{x})$ is the ith constraint that models the failure of the system, and $\boldsymbol{x}^L$ and $\boldsymbol{x}^U$ are the lower and upper limit of the vector of design variables. In deterministic optimization, the designs are obtained without considering uncertainties in the design variables. The resulting optimum based on deterministic optimization is usually associated with a high probability of failure due to little or no latitude for uncertain bounds especially for active constraints.

When the design variables are random with probabilistic constraints, a deterministic optimization problem is replaced with a formulation of RBDO as follows:

$$\min f(\boldsymbol{d}) \tag{3.2}$$

$$s.t. \quad Pr\left[g_j(\boldsymbol{X}) > 0\right] \leq \Phi\left(-\beta_j^t\right), \;\; j = 1, \ldots, m$$

$$\boldsymbol{d}^L \leq \boldsymbol{d} \leq \boldsymbol{d}^U$$

where $f(\boldsymbol{d})$ is the objective function, $\boldsymbol{d}$ is the design vector which assumed to be the mean of the random variable vector $\boldsymbol{X}$, $g_j(\boldsymbol{x}) \leq 0$ is the safe region of the ith constraint, $Pr\left[g_j(\boldsymbol{X}) > 0\right]$ is the fail probability, $\Phi\left(-\beta_j^t\right)$ is the upper limit of fail probability for ith constraint, β_j^t is the target reliability, $\Phi(.)$ is the standard cumulative distribution function of the normal variable, and $\boldsymbol{x}^L$ and $\boldsymbol{x}^U$ are the lower and upper limits of the vector of design variables, respectively.

Researchers have proposed a variety of formulations for performing RBDO under the double-loop structure like reliability index approach (RIA) and performance measure approach (PMA) or better efficiency single/serial loop structure like single-loop single-vector (SLSV) and sequential optimization and reliability assessment (SORA). Double-loop structures are performed by nesting two subproblems: Deterministic optimization problem and reliability analysis.

The formulation based on RIA is presented as follows:

$$\min f(\boldsymbol{d}) \tag{3.3}$$

$$s.t. \quad \beta_j \geq \beta_j^t, \;\; j = 1, \ldots, m$$

$$\boldsymbol{d}^L \leq \boldsymbol{d} \leq \boldsymbol{d}^U$$

The reliability index β_j is determined by solving the minimization problem in the standard normal space (U-space) of random variables

$$\min \beta_j = \boldsymbol{U}^{\boldsymbol{T}}\boldsymbol{U} \tag{3.4}$$

$$s.t. \qquad G_j(\boldsymbol{U}) = 0, \;\; j = 1, \dots, m$$

where $\boldsymbol{U}$ is the vector of random variables in the standard normal space corresponding to the random variable vector $\boldsymbol{X}$. The limit state function $g_j(\boldsymbol{X})$ is the image of $G_j(\boldsymbol{U})$ in the physical space. The double-loop structure formulation based on PMA can be formulated as follows

$$\min f(\boldsymbol{d}) \tag{3.5}$$

$$s.t. \quad \alpha_j \leq 0, \;\; j = 1, \dots, m$$

$$\boldsymbol{d}^L \leq \boldsymbol{d} \leq \boldsymbol{d}^U$$

where α_j is determined by maximization problem for the evaluation of reliability as

$$\max \alpha_j = G_j(\boldsymbol{U}) \tag{3.6}$$

$$s.t. \qquad f(\boldsymbol{U}^{\boldsymbol{T}}\boldsymbol{U}) = \beta_j^t, \;\; j = 1, \dots, m$$

The sub-optimization problem can be solved by simulation-based methods such as direct Monte Carlo Simulation (MCS) (Rubinstein, 1981), Importance Sampling (Melchers, 1989), Adaptive Importance Sampling (Wu, 1994) or approximate analytical methods which include Hasofer and Lind (1974), Advanced Mean Value method (AMV) (Wu and Burnside, 1988), and Hybrid Mean Value method (HMV) (Youn and Choi 2004).

The solution in traditional double-loop approaches for RBDO is carried out in two separate spaces, causing the number of function calls to dramatically increase, especially for systems with a large number of constraints. The enormous computational time makes these approaches impractical.

A more efficient method for probabilistic design optimization is the SLSV approach which provides the same level of accuracy as the previous double-loop methods at a fraction of computational cost. The cost of RBDO based on SLSV increases by less than a factor of two or less as compared to solving the corresponding deterministic design optimization problem.

Single-Loop Single-Vector Method

An RBDO problem with a deterministic objective function and N probabilistic design constraints can be formulated by expanding equation (3.2) as

$$\min f(\boldsymbol{\mu_X}, \boldsymbol{p}) \tag{3.7}$$

$$s.t. \quad Pr\left[g_j(\boldsymbol{X}, \boldsymbol{p}) > 0\right] \leq \Phi\left(-\beta_j^t\right), j = 1, .., N$$

$$\boldsymbol{\mu_X^L} \leq \boldsymbol{\mu_X} \leq \boldsymbol{\mu_X^U}, i = 1, \ldots, ND$$

where $\boldsymbol{\mu_X}$ is the mean of $\boldsymbol{X}$, and $\boldsymbol{p}$ is the vector of deterministic parameters. The total number of design variables is denoted by ND.

For normal random variables, the SLSV formulation (Chen et al. 1997) of the RBDO problem in equation (3.7) is stated as

$$\min f\left(\boldsymbol{\mu_X^{(k)}}, \boldsymbol{p}\right) \tag{3.8}$$

$$s.t. \quad g_j\left(\boldsymbol{X}_j, \boldsymbol{p}\right) \leq 0$$

$$\boldsymbol{\mu_X^L} \leq \boldsymbol{\mu_X} \leq \boldsymbol{\mu_X^U}$$

$$\boldsymbol{X}_j = \boldsymbol{\mu_X^{(k)}} + \beta_j^t \boldsymbol{\sigma_X} \boldsymbol{\alpha}_j^{(k-1)}$$

$$\boldsymbol{\alpha}_j^{(k-1)} = \boldsymbol{\sigma_X} \nabla_X g_j\left(\boldsymbol{X}_j^{(k-1)}\right) / \left\| \boldsymbol{\sigma_X} \nabla_X g_j\left(\boldsymbol{X}_j^{(k-1)}\right) \right\|$$

where $\boldsymbol{\sigma_X}$ is the vector of standard deviations of $\boldsymbol{X}$, and β_j^t is the target value of safety factor associated with the jth constraint. In SLSV, there is no need to calculate the safety index, β_j for the jth constraint. Instead a search is conducted to find $\boldsymbol{\mu_X}$ such that $\boldsymbol{X}_j$ is located on the limit state surface at $g_j = 0$ representing the MPP. $\boldsymbol{X}_j$ can be determined directly from $\boldsymbol{\mu_X}$ as noted in equation (3.8). The parameter k in equation (3.8) is an iteration counter. Equation (3.8) is essentially a deterministic representation of the RBDO problem in equation (3.7).

The SLSV method requires an iterative solution with an algorithm that is as follows:

1. Select an arbitrary initial point in the random space denoted by $\boldsymbol{X}^{(0)}$. Evaluate the normalized constraint gradient vectors, $\boldsymbol{\alpha}_j^{(0)}$ for the *m* potentially active constraints and calculate the resultant unit vector, $\boldsymbol{\alpha}^{(0)}$ as

$$\boldsymbol{\alpha}_j^{(0)} = \frac{\boldsymbol{\sigma_X} \nabla_X g_j(\boldsymbol{X}^{(0)})}{\|\boldsymbol{\sigma_X} \nabla_X g_j(\boldsymbol{X}^{(0)})\|} \tag{3.9}$$

$$\boldsymbol{\alpha}^{(0)} = \frac{\sum_j \boldsymbol{\alpha}_j^{(0)}}{\left\|\sum_j \boldsymbol{\alpha}_j^{(0)}\right\|} \tag{3.10}$$

2. Find the initial estimate of the mean vector $\boldsymbol{\mu}_{\boldsymbol{X}}^{(0)}$ using

$$\boldsymbol{\mu}_{\boldsymbol{X}}^{(0)} = \boldsymbol{X}^{(0)} - \beta_0 \boldsymbol{\sigma_X} \boldsymbol{\alpha}^{(0)} \tag{3.11}$$

3. For the subsequent iterations (i.e., k ≥ 1), the updated vector $\mu_X^{(k)}$ is found by solving the optimization problem defined as

$$\min f\left(\boldsymbol{\mu}_{\boldsymbol{X}}^{(k)}\right) \tag{3.12}$$

$$s.t. \quad g_j\left(\boldsymbol{X}_j\right) \leq 0$$

$$\boldsymbol{X}_j = \boldsymbol{\mu}_{\boldsymbol{X}}^{(k)} + \beta_j^t \boldsymbol{\sigma}_{\boldsymbol{X}} \boldsymbol{\alpha}_j^{(k-1)}$$

$$\boldsymbol{\alpha}_j^{(k-1)} = \frac{\nabla_X g_j\left(\boldsymbol{X}_j^{(k-1)}\right)}{\left\|\nabla_X g_j\left(\boldsymbol{X}_j^{(k-1)}\right)\right\|}$$

$$\boldsymbol{\mu}_{\boldsymbol{X}}^{l} \leq \boldsymbol{\mu}_{\boldsymbol{X}}^{(k)} \leq \boldsymbol{\mu}_{\boldsymbol{X}}^{u}$$

4. After obtaining $\boldsymbol{X}_j^{(1)}$, the constraint gradient vectors are recalculated at $\boldsymbol{X}_j^{(1)}$ for input to the next iteration. Meanwhile, $\boldsymbol{\alpha}_j$ is updated using the new constraint derivatives for the next computation of $\boldsymbol{X}_j$. The vectors $\boldsymbol{\mu}_{\boldsymbol{X}}$ and $\boldsymbol{X}_j$ are alternately updated until the computations converge to a final probabilistic design at coordinates defined by $\boldsymbol{\mu}_{\boldsymbol{X}}$, and a set of final vectors $\boldsymbol{X}_j, j = 1, m$ that describe the MPP for each of the active constraints.

The SLSV can also be applied to RBDO problems with non-normal random variables. For a normal distribution, the relation between design variables, $\boldsymbol{\mu}_{\boldsymbol{X}}^{(k)}$ and the MPP point, $\boldsymbol{X}^{(k)}$ is defined as

$$\boldsymbol{\mu}_{\boldsymbol{X}}^{(k)} = \boldsymbol{X}^{(k)} - \beta \boldsymbol{\sigma}_{\boldsymbol{X}} \boldsymbol{\alpha}^{(k-1)} \tag{3.13}$$

However, in case of non-normal distribution, this relation is implicit and more complex.

For non-normal random variables, the equivalent normal means and standard deviations are calculated first. Suppose that a particular non-normal random variable X with mean μ_X and standard deviation σ_X is described by a cumulative distribution function $F_X(x)$ and a probability density function $f_X(x)$. The equivalent mean μ_X^e and standard deviation σ_X^e are computed at X^* on the limit state function presented by $g = 0$, where the CDF and PDF of the actual function are equal to the normalized CDF and PDF stated as (Nowak and Collins 2000)

$$F_X(x^*) = \Phi\left(\frac{x^* - \mu_X^e}{\sigma_X^e}\right) \tag{3.14}$$

$$f_X(x) = \frac{1}{\sigma_X^e}\phi\left(\frac{x^* - \mu_X^e}{\sigma_X^e}\right) \tag{3.15}$$

where Φ is the CDF and ϕ is the PDF of the standard normal distribution. The μ_X^e and σ_X^e can be obtained as

$$\mu_X^e = x^* - \sigma_X^e\left[\Phi^{-1}\left(F_X(x^*)\right)\right] \tag{3.16}$$

$$\sigma_X^e = \frac{1}{f_X(x^*)}\phi\left[\Phi^{-1}\left(F_X(x^*)\right)\right] \tag{3.17}$$

Thus, the SLSV with non-normal distributions can be reformulated as

$$\min f\left(\boldsymbol{\mu}_{\boldsymbol{X}}^{(k)}, \boldsymbol{p}\right) \tag{3.18}$$

$$s.t. \quad g_j\left(\boldsymbol{X}_j, \boldsymbol{p}\right) \leq 0$$

$$\boldsymbol{\mu}_{\boldsymbol{X}}^l \leq \boldsymbol{\mu} \leq \boldsymbol{\mu}_{\boldsymbol{X}}^u$$

$$\boldsymbol{X}_j = \boldsymbol{\mu}_{\boldsymbol{X}}^{e(k)} - \beta_j^t \boldsymbol{\sigma}_{\boldsymbol{X}}^e \boldsymbol{\alpha}_j^{(k-1)}$$

$$\boldsymbol{\alpha}_j^{(k-1)} = \nabla_X g_j\left(\boldsymbol{X}^{(k-1)}\right) / \left\|\nabla_X g_j\left(\boldsymbol{X}^{(k-1)}\right)\right\|$$

The step-by-step algorithm for SLSV with non-normal distribution is described as follows:

1. Set the initial design $\boldsymbol{\mu}_{\boldsymbol{X}}^{(k)}$, and the initial estimate for MPP $\boldsymbol{X}^{(k)}$, where k is set to 0.
2. Find the design $\boldsymbol{\mu}_{\boldsymbol{X}}^{(k+1)}$ by solving the following optimization problem

$$\min f\left(\boldsymbol{\mu}_{\boldsymbol{X}}^{(k+1)}, \boldsymbol{p}\right) \tag{3.19}$$

$$s.t. \quad g_j\left(\boldsymbol{X}_j, \boldsymbol{p}\right) \leq 0$$

$$\boldsymbol{\mu}_{\boldsymbol{X}}^{l} \leq \boldsymbol{\mu} \leq \boldsymbol{\mu}_{\boldsymbol{X}}^{u}$$

$$\boldsymbol{\sigma}_{\boldsymbol{X}}^{e(k+1)} = \frac{1}{f_X\left(\boldsymbol{X}^{(k)}\right)} \phi\left[\Phi^{-1}\left(F_X\left(\boldsymbol{X}^{(k)}\right)\right)\right]$$

$$\boldsymbol{\mu}_{\boldsymbol{X}}^{e(k+1)} = \boldsymbol{X}^{(k)} - \boldsymbol{\sigma}_{\boldsymbol{X}}^{e(k)}\left[\Phi^{-1}\left(F_X\left(\boldsymbol{X}^{(k)}\right)\right)\right]$$

$$\boldsymbol{X}_j = \boldsymbol{\mu}_{\boldsymbol{X}}^{e(k+1)} - \beta_j^t \boldsymbol{\sigma}_{\boldsymbol{X}}^{e(k+1)} \boldsymbol{\alpha}_j^{(k)}$$

$$\boldsymbol{\alpha}_j^{(k)} = \nabla_X g_j\left(\boldsymbol{X}^{(k)}\right) / \left\|\nabla_X g_j\left(\boldsymbol{X}^{(k)}\right)\right\|$$

3. The random vector (MPP) is updated as follows

$$\boldsymbol{X}^{(k+1)} = \boldsymbol{\mu}_{\boldsymbol{X}}^{e(k+1)} - \beta_j^t \boldsymbol{\sigma}_{\boldsymbol{X}}^{e(k+1)} \boldsymbol{\alpha}_j^{(k)} \tag{3.20}$$

4. Check the convergence criterion; if it is satisfied, $\boldsymbol{\mu}_{\boldsymbol{X}}^{(k+1)}$ is considered the optimum solution. Otherwise, set k to $k+1$, and go back to step (2) for continuing the algorithm.

Augmented Lagrangian Penalty Method

Using the notational system in Tosserams et al. (2006) for a decomposed system with N levels and M elements, the subscripts ij denote the jth element of the system in the ith level. The vector of local variables in element ij is denoted by $\mathbf{x}_{\mathrm{ij}}$ with $\boldsymbol{t}_{ij}$ as the vector of target variables shared by element ij and its parent at level $i-1$; E_i is the set of elements at level i (e.g., $E_3 = \{4,5,6\}$); $D_{ij} = \left\{k_1, \ldots, k_{D_{ij}}\right\}$ is the set of children of element ij (e.g., $D_{22} = \{4,5\}$); f_{ij} is the local objective function, with $\boldsymbol{g}_{ij}$ and $\boldsymbol{h}_{ij}$ as the vectors of local inequality and equality constraints, respectively.

The subproblem for element ij (P_{ij}) involves only a subset of decision variables $\overline{\boldsymbol{x}}_{ij}$ and it is formulated as

$$
\begin{aligned}
& min_{\overline{\mathbf{x}}_{ij}}\, f_{ij}\left(\overline{\mathbf{x}}_{ij}\right) + \pi\left(\mathbf{c}(\overline{\mathbf{x}}_{11}, \ldots, \overline{\mathbf{x}}_{NM})\right) \\
& s.t. \quad \boldsymbol{g}_{ij}\left(\overline{\boldsymbol{x}}_{ij}\right) \leq 0 \\
& \qquad\quad \boldsymbol{h}_{ij}\left(\overline{\boldsymbol{x}}_{ij}\right) = 0
\end{aligned} \tag{3.21}
$$

where $\overline{\boldsymbol{x}}_{ij} = \left[\boldsymbol{x}_{ij}, \boldsymbol{r}_{ij}, \boldsymbol{t}_{(i+1)k_1}, \ldots, \boldsymbol{t}_{(i+1)k_{D_{ij}}}\right]$ and π represents the penalty term on the inconsistency constraints $\boldsymbol{c}_{ij} = \boldsymbol{t}_{ij} - \boldsymbol{r}_{ij} = 0$, with the response copies $\boldsymbol{r}_{ij}$ introduced to make the objective function and constraints separable.

In the Augmented Lagrangian Penalty (ALP) formulation of ATC, the penalty term is defined as

$$
\pi_{AL}\left(\boldsymbol{t}_{ij} - \boldsymbol{r}_{ij}\right) = \boldsymbol{\lambda}_{ij}^{T}\left(\boldsymbol{t}_{ij} - \boldsymbol{r}_{ij}\right) + \left\|\boldsymbol{w}_{ij} \circ \left(\boldsymbol{t}_{ij} - \boldsymbol{r}_{ij}\right)\right\|_2^2 \tag{3.22}
$$

where $\boldsymbol{\lambda}_{ij}$ and $\mathbf{w}_{ij}$ are the penalty parameters.

The AL method contains two loops. In the inner loop, the decomposed ATC problem is solved for fixed penalty parameters while in the outer loop, an algorithm is applied to update the parameters $\boldsymbol{\lambda}$ and $\boldsymbol{w}$ as

$$
\boldsymbol{\lambda}^{(k+1)} = \boldsymbol{\lambda}^{(k)} + 2\, \boldsymbol{w}^{(k)} \circ \boldsymbol{w}^{(k)} \circ \boldsymbol{c}^{(k)} \tag{3.23}
$$

$$\boldsymbol{w}^{(k+1)} = \eta \boldsymbol{w}^{(k)} \quad (3.24)$$

where the penalty parameter updating coefficient $\eta \geq 1$ for convex objective functions.

The outer-loop convergence criterion is satisfied when the reduction of inconsistencies in two successive solution estimates is sufficiently small (i.e., $\left\|\boldsymbol{c}^{(k)} - \boldsymbol{c}^{(k-1)}\right\|_{\infty} < \tau$, where $\mathbf{c}^{(k)}$ denotes the vector of all inconsistencies in the outer loop iteration k, and τ is a user-defined termination tolerance).

Single Loop Single Vector + Augmented Lagrangian Approach

In integrating SLSV and AL, the uncertain parameters are defined as random variables and denoted by upper case Latin symbols. The mean values of the random variables are treated as design variables and the corresponding standard deviations are either held fixed (Kokkolaras et al. 2006) or included as design variables (Liu et al. 2006). Thus, the general optimization subproblem P_{ij} takes the form

$$min_{\boldsymbol{\mu}_{\boldsymbol{X}_{ij}},\boldsymbol{\sigma}_{\boldsymbol{X}_{ij}}} f_{ij}\left(\boldsymbol{\mu}_{\boldsymbol{X}_{ij}}, \boldsymbol{p}\right) + \boldsymbol{\lambda}_{ij}^{T}\left(\boldsymbol{\mu}_{\boldsymbol{T}_{ij}} - \boldsymbol{\mu}_{\boldsymbol{R}_{ij}}\right) + \left\|\boldsymbol{w}_{ij} \circ \left(\boldsymbol{\mu}_{\boldsymbol{T}_{ij}} - \boldsymbol{\mu}_{\boldsymbol{R}_{ij}}\right)\right\|_{2}^{2} +$$

$$\boldsymbol{\lambda}_{ij}^{T}\left(\boldsymbol{\sigma}_{\boldsymbol{T}_{ij}} - \boldsymbol{\sigma}_{\boldsymbol{R}_{ij}}\right) + \left\|\boldsymbol{w}_{ij} \circ \left(\boldsymbol{\sigma}_{\boldsymbol{T}_{ij}} - \boldsymbol{\sigma}_{\boldsymbol{R}_{ij}}\right)\right\|_{2}^{2} \quad (3.25)$$

$$g_{ij}^{M}\left(\boldsymbol{X}_{ij}, \boldsymbol{p}\right) \leq 0$$

$$\boldsymbol{\mu}_{\boldsymbol{X}_{ij}}^{l} \leq \boldsymbol{\mu} \leq \boldsymbol{\mu}_{\boldsymbol{X}_{ij}}^{u}$$

$$\boldsymbol{X}_{M} = \boldsymbol{\mu}_{\boldsymbol{X}_{ij}}^{(s)} - \beta_{0}^{j} \boldsymbol{\sigma}_{\boldsymbol{X}_{ij}} \boldsymbol{\alpha}_{M}^{(s-1)}$$

$$\boldsymbol{\alpha}_{M}^{(s-1)} = \nabla_{X} g_{M}\left(\boldsymbol{X}^{(s-1)}\right) / \left\|\nabla_{X} g_{M}\left(\boldsymbol{X}^{(s-1)}\right)\right\|$$

where M is the number of constraints in the current subproblem and $\boldsymbol{X}_M$ is the random variable vector corresponding to the local design constraints g_{ij}^M. In equation (3.25), the inconsistency between the target mean and the corresponding response mean as well as that for the standard deviations are brought into the penalty term forcing the target and response moments to match (Liu et al. 2006).

The algorithm for solving SLSV+AL is presented below; there are two loops for the ATC procedure and one loop for solving the RBDO problem in each element using the SLSV approach.

1. At the initial stage ($k = 0$), the decomposed problem is defined with the initial estimates $\boldsymbol{X}^{(0)}$, $\boldsymbol{\mu}_{\mathbf{T}}^{(0)}$, $\boldsymbol{\mu}_{\mathbf{R}}^{(0)}$ and penalty parameters $\boldsymbol{\lambda}^{(0)}$ and $\mathbf{w}^{(0)}$.
2. Inner loop (solve the ATC problem under uncertainty): Since the efficiency of SLSV depends highly on the initial design point, first solve each element as a deterministic problem to determine the initial point for the SLSV approach to solve the probabilistic problem in each element. There are several loops for each probabilistic optimization problem. Solve the decomposed problem with fixed $\boldsymbol{\lambda}^{(\mathrm{k})}$ and $\mathbf{w}^{(\mathrm{k})}$ and obtain new solution estimates $\boldsymbol{X}^{(k+1)}$, $\boldsymbol{\mu}_{\mathbf{T}}^{(\mathrm{k+1})}$, and $\boldsymbol{\mu}_{\mathbf{R}}^{(\mathrm{k+1})}$.
3. Check convergence: When the outer loop has converged, set $k = \mathrm{K}$ and stop; otherwise $k = k + 1$ and proceed to step 4.
4. Outer loop (update the penalty parameters): Update $\boldsymbol{\lambda}$ and $\mathbf{w}$ to $\boldsymbol{\lambda}^{(\mathrm{k+1})}$ and $\mathbf{w}^{(\mathrm{k+1})}$ using equations (3.23) and (3.24) and the results from step 2, and return to step 2.

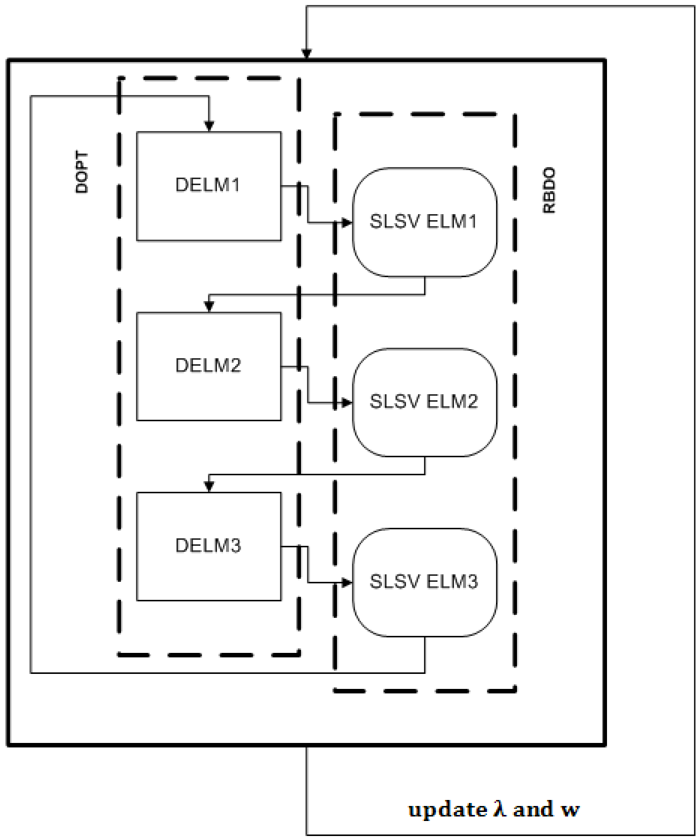

Figure 3.1 Flowchart for SLSV+AL Approach

Figure 3.1 shows the flowchart of the prescribed algorithm for a 3-level problem where DOPT and DELM represent the deterministic optimization and deterministic elements, respectively. The SLSV+AL approach was implemented into a MATLAB code as part of this study and used in the solution of the example problems described next.

Numerical Example Problems

In order to verify the accuracy of the presented SLSV+AL approach, three example problems are solved with the results compared to those for the all-at-once (AAO) formulation found using RIA, PMA, SLSV, and SORA provided in the literature

(Cho et al. 2011). The standard deviations of the random variables are known for problems 1 and 2 and treated as design variables in problem 3.

Problem 1

The first RBDO example problem (Cho et al. 2011) has ten random variables defined by vector $\boldsymbol{X}$ and eight probabilistic design constraints. The AAO problem optimizes a nonlinear objective function that depends on the design variable vector $\mathbf{d} = [d_1, d_2, d_3, d_4, d_5, d_6, d_7, d_8, d_9, d_{10}]^{\mathrm{T}}$ that represents the mean values of the random variables and it is formulated as

$$\min\ f(\mathbf{d}) = d_1^2 + d_2^2 + d_1 d_2 - 14d_1 - 16d_2 + (d_3 - 10)^2 + 4(d_4 - 5)^2 +$$

$$(d_5 - 3)^2 + 2(d_6 - 1)^2 + 5d_7^2 + 7(d_8 - 11)^2 + 2(d_9 - 10)^2 + (d_{10} - 7)^2 + 45$$

$$s.t.\quad Pr\left[g_j(\boldsymbol{X}) > 0\right] \le \Phi\left(-\beta_0^j\right),\ j = 1,8 \tag{3.26}$$

$$g_1(\boldsymbol{X}) = (4X_1 + 5X_2 - 3X_7 + 9X_8)/105 - 1$$

$$g_2(\boldsymbol{X}) = 10X_1 - 8X_2 - 17X_7 + 2X_8$$

$$g_3(\boldsymbol{X}) = (-8X_1 + 2X_2 + 5X_9 - 2X_{10})/12 - 1$$

$$g_4(\boldsymbol{X}) = (3(X_1 - 2)^2 + 4(X_2 - 3)^2 + 2X_3^2 - 7X_4)/120 - 1$$

$$g_5(\boldsymbol{X}) = (5X_1^2 + 8X_2 + (X_3 - 6)^2 - 2X_4)/40 - 1$$

$$g_6(\boldsymbol{X}) = (0.5(X_1 - 8)^2 + 2(X_2 - 4)^2 + 3X_5^2 - X_6)/30 - 1$$

$$g_7(\boldsymbol{X}) = X_1^2 + 2(X_2 - 2)^2 - 2X_1X_2 + 14X_5 - 6X_6$$

$$g_8(\boldsymbol{X}) = -3X_1 + 6X_2 + 12(X_9 - 8)^2 - 7X_{10}$$

$$d_i \ge 0,\ i = 1{,}10, \beta_0^j = 3.0,\ j = 1{,}8$$

$$X_i \sim N(d_i, 0.02^2),\ \ i = 1{,}10$$

$$\mathbf{d}^{(0)} = [2.17{,}2.36{,}8.77{,}5.10{,}0.99{,}1.43{,}1.32{,}9.83{,}8.28{,}8.38]^T$$

All random variables are assumed to be independent and follow normal probability density function with standard deviation of 0.02. The selected initial design point is the same as that reported in the literature (Cho et al. 2011).

The decomposition model consists of three elements at two levels: a top-level element (1) with two children (2 and 3) at level 2. Elements 2 and 3 are coupled through d_1 and d_2, which serve as the linking variables and are coordinated by element 1. The remaining eight variables (d_3, d_4, d_5, d_6), (d_7, d_8), and (d_9, d_{10}) are the local design variables of elements 1, 2, and 3, respectively. The probabilistic design constraints on (g_4, g_5, g_6, g_7), (g_1, g_2), and (g_3, g_8) are allocated to elements 1, 2, and 3, respectively. Termination tolerances are set to $\tau = 10^{-2}$. The initial values of the penalty parameters are set to $\boldsymbol{\lambda}^{(\mathbf{0})} = 0$ and $\mathbf{w}^{(\mathbf{0})} = 1$ with $\eta = 2$.

Table 3.1 shows the results obtained by the multilevel SLSV+AL approach as well as those for the AAO RBDO problem solved[21] using four separate approaches. The last column shows the maximum relative difference between the value found by SLSV+AL and that by any of the other four methods listed.

Table 3.2 Comparison of results for the RBDO Problem 1

	Solution Method					
	RIA	PMA	SORA	SLSV	SLSV+AL	%diff
$f(\boldsymbol{d})$	27.749	27.749	27.750	27.751	27.656	-0.34
d_1	2.131	2.133	2.135	2.138	2.131	-0.33
d_2	2.340	2.336	2.330	2.323	2.342	0.81
d_3	8.711	8.710	8.709	8.705	8.714	0.10
d_4	5.101	5.099	5.101	5.094	5.115	0.41
d_5	0.934	0.931	0.930	0.922	0.925	0.28
d_6	1.467	1.463	1.464	1.449	1.445	-0.29
d_7	1.382	1.384	1.389	1.395	1.380	-1.11
d_8	9.804	9.806	9.810	9.815	9.802	-0.13
d_9	8.147	8.146	8.152	8.154	8.152	-0.02
d_{10}	8.477	8.466	8.463	8.452	8.478	0.31

The results of SLSV+AL in Table 3.1 compare fairly well in terms of solution accuracy. The optimum objective function values are nearly identical while the maximum percent difference among the design variable values is less than 1.2, which is negligible.

In terms of computational cost, it is difficult to have a direct comparison as no cost data was provided for the other methods in the literature. However, SLSV+AL is expected to have better performance than PATC (Liu et al. 2006, Kokkolaras et al. 2006) due to efficiencies in both the SLSV and AL portions of the solution algorithm. The overall computational cost and the number of subproblem optimizations can be reduced by large orders of magnitude using an augmented Lagrangian relaxation approach in place of quadratic penalty function method (Han 2008) used in PATC. Also, SLSV is more efficient than AMV or MCS in solving the RBDO problem in each element of the hierarchy (Yang and Gu 2004). In this problem, the SLSV+AL solution converged in 12 inner loop and 6 outer loop iterations using the stopping criterion of $\tau = 0.01$.

Problem 2

This is a gear reducer optimization problem (Cho et al. 2011). It has seven random variables and 11 probabilistic constraints. The objective function is the volume (surrogate for weight) of the system. The physical quantities such as bending stress in the gear tooth, contact stress in the gear tooth, longitudinal displacement of the shaft, stress in the shaft, and dimensional restriction are treated as probabilistic constraints. The random design variables are: X_1 (gear width), X_2 (gear module), X_3 (the number of pinion teeth), X_4, X_5 (distances between bearings), and X_6, X_7 (diameters of the two shafts). All random variables have normal distribution and are statistically independent. The design variables represent the mean values of the random variables, $\mathbf{d} = [d_1, d_2, d_3, d_4, d_5, d_6, d_7]^{\mathbf{T}}$ and the initial design point for the RBDO problem is selected as the result of the corresponding deterministic optimization problem. The AAO RBDO problem of the speed reducer is formulated as

$$\min f(\mathbf{d}) = 0.7854 d_1 d_2^2 (3.3333 d_3^2 + 14.9334 d_3 - 43.0934) + 1.508 d_1 (d_6^2 + d_7^2) + 7.477(d_6^3 + d_7^3) + 0.7854(d_4 d_6^2 + d_5 d_7^2) \tag{3.27}$$

$$s.t. \quad Pr\left[g_j(\boldsymbol{X}) > 0\right] \leq \Phi\left(-\beta_0^j\right),\ \beta_0^j = 3.0,\ \ j = 1, 11$$

$$g_1(\boldsymbol{X}) = 27/(X_1X_2^2X_3) - 1$$

$$g_2(\boldsymbol{X}) = 397.5/(X_1X_2^2X_3^2) - 1$$

$$g_3(\boldsymbol{X}) = 1.93X_4^3/(X_2X_3X_6^4) - 1$$

$$g_4(\boldsymbol{X}) = 1.93X_5^3/(X_2X_3X_7^4) - 1$$

$$g_5(\boldsymbol{X}) = \sqrt{\left[\left(\frac{745X_4}{X_2X_3}\right)^2 + 16.9\times10^6\right]\Big/(0.1X_6^3)} - 1100$$

$$g_6(\boldsymbol{X}) = \sqrt{\left[\left(\frac{745X_5}{X_2X_3}\right)^2 + 157.5\times10^6\right]\Big/(0.1X_7^3)} - 850$$

$$g_7(\boldsymbol{X}) = X_2X_3 - 40$$

$$g_8(\boldsymbol{X}) = 5 - X_1/X_2$$

$$g_9(\boldsymbol{X}) = X_1/X_2 - 12$$

$$g_{10}(\boldsymbol{X}) = (1.5X_6 + 1.9)/X_4 - 1$$

$$g_{11}(\boldsymbol{X}) = (1.1X_7 + 1.9)/X_5 - 1$$

$$2.6 \le d_1 \le 3.6\,, 0.7 \le d_2 \le 0.8, 17 \le d_3 \le 28$$

$$7.3 \le d_4 \le 8.3, 7.3 \le d_5 \le 8.3, 2.9 \le d_6 \le 3.9, 5.0 \le d_7 \le 5.5$$

$$X_i \sim N(d_i, 0.005^2),\quad i = 1, 7$$

$$\mathbf{d}^{(0)} = [3.5,0.7,17.0,7.3,7.72,3.35,5.29]^T$$

The decomposition model consists of three elements at two levels: a top-level element (1) with two children (2 and 3) at level 2. Elements 2 and 3 are coupled through the linking variables d_1, d_2, and d_3 which are coordinated by element 1. The other four variables (d_4, d_6), (d_5, d_7), are treated as the local design variables of elements 2 and 3, respectively. The probabilistic design constraints on $(\mathrm{g}_1, \mathrm{g}_2, \mathrm{g}_7, \mathrm{g}_8, \mathrm{g}_9)$, $(\mathrm{g}_3, \mathrm{g}_5, \mathrm{g}_{10})$, and $(\mathrm{g}_4, \mathrm{g}_6, \mathrm{g}_{11})$ are allocated to elements 1, 2, and 3, respectively. Termination tolerances are set to $\tau = 10^{-2}$. The initial values of the penalty parameters are set to $\boldsymbol{\lambda}^{(\mathbf{0})} = 0$ and $\mathbf{w}^{(\mathbf{0})} = 1$ with $\eta = 2$.

Table 3.3 Comparison of results for the RBDO Problem 2

	Solution Method					
	RIA	PMA	SORA	SLSV	SLSV+AL	%diff
$f(\boldsymbol{d})$	3464.4	3465.5	3465.5	3472.5	3436.0	-1.05
d_1	3.58	3.58	3.58	3.59	3.58	-0.35
d_2	0.70	0.70	0.70	0.70	0.70	0.00
d_3	17.0	17.0	17.0	17.0	17.0	0.00
d_4	7.30	7.30	7.30	7.30	7.30	0.00
d_5	7.75	7.76	7.76	7.78	7.75	-0.38
d_6	3.37	3.37	3.37	3.37	3.36	-0.16
d_7	5.30	5.30	5.30	5.31	5.30	-0.11

The RBDO results of the multilevel SLSV+AL approach are shown in Table 3.2 and compared with those for the AAO RBDO problem solved (Yi et al. 2008) using four separate approaches. The results of SLSV+AL appear to be fairly consistent with the others listed in Table 3.2. As in Table 3.1, the last column shows the relative difference in the values found by SLSV+AL and those by any of the other four methods. The SLSV+AL solution converges after only 8 inner loop and 3 outer loop iterations with a stopping criterion of $\tau = 0.01$.

Problem 3

This problem is more complex than the previous two. There are 8 deterministic $\{x_4, x_5, x_7, x_9, x_{10}, x_{12}, x_{13}, x_{14}\}$ and 6 random $\{X_1, X_2, X_3, X_6, X_8, X_{11}\}$ variables. The standard deviations for four of the random variables are not known and treated as decision variables. The other two are independent and normally distributed with constant standard deviations. Given $T^{\mu_{X_1}}, T^{\sigma_{X_1}}, T^{\mu_{X_2}}, T^{\sigma_{X_2}}, \sigma_{X_8}, \sigma_{X_{11}}$, the probabilistic AAO (PAIO) (Liu et al. 2006) problem is to find $x_4, x_5, x_7, \mu_{X_8}, x_9, x_{10}, \mu_{X_{11}} x_{12}, x_{13}, x_{14} \geq 0$ to

$$\min\left(T^{\mu_{X_1}} - \mu_{X_1}\right)^2 + \left(T^{\sigma_{X_1}} - \sigma_{X_1}\right)^2 + \left(T^{\mu_{X_2}} - \mu_{X_2}\right)^2 + \left(T^{\sigma_{X_2}} - \sigma_{X_2}\right)^2$$

$$s.t. \quad Pr\left[g_j(\boldsymbol{X}) \leq 0\right] \geq \Phi\left(\beta_0^j\right),\ \beta_0^j = 3.0,\ j = 1, 6 \tag{3.28}$$

$$g_1 = (X_3^{-2} + x_4^2)/x_5^2 - 1$$

$$g_2 = (x_5^2 + X_6^{-2})/x_7^2 - 1$$

$$g_3 = (X_8^2 + x_9^2)/X_{11}^2 - 1$$

$$g_4 = (X_8^{-2} + x_{10}^2)/X_{11}^2 - 1$$

$$g_5 = (X_{11}^2 + x_{12}^{-2})/x_{13}^2 - 1$$

$$g_6 = (X_{11}^2 + x_{12}^2)/x_{14}^2 - 1$$

$$X_1 = (X_3^2 + x_4^{-2} + x_5^2)^{1/2}$$

$$X_2 = (x_5^2 + X_6^2 + x_7^2)^{1/2}$$

$$X_3 = (X_8^2 + x_9^{-2} + x_{10}^{-2} + X_{11}^2)^{1/2}$$

$$X_6 = (X_{11}^2 + x_{12}^2 + x_{13}^2 + x_{14}^2)^{1/2}$$

In this problem, $[T^{\mu_{X_1}}, T^{\mu_{X_2}}] = [0,0]$ and $[T^{\sigma_{X_1}}, T^{\sigma_{X_2}}] = [0,0]$. X_8 and X_{11} are normally distributed with standard deviations equal to 0.1. The decomposition model selected for this problem consists of three elements at two levels: a top-level element (1) with two children (2 and 3) at level 2. The response/target variable for elements 1 and 2 is X_3 and that for elements 1 and 3 is X_6. Elements 2 and 3 are coupled through variable X_{11}, which is coordinated by element 1. The variables $(X_1, X_2, x_4, x_5, x_7)$, (X_8, x_9, x_{10}), and (x_{12}, x_{13}, x_{14}) are local variables of elements 1, 2, and 3, respectively. The probabilistic constraints on $(\mathrm{g}_1, \mathrm{g}_2)$, $(\mathrm{g}_3, \mathrm{g}_4)$, and $(\mathrm{g}_5, \mathrm{g}_6)$ are allocated to elements 1, 2, and 3, respectively. Termination tolerances are set to $\tau = 10^{-2}$. The initial values of the penalty parameters are set to $\boldsymbol{\lambda}^{(\mathbf{0})} = 0$ and $\mathbf{w}^{(\mathbf{0})} = 1$ with $\eta = 2$.

Table 3.4 Comparison of results for the RBDO Problem 3

	Solution Method				
	PAIO	PATC	SLSV	SLSV+AL	%diff
x_4	0.7599	0.7597	0.7598	0.7598	0.00
x_5	0.8676	0.8659	0.8496	0.8493	-0.03
x_7	0.9208	0.9209	0.8963	0.8963	0.00
μ_{X_8}	1.1984	1.2013	1.0330	1.0333	0.03
x_9	0.8098	0.7912	0.7800	0.7728	-0.92
x_{10}	0.7350	0.7229	0.8116	0.8058	-0.71
$\mu_{X_{11}}$	1.4931	1.4737	1.6526	1.6488	-0.23
x_{12}	0.8409	0.8419	0.8409	0.8409	0.00
x_{13}	2.1333	2.1080	2.1724	2.1686	-0.18
x_{14}	1.9606	1.9344	2.0281	2.0240	-0.20

For this problem also there is a good consistency between the ATC and AAO approaches. The maximum percentage difference is 0.92. The SLSV+AL solution converges after 76 inner loop and 7 outer loop iterations with a stopping criterion of $\tau = 0.01$.

Problem 4

This problem is similar to problem 1, but the design variables, $\{X_1, \dots, X_{10}\}$, follow three different types of random distributions: normal, lognormal, and Gumbel with standard deviation 0.5. The target reliability indices are set equal to 2.0.

$$\min\ f(\mathbf{d}) = d_1^2 + d_2^2 + d_1 d_2 - 14d_1 - 16d_2 + (d_3 - 10)^2 + 4(d_4 - 5)^2 + (d_5 - 3)^2 + 2(d_6 - 1)^2 + 5d_7^2 + 7(d_8 - 11)^2 + 2(d_9 - 10)^2 + (d_{10} - 7)^2 + 45$$

$$s.t. \quad Pr\left[g_j(\boldsymbol{X}) > 0\right] \leq \Phi\left(-\beta_0^j\right),\ j = 1,8 \tag{3.29}$$

$$g_1(\boldsymbol{X}) = (4X_1 + 5X_2 - 3X_7 + 9X_8)/105 - 1$$

$$g_2(\boldsymbol{X}) = 10X_1 - 8X_2 - 17X_7 + 2X_8$$

$$g_3(\boldsymbol{X}) = (-8X_1 + 2X_2 + 5X_9 - 2X_{10})/12 - 1$$

$$g_4(\boldsymbol{X}) = (3(X_1 - 2)^2 + 4(X_2 - 3)^2 + 2X_3^2 - 7X_4)/120 - 1$$

$$g_5(\boldsymbol{X}) = (5X_1^2 + 8X_2 + (X_3 - 6)^2 - 2X_4)/40 - 1$$

$$g_6(\boldsymbol{X}) = (0.5(X_1 - 8)^2 + 2(X_2 - 4)^2 + 3X_5^2 - X_6)/30 - 1$$

$$g_7(\boldsymbol{X}) = X_1^2 + 2(X_2 - 2)^2 - 2X_1X_2 + 14X_5 - 6X_6$$

$$g_8(\boldsymbol{X}) = -3X_1 + 6X_2 + 12(X_9 - 8)^2 - 7X_{10}$$

$$d_i \geq 0,\ i = 1,10, \beta_0^j = 2.0,\ j = 1,8$$

$$\mathbf{d}^{(0)} = [2.17,2.36,8.77,5.10,0.99,1.43,1.32,9.83,8.28,8.38]^T$$

The same decomposition model as that in problem 1 is used with three elements at two levels. The optimum results are presented in Table 3.4. For every distribution type (normal, lognormal, and Gumbel), the results for SLSV+AL and SLSV are nearly identical. Through this problem, it is shown that the SLSV+AL approach can be used in the case of non-normal random distribution.

Table 3.5 Comparison of results for RBDO problem 4

	normal		lognormal		Gumbel	
	SLSV	SLSV+AL	SLSV	SLSV+AL	SLSV	SLSV+AL
$f(\boldsymbol{d})$	256.5175	256.5160	176.9965	176.7921	164.1902	164.8615
d_1	1.1258	1.1247	1.1332	1.1311	1.1693	1.1644
d_2	3.2135	3.2217	2.9353	2.9479	2.8829	2.9114
d_3	6.3549	6.3542	6.5438	6.5438	6.6643	6.6681
d_4	7.3109	7.3052	6.6180	6.6154	6.3797	6.3835
d_5	0.0160	0.0159	0.2841	0.2835	0.0821	0.0827
d_6	5.2911	5.2406	3.8001	3.7741	3.4887	3.4983
d_7	1.6477	1.6417	1.5130	1.5053	1.5064	1.4870
d_8	8.4042	8.4008	8.7748	8.7694	8.7037	8.6904
d_9	7.5551	7.5449	7.6565	7.6471	7.3780	7.3617
d_{10}	17.5074	17.4888	15.8903	15.8941	15.1844	15.2131

Conclusion

In this study, the capabilities of the single loop single vector (SLSV) methodology were integrated with those of the augmented Lagrangian penalty (ALP) formulation of analytical target cascading (ATC) for efficient and accurate solution of hierarchically decomposed reliability-based design optimization (RBDO) problems. The proposed SLSV+AL approach can be used to solve problems of varying degrees of complexity where the uncertainties are propagated from one element to another by matching one or two statistical moments of the responses of interest with those of the corresponding targets. The method can be applied to problems with both normal and non-normal probability density functions. The main feature of SLSV+AL is its ability to efficiently solve the RBDO problem in each element of the hierarchical system.

The SLSV+AL approach was successfully applied to the solution of three diverse RBDO problems reported in the literature. The results obtained here were in excellent agreement with those found using the other methods. Due to the unavailability of the computational cost information associated with the other RBDO methods used as reference in this study, no direct cost comparison can be made. However, the proposed method with its use of SLSV approach offers more efficient solution of RBDO problem in each element than those that rely on the double-loop approach (i.e., reliability-index approach). Similarly, the use of AL within the ATC framework offers a more efficient and accurate decomposition and coordination strategy compared with the others reported in the literature. Hence, the overall computational efficiency of SLSV+AL is expected to be similar or better than those used for comparison.

CHAPTER IV

EXPONENTIAL PENALTY FUNCTION FORMULATION FOR MULTILEVEL OPTIMIZATION

In this chapter, a penalty function formulation based on the exponential method of multipliers (Kort and Bertsekas 1972) is presented for solving multilevel optimization problems within the framework of ATC. Both single- and double-loop coordination strategies are considered. By means of the exponential penalty function (EPF) relaxation, ill-conditioning is reduced in the inner loop because accurate solutions can be obtained for even small fixed weights without using any parameter adjusting scheme. An overview of ATC is provided and the previous formulations and coordination strategies are briefly described. The EPF I and II approaches are discussed. Four benchmark problems are presented with solution accuracy and computational efficiency of the proposed approaches compared with those from four other techniques presented in the literature.

An all-in-one (AIO) problem according to the notation and problem structure described in Chapter 2 is defined as

$$\min_{\bar{\boldsymbol{x}}_{11},\ldots,\bar{\boldsymbol{x}}_{NM}} \sum_{i=1}^{N} \sum_{j\,\in\,\mathrm{E}_i} f_{ij}\left(\bar{\boldsymbol{x}}_{ij}\right) \tag{4.1}$$

$$s.t. \quad \boldsymbol{g}_{ij}\left(\bar{\boldsymbol{x}}_{ij}\right) \leq 0$$

$$\boldsymbol{h}_{ij}\left(\bar{\boldsymbol{x}}_{ij}\right) = 0$$

$$\forall j \in \mathrm{E}_i, i = 1, \ldots, N$$

where $\overline{\boldsymbol{x}}_{ij} = \left[\boldsymbol{x}_{ij}, \boldsymbol{t}_{(i+1)k_1}, \dots, \boldsymbol{t}_{(i+1)k_{n_{ij}}}\right]$.

To make the objective functions and constraints in equation (4.1) separable, response copies $\boldsymbol{r}_{ij}$ are introduced, which leads to the modified AIO formulation with addition of consistency constraints $\boldsymbol{c}_{ij} = \boldsymbol{t}_{ij} - \boldsymbol{r}_{ij} = 0$ to equation (4.1), where $\boldsymbol{t}_{ij}$ is the vector of known targets. Using method of multipliers with elimination of consistency constraints results in the relaxed AIO problem expressed as

$$\min_{\overline{\boldsymbol{x}}_{11},\dots,\overline{\boldsymbol{x}}_{NM}} \sum_{i=1}^{N} \sum_{j \in E_i} f_{ij}(\overline{\boldsymbol{x}}_{ij}) + \pi(\boldsymbol{c}_{ij}) \tag{4.2}$$

$$s.t. \quad \boldsymbol{g}_{ij}(\overline{\boldsymbol{x}}_{ij}) \leq 0$$

$$\boldsymbol{h}_{ij}(\overline{\boldsymbol{x}}_{ij}) = 0$$

$$\forall j \in \mathrm{E}_i, i = 1, \dots, N$$

where $\overline{\boldsymbol{x}}_{ij} = \left[\boldsymbol{x}_{ij}, \boldsymbol{r}_{ij}, \boldsymbol{t}_{(i+1)k_1}, \dots, \boldsymbol{t}_{(i+1)k_{n_{ij}}}\right]$ and $\boldsymbol{c} = [\boldsymbol{c}_{22}, \dots, \boldsymbol{c}_{\mathrm{NM}}]$ is the vector of inconsistencies.

For a general relaxing function π, the AIO problem can be decomposed into a hierarchical system with the general problem for element *ij*, named P_{ij}, given by

$$\min_{\overline{\boldsymbol{x}}_{ij}} f_{ij}(\overline{\boldsymbol{x}}_{ij}) + \pi(\boldsymbol{c}_{ij}) \tag{4.3}$$

$$s.t. \quad \boldsymbol{g}_{ij}(\overline{\boldsymbol{x}}_{ij}) \leq 0$$

$$\boldsymbol{h}_{ij}(\overline{\boldsymbol{x}}_{ij}) = 0$$

where $\overline{\boldsymbol{x}}_{ij} = \left[\boldsymbol{x}_{ij}, \boldsymbol{r}_{ij}, \boldsymbol{t}_{(i+1)k_1}, \dots, \boldsymbol{t}_{(i+1)k_{n_{ij}}}\right]$ represents the vector of local decision variables.

Within the ATC framework, three different formulations have been proposed, i.e., the quadratic penalty (QP), ordinary Lagrangian (OL), and augmented Lagrangian (AL) penalty. These formulations differ only in the way the relaxing function π is defined such that

$$\pi_{QP}(\boldsymbol{c}_{ij}) = \left\|\boldsymbol{w}_{ij} \circ \boldsymbol{c}_{ij}\right\|_2^2 \tag{4.4}$$

$$\pi_{OL}(\boldsymbol{c}_{ij}) = \boldsymbol{\lambda}_{ij}^T \boldsymbol{c}_{ij} \tag{4.5}$$

$$\pi_{AL}(\boldsymbol{c}_{ij}) = \boldsymbol{\lambda}_{ij}^T \boldsymbol{c}_{ij} + \left\|\boldsymbol{w}_{ij} \circ \boldsymbol{c}_{ij}\right\|_2^2 \tag{4.6}$$

where $\mathbf{w} \circ \mathbf{c}$ is a vector product found by multiplication of terms with identical indices in vectors $\mathbf{w}$ and $\mathbf{c}$.

The variety of approaches used for defining and updating the weight factor $\boldsymbol{w}_{ij}$ diversifies the QP and AL formulations (Kim et al. 2003; Michalek and Papalambros 2005). Similarly, different approaches have been suggested for updating the parameter $\boldsymbol{\lambda}_{ij}$.

Generally, the procedure of solving an AL formulated decomposed problem is divided into two parts. In the first part, the decomposed problem (hierarchical or parallel structure) is solved with parameters $\boldsymbol{\lambda}$ and $\boldsymbol{w}$ held fixed, whereas in the second part, the values of $\boldsymbol{\lambda}$ and $\boldsymbol{w}$ are updated.

In the double-loop coordination strategy, the decomposed problem is solved until convergence is reached in the inner loop before updating the parameters in the outer loop to arrive at the solution with a prescribed inconsistency tolerance. However, in the single-loop coordination strategy, the decomposed problem is solved while the parameters are updated in the same loop.

The inner-loop elemental structure in the double-loop strategy can be either hierarchical called AL (Tosserams et al. 2006) or parallel called DQA for diagonal quadratic approximation (Li et al. 2008). The hierarchical structure uses the difference in the objective function values between two consecutive iterations as the inner-loop convergence criterion while in DQA, the inner-loop convergence is based on improving linearization.

In the single-loop strategy, structural elements are either in a two-level order, named alternative direction method of multipliers (AL-AD), (Tosserams et al. 2006) or parallel order, named truncated DQA (TDQA), (Li et al. 2008). The two-level order contains elements of odd levels of hierarchical structure in one level and elements of even levels in the other level.

The parameters $\boldsymbol{\lambda}$ and $\boldsymbol{w}$ are updated as

$$\boldsymbol{\lambda}^{(k+1)} = \boldsymbol{\lambda}^{(k)} + 2\,\boldsymbol{w}^{(k)} \circ \boldsymbol{w}^{(k)} \circ \boldsymbol{c}^{(k)} \tag{4.7}$$

$$\boldsymbol{w}^{(k+1)} = \beta \boldsymbol{w}^{(k)} \tag{4.8}$$

where k represents the iteration number and $\beta \geq 1$ for convex objective functions (Tosserams et al. 2006).

The AL formulation avoids setting arbitrarily large weight factors that can often cause ill-conditioning of the ATC problem. The first part of AL solution tends to be very computationally expensive in comparison to the second part. It has been shown in the literature (Tosserams et al. 2006, Li et al. 2008) that AL can reduce the computational cost of solving a decomposed optimization problem without loss of accuracy.

Exponential Penalty Function Formulation

For an all-at-once (AAO) constrained optimization problem of the form

$$\min f(\boldsymbol{x}) \tag{4.9}$$

$$s.t. \quad g_j(\boldsymbol{x}) \leq 0\,, j = 1, r$$

an equivalent unconstrained optimization problem using method of multipliers is expressed as (Kort and Bertsekas 1972)

$$\min_{\boldsymbol{x}^k} f(\boldsymbol{x}) + \sum_{j=1}^{r} \frac{\mu_j^k}{a_j^k} \psi\left(a_j^k g_j(\boldsymbol{x})\right) \tag{4.10}$$

where μ_j^k and a_j^k are the multiplier and penalty parameters for constraint j, respectively. For second-order solution methods, the penalty function ψ must be at least twice differentiable with the following properties: $\nabla^2\psi(t) > 0\ \forall\ t \in \Re$; $\psi(0) = 0, \nabla\psi(0) = 1$; $\lim_{t\to-\infty} \psi(t) > -\infty$; $\lim_{t\to-\infty} \nabla\psi(t) = 0$ and $\lim_{t\to\infty} \nabla\psi(t) = \infty$. Satisfying the above properties is exponential penalty function (EPF) of the form $\psi(t) = e^t - 1$.

Analysis and convergence proof of this method was presented by Tseng and Bertsekas (1993) for the AAO problems. Based on observations by Kort and Bertsekas (1972) for problems cast in the form of equation (4.10), the advantage of exponential method of multipliers is expected to be greater for convex rather than non-convex optimization problems.

For ATC application of EPF, consistency constraints are converted into inequality form such that

$$\mathbf{c}_{ij} = \boldsymbol{t}_{ij} - \boldsymbol{r}_{ij} = 0 \quad \equiv \quad \begin{cases} \boldsymbol{t}_{ij} - \boldsymbol{r}_{ij} \leq 0 \\ \boldsymbol{r}_{ij} - \boldsymbol{t}_{ij} \leq 0 \end{cases} \tag{4.11}$$

which results in P_{ij} to be formulated as

$$\min_{\overline{\boldsymbol{x}}_{ij}} f_{ij}(\overline{\boldsymbol{x}}_{ij}) + \left\{\frac{\boldsymbol{\mu}_{ij}}{\boldsymbol{a}_{ij}}\left(e^{\boldsymbol{a}_{ij}\,(\boldsymbol{t}_{ij}-\boldsymbol{r}_{ij})} - 1\right) + \frac{\boldsymbol{\gamma}_{ij}}{\boldsymbol{b}_{ij}}\left(e^{\boldsymbol{b}_{ij}\,(\boldsymbol{r}_{ij}-\boldsymbol{t}_{ij})} - 1\right)\right\} +$$

$$\sum_{k\in D_{ij}} \left\{\frac{\boldsymbol{\mu}_{(i+1)k}}{\boldsymbol{a}_{(i+1)k}}\left(e^{\boldsymbol{a}_{(i+1)k}\,(\boldsymbol{t}_{(i+1)k}-\boldsymbol{r}_{(i+1)k})} - 1\right) + \frac{\boldsymbol{\gamma}_{(i+1)k}}{\boldsymbol{b}_{(i+1)k}}\left(e^{\boldsymbol{b}_{(i+1)k}\,(\boldsymbol{r}_{(i+1)k}-\boldsymbol{t}_{(i+1)k})} - 1\right)\right\} \quad (4.12)$$

$$s.t. \quad \boldsymbol{g}_{ij}(\overline{\boldsymbol{x}}_{ij}) \leq 0$$

$$\boldsymbol{h}_{ij}(\overline{\boldsymbol{x}}_{ij}) = 0$$

where $\overline{\boldsymbol{x}}_{ij} = \left[\boldsymbol{x}_{ij}, \boldsymbol{r}_{ij}, \boldsymbol{t}_{(i+1)k_1}, \ldots, \boldsymbol{t}_{(i+1)k_{n_{ij}}}\right]$.

The initial values for multipliers $\boldsymbol{\mu}_{ij}^{0}$ and $\boldsymbol{\gamma}_{ij}^{0}$ are set equal to arbitrary positive numbers and updated using

$$\boldsymbol{\mu}_{ij}^{k+1} = \boldsymbol{\mu}_{ij}^{k}\psi_{ij}^{k} = \boldsymbol{\mu}_{ij}^{k} e^{\boldsymbol{a}_{ij}^{k}\left(\boldsymbol{t}_{ij}^{k}-\boldsymbol{r}_{ij}^{k}\right)} \quad (4.13)$$

$$\boldsymbol{\gamma}_{ij}^{k+1} = \boldsymbol{\gamma}_{ij}^{k}\bar{\psi}_{ij}^{k} = \boldsymbol{\gamma}_{ij}^{k} e^{\boldsymbol{b}_{ij}^{k}\left(\boldsymbol{r}_{ij}^{k}-\boldsymbol{t}_{ij}^{k}\right)} \quad (4.14)$$

There are two ways of choosing the penalty parameters $\boldsymbol{a}_{ij}$ and $\boldsymbol{b}_{ij}$. One way is to set $\boldsymbol{a}_{ij}^{k} = \boldsymbol{a}_0$ and $\boldsymbol{b}_{ij}^{k} = \boldsymbol{b}_0\ \forall k$ or $\boldsymbol{a}_{ij}^{k+1} = \beta\boldsymbol{a}_{ij}^{k} > \boldsymbol{a}_{ij}^{k}$ and $\boldsymbol{b}_{ij}^{k+1} = \beta\boldsymbol{b}_{ij}^{k} > \boldsymbol{b}_{ij}^{k}\ \forall k$ with no dependence on values of the multipliers, whereas in the alternative way, the penalty parameters depend on values of the multipliers at the kth iteration such that $\boldsymbol{a}_{ij}^{k} = \boldsymbol{\omega}_{ij}^{k}/\boldsymbol{\mu}_{ij}^{k}\ \forall k$ and $\boldsymbol{b}_{ij}^{k} = \boldsymbol{\nu}_{ij}^{k}/\boldsymbol{\gamma}_{ij}^{k}\ \forall k$, where $\boldsymbol{\omega}_{ij}^{k+1} \geq \boldsymbol{\omega}_{ij}^{k}$ and $\boldsymbol{\nu}_{ij}^{k+1} \geq \boldsymbol{\nu}_{ij}^{k}$.

As part of this research, both the dependent and independent approaches were examined for one example problem. The results presented in Appendix I indicate that for the same level of accuracy, the number of function evaluations and computational time are generally reduced when the penalty parameters are kept independent of the multipliers. Also, by allowing the penalty parameters to be updated during the optimization process, solution efficiency improves. Although the results for the updating approach is slightly better than the one holding the penalty parameters fixed, in all the benchmark problems presented in the next section, the penalty parameters are held fixed $(\mathrm{i.e.}, \boldsymbol{a}_{ij}, \boldsymbol{b}_{ij} = 1)$. Merit of the EPF formulation can be more accurately measured by making the solution independent of a particular choice of updating formula.

The EPF formulation is combined with two coordination and updating strategies as shown in figure 4.3. EPF I uses a double-loop approach (i.e., inner-loop coordination and outer-loop parameter updating) whereas in EPF II, coordination and parameter updating are both performed in a single loop.

EPF I Approach:

0. Decompose the problem and select an initial design point $\bar{\boldsymbol{x}}^0$. Set $k = 0$ and choose values for $\boldsymbol{\mu}^0$ and $\boldsymbol{\gamma}^0$.
1. (Inner loop) Set $i_l = 0$ and solve element problems in hierarchical order with fixed $\boldsymbol{\mu}^k$ and $\boldsymbol{\gamma}^k$. By solving each element, the targets and the upper values of linking variables for the corresponding children are found. Responses and the lower values of linking variables are determined at the end of hierarchy. Set $i_l = i_l + 1$ and continue the iterative process until the inner loop converges.
2. If the outer loop has converged, set $k = \mathrm{K}$ and stop; otherwise, proceed to step 3.
3. (Outer loop) Find the updated parameters $\boldsymbol{\mu}^{k+1}$ and $\boldsymbol{\gamma}^{k+1}$ using equations (4.13) and (4.14), and return to step 1.

EPF II Approach:

0. Decompose the problem and select an initial design point $\bar{\boldsymbol{x}}^0$. Set $k = 0$ and choose values for $\boldsymbol{\mu}^0$ and $\boldsymbol{\gamma}^0$.
1. Solve element problems in hierarchical order with fixed $\boldsymbol{\mu}^k$ and $\boldsymbol{\gamma}^k$.
2. If the convergence criterion is satisfied, set $k = \mathrm{K}$ and stop; otherwise, proceed to step 3.
3. (Outer loop) Find the updated parameters $\boldsymbol{\mu}^{k+1}$ and $\boldsymbol{\gamma}^{k+1}$ using equations (4.13) and (4.14), and return to step 1.

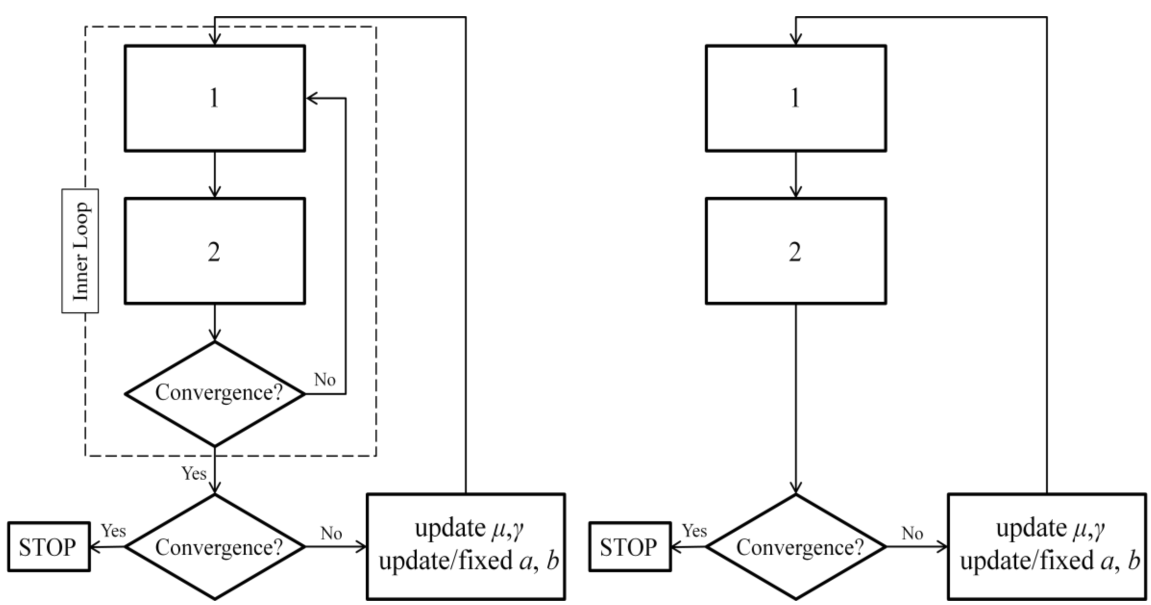

Figure 4.1 Flowcharts of EPF I (left) and EPF II approaches

The convergence criteria and coordination strategy used for EPF I are similar to those of AL (Tosserams et al. 2006). The inner loop convergence in EPF I is reached when reduction in the augmented objective function of the relaxed problem between two consecutive inner loop iterations is less than the termination tolerance $\tau^{ATC} = \tau/10$. The outer loop convergence criterion in EPF I and EPF II is defined based on reduction of the inconsistencies in two successive solutions as

$$\left\|\boldsymbol{c}^{(k)} - \boldsymbol{c}^{(k-1)}\right\|_{\infty} < \tau \tag{4.15}$$

Performance is measured using three quantities: solution error, total number of function evaluations, and the total CPU time required to solve the decomposed optimization problem. Solution error e is defined as (Tosserams et al. 2006)

$$e = \|\boldsymbol{x}^{*} - \boldsymbol{x}^{ATC}\| \tag{4.16}$$

where $\boldsymbol{x}^{*}$ is the known optimal solution and $\boldsymbol{x}^{ATC}$ is the solution found by the particular ATC formulation.

Solution error can be controlled by changing the termination tolerance τ. The computational efficiency is measured by the CPU time and the total number of function evaluations reported by the fmincon solver in MATLAB[1].

Unlike the penalty parameter $\boldsymbol{w}$ in equations (4.7) and (4.8), the EPF parameters $\boldsymbol{a}$ and $\boldsymbol{b}$ in equation (4.12) can be given arbitrary values. According to Kort and Bertsekas (1972), for AAO problems cast in the form of equation (4.10), the exponential method of multipliers converges from any starting point, it does not require any parameter adjusting scheme, and the subsequent sequence of unconstrained minimizations of equation (4.10) does not become ill-conditioned during the solution

[1] MATLAB Version 7.12.0.635 (R2011a); OS: XP SP3; Processor: Intel(R) Core(TM)2 Duo CPU E8400 @ 3 GHz and 3.25 GB RAM.

process. Moreover, when converting the AAO problem in equation (4.9) to an equivalent unconstrained minimization problem, EPF provides greater efficiency than AL if the AAO is a convex programming problem (Kort and Bertsekas 1972). These advantages are the motivating factors for the application of EPF to the ATC framework.

In the next section, four benchmark (one convex and three non-convex) optimization problems are presented with the solution to each problem obtained using the proposed EPF I and EPF II approaches as well as four other approaches (i.e., AL, AL-AD, DQA, TDQA) found in the literature.

Benchmark Problems

Problem 1

A ten-variable nonlinear constrained optimization problem is formulated as (Montes and Coello 2005)

$$\min_{x_1,\dots,x_{10}} \; f(x) = x_1^2 + x_2^2 + x_1 x_2 - 14x_1 - 16x_2 + 45 + (x_3 - 10)^2 + 4(x_4 - 5)^2 + (x_5 - 3)^2 + 2(x_6 - 1)^2 + 5x_7^2 + 7(x_8 - 11)^2 + 2(x_9 - 10)^2 + (x_{10} - 7)^2 \tag{4.17}$$

$$s.t. \quad g_1(x) = -105 + 4x_1 + 5x_2 - 3x_7 + 9x_8 \le 0$$

$$g_2(x) = 10x_1 - 8x_2 - 17x_7 + 2x_8 \le 0$$

$$g_3(x) = -8x_1 + 2x_2 + 5x_9 - 2x_{10} - 12 \le 0$$

$$g_4(x) = 3(x_1 - 2)^2 + 4(x_2 - 3)^2 + 2x_3^2 - 7x_4 - 120 \le 0$$

$$g_5(x) = 5x_1^2 + 8x_2 + (x_3 - 6)^2 - 2x_4 - 40 \le 0$$

$$g_6(x) = x_1^2 + 2(x_2 - 2)^2 - 2x_1 x_2 + 14x_5 - 6x_6 \le 0$$

$$g_7(x) = 0.5(x_1 - 8)^2 + 2(x_2 - 4)^2 + 3x_5^2 - x_6 - 30 \le 0$$

$$g_8(x) = -3x_1 + 6x_2 + 12(x_9 - 8)^2 - 7x_{10} \le 0$$

$$-10 \le x_1, \dots, x_{10} \le 10$$

This is a convex programming problem since the objective function and all design constraints have positive definite Hessians. The unique global optimum is located at $\boldsymbol{x}^*$ = [2.172, 2.364, 8.774, 5.095, 0.991, 1.431, 1.322, 9.829, 8.280, 8.376], where $f(\boldsymbol{x}^*)$ = 24.306 and constraints g_1 through g_6 are active.

The decomposition selected for this problem consists of four elements in two levels, element 1 at the top level and elements 2 through 4 at the bottom as shown in figure 4.4. The linking variables x_1 and x_2 are shared among elements 2 through 4 and coordinated by element 1. The objective function is also decomposed to four parts based on the local variables in each element. The corresponding EPF formulation is also shown in figure 4.4.

The relaxed AIO formulation of the decomposed problem is stated as

$$\min_{x_{1s1},\dots,x_{1s4},x_{2s1},\dots,x_{2s4},x_3,\dots,x_{10}} f'^{(x)} = x_{1s1}^2 + x_{2s1}^2 + x_{1s1}x_{2s1} - 14x_{1s1} - 16x_{2s1} + 45 +$$
$$(x_3 - 10)^2 + 4(x_4 - 5)^2 + (x_5 - 3)^2 + 2(x_6 - 1)^2 + 5x_7^2 + 7(x_8 - 11)^2 +$$
$$2(x_9 - 10)^2 + (x_{10} - 7)^2 +$$
$$\pi\big((x_{1s1} - x_{1s2}, x_{1s1} - x_{1s3}, x_{1s1} - x_{1s4}, x_{2s1} - x_{2s2}, x_{2s1} - x_{2s3}, x_{2s1} - x_{2s4})\big) \qquad (4.18)$$

$$s.t. \quad g'_1(x) = -105 + 4x_{1s3} + 5x_{2s3} - 3x_7 + 9x_8 \le 0$$

$$g'_2(x) = 10x_{1s3} - 8x_{2s3} - 17x_7 + 2x_8 \le 0$$

$$g'_3(x) = -8x_{1s4} + 2x_{2s4} + 5x_9 - 2x_{10} - 12 \le 0$$

$$g'_4(x) = 3(x_{1s1} - 2)^2 + 4(x_{2s1} - 3)^2 + 2x_3^2 - 7x_4 - 120 \le 0$$

$$g'_5(x) = 5x_{1s1}^2 + 8x_{2s1} + (x_3 - 6)^2 - 2x_4 - 40 \le 0$$

$$g'_6(x) = x_{1s2}^2 + 2(x_{2s2} - 2)^2 - 2x_{1s2}x_{2s2} + 14x_5 - 6x_6 \leq 0$$

$$g'_7(x) = 0.5(x_{1s2} - 8)^2 + 2(x_{2s2} - 4)^2 + 3x_5^2 - x_6 - 30 \leq 0$$

$$g'_8(x) = -3x_{1s4} + 6x_{2s4} + 12(x_9 - 8)^2 - 7x_{10} \leq 0$$

$$-10 \leq x_3, \ldots, x_{10} \leq 10; \; -10 \leq x_{isj} \leq 10 \; \forall i = 1,2 \text{ and } j = 1,4$$

The relaxed AIO problem using AL and EPF formulations is solved with the results shown in Table 4.1. Although both EPF and AL have the same level of accuracy, AL appears to be more computationally efficient in solving the AIO problem.

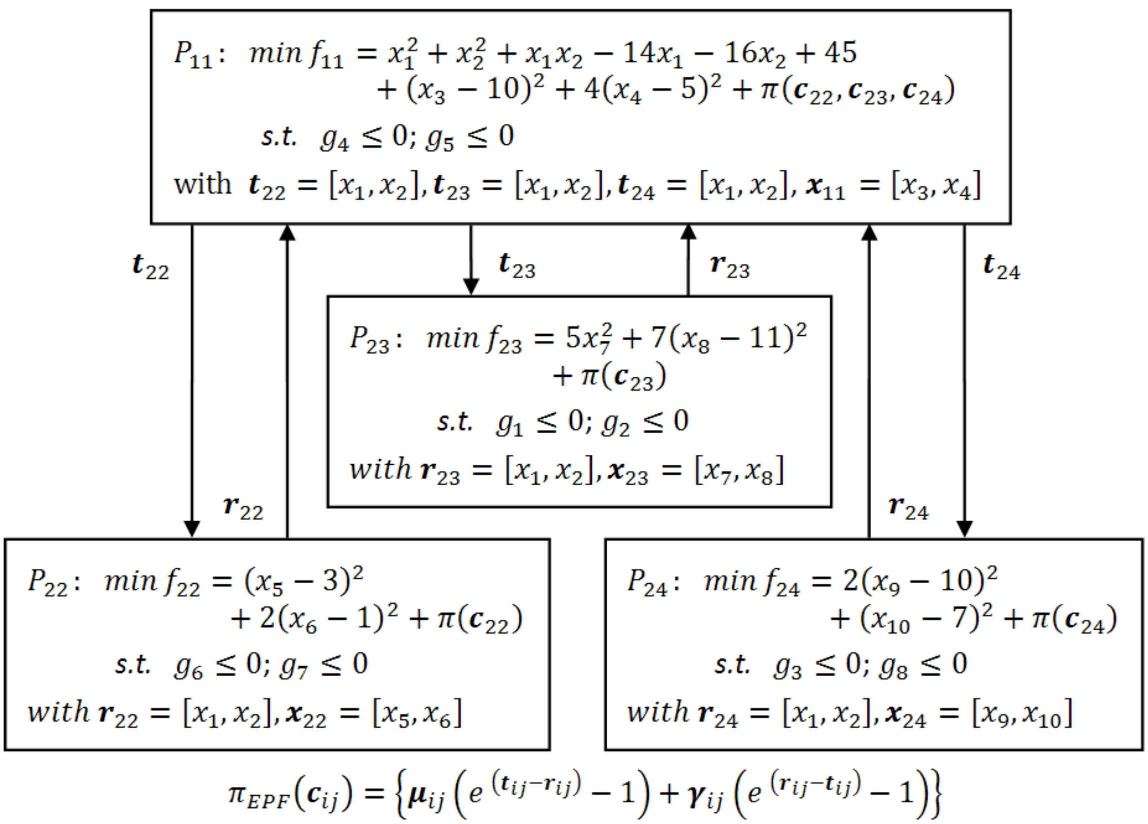

Figure 4.2 Hierarchical decomposition of Problem 1

For an AIO problem such as the one considered here, the AL and EPF formulations only augment the objective function with the consistency constraints while the other design constraints are kept intact. Consequently, the superiority of EPF over AL for the AAO problems (Kort and Bertsekas 1972) is not observed here. However, the same cannot be said when solving the decomposed multilevel system as noted below.

Figure 4.5 shows the plots of function evaluation and the CPU time versus the absolute solution error e from equation (4.16) for the six different approaches at termination tolerances τ = 10^{-2}, 10^{-3}, 10^{-4}, 10^{-5} (shown from left to right). The initial values for the penalty parameters in AL, AL-AD, DQA and TDQA are set to $\lambda^{(0)} = 0$ and $w^{(0)} = 1$; in EPF I and EPF II, $\mu^{(0)} = 1$ and $\gamma^{(0)} = 1$. The starting design point is $\boldsymbol{x}^{(0)} = [0, 0, 0, 0, 0, 0, 0, 0, 0, 0]$ for all the formulations. For AL and DQA, $\beta = 2$, and for AL-AD and TDQA, $\beta = 1$.

Table 4.1 Comparison of AL and EPF results for the relaxed AIO of Problem 1

Formulation	Error, e	No. of Function Evaluations	No. of Iterations	f^*
AL	4.44E-04	2440	127	24.306
EPF	5.98E-04	3593	195	24.306

Given the analytical nature of the benchmark problems considered, the CPU time for all the solution schemes is very small. However, relatively speaking, the results show EPF to be more efficient than AL as τ value is reduced for increasing the solution accuracy. More importantly, EPF II requires much fewer function calls (noting the log scale of figure 4.5) than all the others, while EPF I offers better performance than the double-loop approaches (AL and DQA). As an example, for $\tau = 10^{-2}$, EPF II requires 23% fewer function evaluations than the next best approach (i.e., AL-AD) and nearly 88% less than that required by DQA. The difference grows even wider as τ value is reduced.

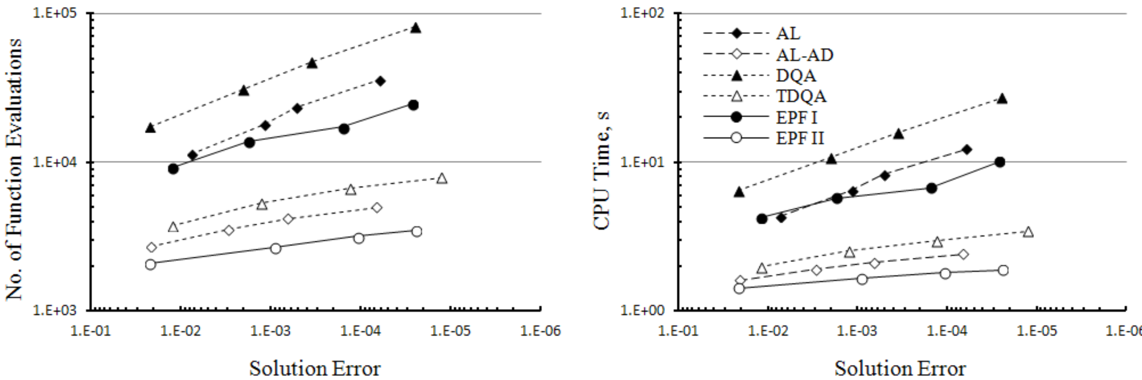

(a) (b)

Figure 4.3 Function evaluations (a) and CPU time (b) versus solution error in Problem 1

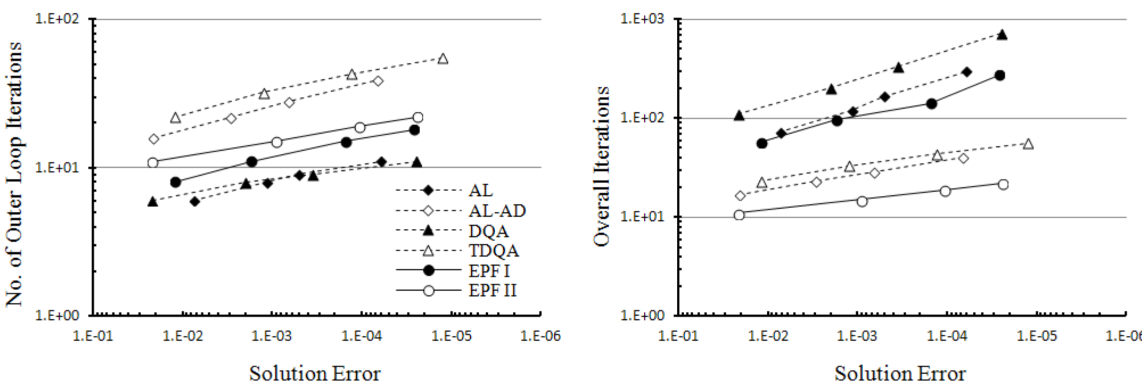

(a) (b)

Figure 4.4 Number of Outer Loop (a) and Overall (b) iterations versus solution error in Problem 1

A closer look at the results in Table 4.1 and figure 4.5 led to examination of the numbers of outer-loop iterations (i.e., AL-AD, TDQA, EPF II) and overall (inner- plus outer-loop) iterations (i.e., AL, DQA, EPF I) among the six approaches considered. The plotted data in figure 4.6 show that DQA has the lowest number of outer-loop iterations but the highest overall number of iterations. In comparison, EPF II requires the fewest overall number of iterations among all six approaches, but it falls in the middle of the pack when considering the number of outer-loop iterations.

These results indicate that all single-loop approaches are more computationally efficient than their double-loop counterparts, and that the EPF II approach requires fewer function evaluations than AL-AD and TDQA.

Problem 2

A seven-variable nonlinear constrained optimization problem is formulated as

$$\min_{x_1,\ldots,x_7} \quad f = x_1^2 + x_2^2 \tag{4.19}$$

$$s.t. \quad g_1 = \frac{x_3^{-2}+x_4^2}{x_5^2} - 1 \le 0$$

$$g_2 = \frac{x_5^2+x_6^{-2}}{x_7^2} - 1 \le 0$$

$$h_1 = x_1^2 - x_3^2 - x_4^{-2} - x_5^2 = 0$$

$$h_2 = x_2^2 - x_5^2 - x_6^2 - x_7^2 = 0$$

$$x_1, \ldots, x_7 \ge 0$$

where at the point of optimum $\boldsymbol{x}^* = [2.149, 2.076, 1.316, 0.760, 1.075, 1.000, 1.468]$, $f^* = 8.93$ and all the constraints are active. Although the objective function is convex, the constraint set is not, as can be easily noted by presence of nonlinear equality constraints. Hence, this is a non-convex optimization problem.

The problem is decomposed into a two-level hierarchy (Tosserams 2004) with one element at each level as shown in figure 4.7. The EPF formulation, objective function, design constraints, and local variables in each element are also shown. The target variable in this problem is x_5.

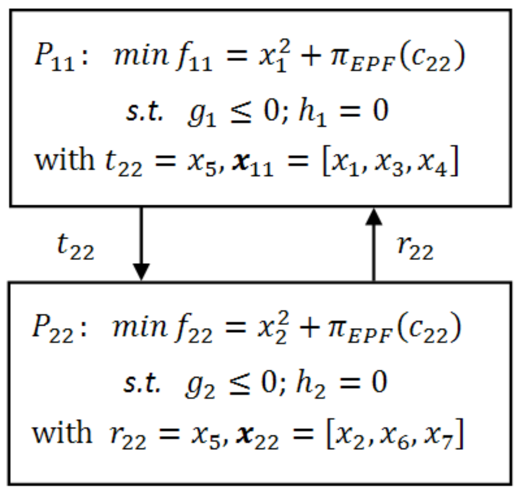

$$\pi_{EPF}(c_{22}) = \left\{\mu_{22}\left(e^{\,(t_{22}-r_{22})} - 1\right) + \gamma_{22}\left(e^{\,(r_{22}-t_{22})} - 1\right)\right\}$$

Figure 4.5 Hierarchical decomposition of Problem 2

Besides the formulation in figure 4.7, the decomposed problem is also solved using AL, AL-AD, DQA, and TDQA formulations of ATC. The initial values for the penalty parameters in AL, AL-AD, DQA and TDQA are chosen as $\lambda^{(0)} = 0$ and $w^{(0)} = 1$ whereas in EPF I and EPF II, $\mu^{(0)} = 1$ and $\gamma^{(0)} = 1$. The starting design point is chosen as $\boldsymbol{x}^{(0)} = [3, 3, 3, 3, 3, 3, 3]$ for all the formulations. For AL and DQA, $\beta = 2$, and for AL-AD and TDQA, $\beta = 1$.

Figure 4.8 shows the plots of the number of function evaluations and CPU time versus the absolute solution error e for the six different approaches at termination tolerances $\tau = 10^{-2}, 10^{-3}, 10^{-4}, 10^{-5}$.

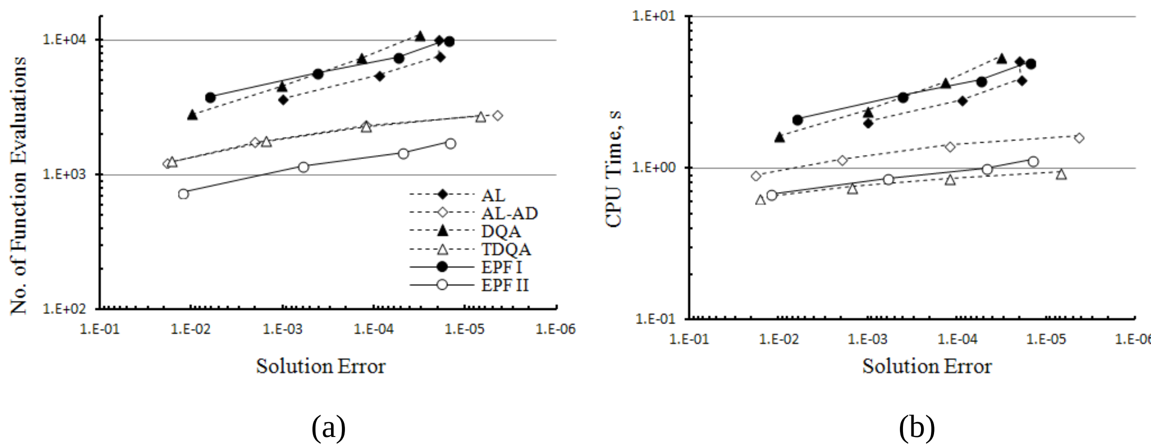

Figure 4.6 Function evaluations (a) and CPU time (b) versus solution error in Problem 2

In terms of the number of function evaluations, EPF II appears to be the most efficient followed by TDQA and AL-AD, with the latter two requiring, on average, at least 57% more function evaluations than EPF II. In terms of CPU time, TDQA is the most efficient with EPF II closely behind. In terms of CPU time, both TDQA and EPF II are, on average, at least 40% more efficient than the other approaches considered. In terms of function evaluation, EPF II is 40% more efficient than TDQA and much more efficient than the others.

Problem 3

A fourteen-variable nonlinear constrained optimization problem is formulated as

$$\min_{x_1,\ldots,x_{14}} \ f = x_1^2 + x_2^2 \tag{4.20}$$

$$s.t. \quad g_1 = \frac{x_3^{-2}+x_4^2}{x_5^2} - 1 \le 0$$

$$g_2 = \frac{x_5^2+x_6^{-2}}{x_7^2} - 1 \le 0$$

$$g_3 = \frac{x_8^2+x_9^2}{x_{11}^2} - 1 \le 0$$

$$g_4 = \frac{x_8^{-2}+x_{10}^2}{x_{11}^2} - 1 \le 0$$

$$g_5 = \frac{x_{11}^2+x_{12}^{-2}}{x_{13}^2} - 1 \le 0$$

$$g_6 = \frac{x_{11}^2+x_{12}^2}{x_{14}^2} - 1 \le 0$$

$$h_1 = x_1^2 - (x_3^2 + x_4^{-2} + x_5^2) = 0$$

$$h_2 = x_2^2 - (x_5^2 + x_6^2 + x_7^2) = 0$$

$$h_3 = x_3^2 - (x_8^2 + x_9^{-2} + x_{10}^{-2} + x_{11}^2) = 0$$

$$h_4 = x_6^2 - (x_{11}^2 + x_{12}^2 + x_{13}^2 + x_{14}^2) = 0$$

$$x_1, \ldots, x_{14} \ge 0$$

where at the point of optimum $\boldsymbol{x}^* =$ [2.835, 3.090, 2.356, 0.760, 0.870, 2.812, 0.940, 0.972, 0.865, 0.796, 1.301, 0.841, 1.763, 1.549], $f^* = 17.61$ and all the constraints are active. The nonlinear equality constraints make this a non-convex optimization problem.

The problem is decomposed into a three-level hierarchy (Kim 2001) with five elements, one element at the top and two elements each at levels two and three as shown in figure 4.9.

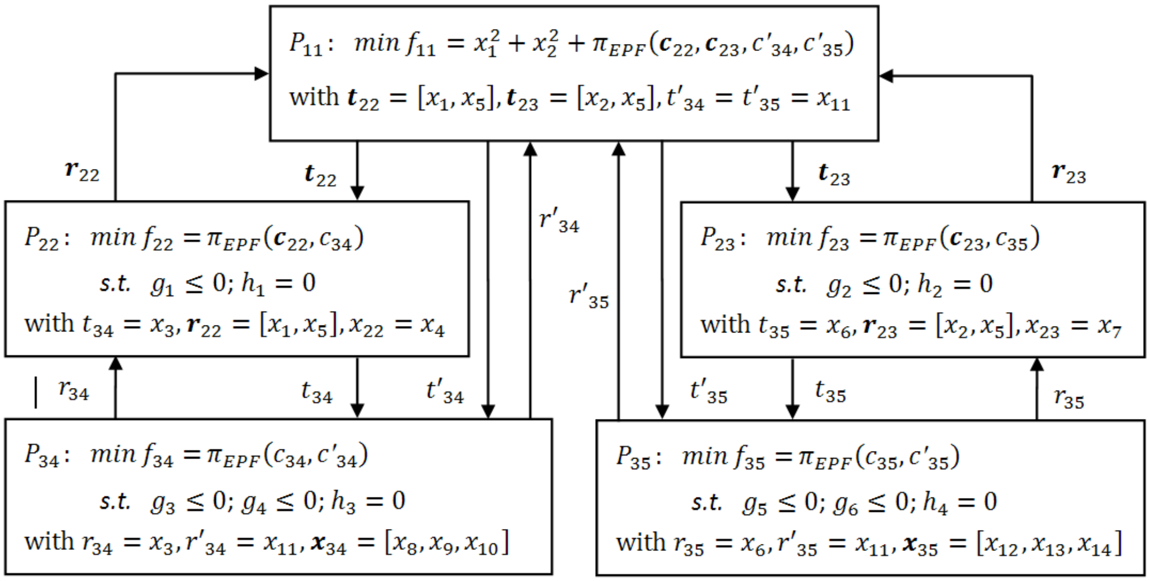

$$\boldsymbol{\pi_{EPF}(c_{ij})} = \left\{\boldsymbol{\mu_{ij}}\left(\boldsymbol{e}^{(t_{ij}-r_{ij})} - \boldsymbol{1}\right) + \boldsymbol{\gamma_{ij}}\left(\boldsymbol{e}^{(r_{ij}-t_{ij})} - \boldsymbol{1}\right)\right\} + \sum_{\boldsymbol{k \in D_{ij}}} \left\{\boldsymbol{\mu_{(i+1)k}}\left(\boldsymbol{e}^{(t_{(i+1)k}-r_{(i+1)k})} - \boldsymbol{1}\right) + \boldsymbol{\gamma_{(i+1)k}}\left(\boldsymbol{e}^{(r_{(i+1)k}-t_{(i+1)k})} - \boldsymbol{1}\right)\right\}$$

Figure 4.7 Hierarchical decomposition of Problem 3

The EPF formulation, local variables and design constraints in each element are also identified in figure 4.9. The target variables x_1 and x_2 link element 1 and its (children) elements 2 and 3, respectively. Similarly, element 2 is linked to element 4 via x_3 while element 3 is linked to element 5 through x_6. The linking variable x_5 is a shared variable in elements 2 and 3 whereas x_{11} is a shared variable in elements 4 and 5. The values of x_5 and x_{11} are coordinated in element 1. Because elements 34 and 35 do not share the same parent, the linking variable x_{11} is coordinated at the common grandparent element.

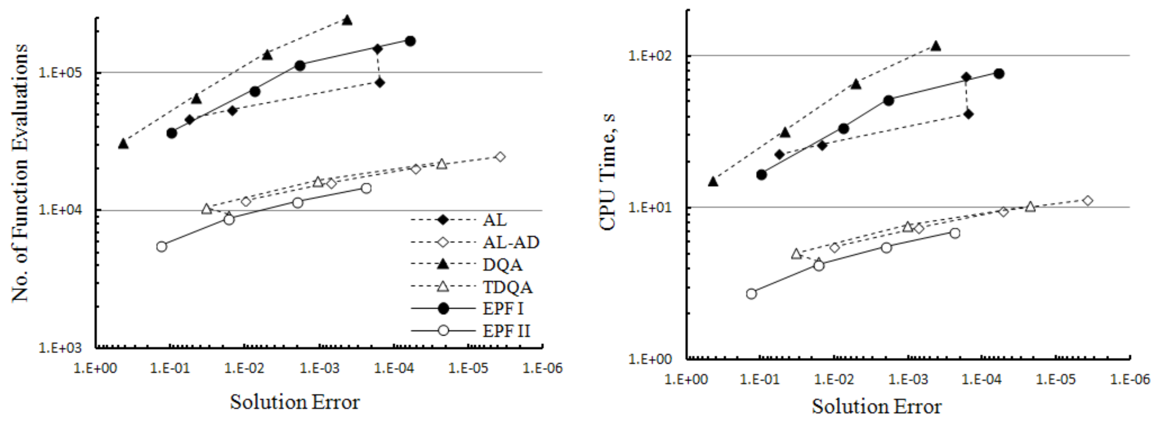

(a) (b)

Figure 4.8 Function evaluations (a) and CPU time (b) versus solution error in Problem 3

Besides the formulation in figure 4.9, the decomposed problem is also solved using AL, AL-AD, DQA, and TDQA formulations. In AL, AL-AD, DQA and TDQA, the penalty parameters are initialized as $\lambda^{(0)} = 0$ and $w^{(0)} = 1$; in EPF I and EPF II, $\mu^{(0)} = 1$ and $\gamma^{(0)} = 1$. The starting point is $x^{(0)} =$ [5.0, 5.0, 2.76, 0.25, 1.26, 4.64, 1.39, 0.67, 0.76, 1.7, 2.26, 1.41, 2.71, 2.66] for all the formulations. For AL and DQA, $\beta = 2$, and for AL-AD and TDQA, $\beta = 1$.

Figure 4.10 shows the plots of the number of function evaluations and CPU time versus the absolute solution error e for the six different approaches at termination tolerances $\tau = 10^{-2}, 10^{-3}, 10^{-4}, 10^{-5}$.

Similar to the previous problem, EPF II appears to be the most efficient approach in terms of the number of function evaluations followed by TDQA and AL-AD, with the latter two requiring, on average, at least 45% more function evaluations than EPF II. In terms of CPU time, unlike the previous problem, EPF II is the most efficient with TDQA and AL-AD behind. EPF II is, on average, at least 40% more efficient than the rest.

In Appendix II, Problem 3 is solved using EPF I and EPF II for two other decompositions with the results compared with those in figure 4.9.

Problem 4

A seven-variable nonlinear constrained optimization problem is formulated as (Montes and Coello 2005)

$$\min_{x_1,\dots,x_7} f = (x_1-10)^2 + 5(x_2-12)^2 + x_3^4 + 3(x_4-11)^2 + 10x_5^6 + 7x_6^2 + x_7^4 - 4x_6x_7 - 10x_6 - 8x_7 \tag{4.21}$$

$$\begin{aligned} s.t. \quad & g_1 = -127 + 2x_1^2 + 3x_2^4 + x_3 + 4x_4^2 + 5x_5 \le 0 \\ & g_2 = -282 + 7x_1 + 3x_2 + 10x_3^2 + x_4 - x_5 \le 0 \\ & g_3 = -196 + 23x_1 + x_2^2 + 6x_6^2 - 8x_7 \le 0 \\ & g_4 = 4x_1^2 + x_2^2 - 3x_1x_2 + 2x_3^2 + 5x_6 - 11x_7 \le 0 \\ & -10 \le x_i \le 10, i = 1, \dots, 7 \end{aligned}$$

where at the optimum point $x^* = (2.331, 1.951, -0.478, 4.366, -0.625, 1.038, 1.594)$, $f^* = 680.63$ and constraints g_1 and g_4 are active. This is not a convex programming problem since Hessian of the objective function is indefinite.

The decomposed problem and the corresponding EPF formulations are shown in figure 4.11. There is no local design variable or design constraint in element 1. The linking variables x_1, x_2 and x_3 are shared between elements 2 and 3 and coordinated in element 1.

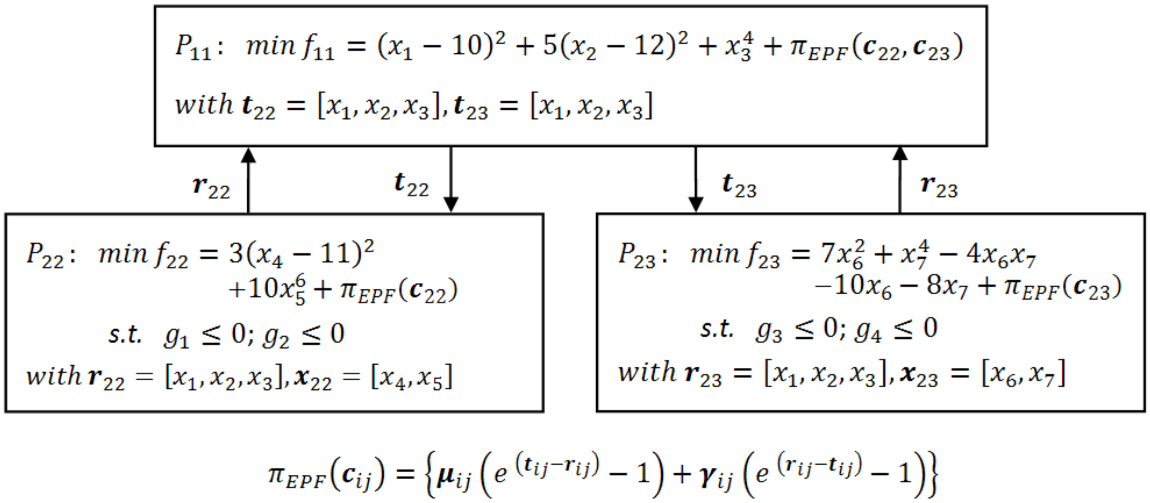

Figure 4.9 Hierarchical decomposition of Problem 4

Besides the formulations in figure 4.11, the decomposed problem is also solved using AL, AL-AD, DQA, and TDQA formulations of ATC. In AL, AL-AD, DQA and TDQA the initial parameters are set as $\lambda^{(0)} = 0$ and $w^{(0)} = 1$. In EPF I and EPF II, $\mu^{(0)} = 1$ and $\gamma^{(0)} = 1$. The starting point is $x^{(0)} = [0, 0, 0, 0, 0, 0, 0]$ for all the formulations. For AL and DQA, $\beta = 2$, and for AL-AD and TDQA, $\beta = 1$.

Figure 4.12 shows the plots of the number of function evaluations and CPU time versus the absolute solution error e for the six different approaches at termination tolerances $\tau = 10^{-2}, 10^{-3}, 10^{-4}, 10^{-5}$.

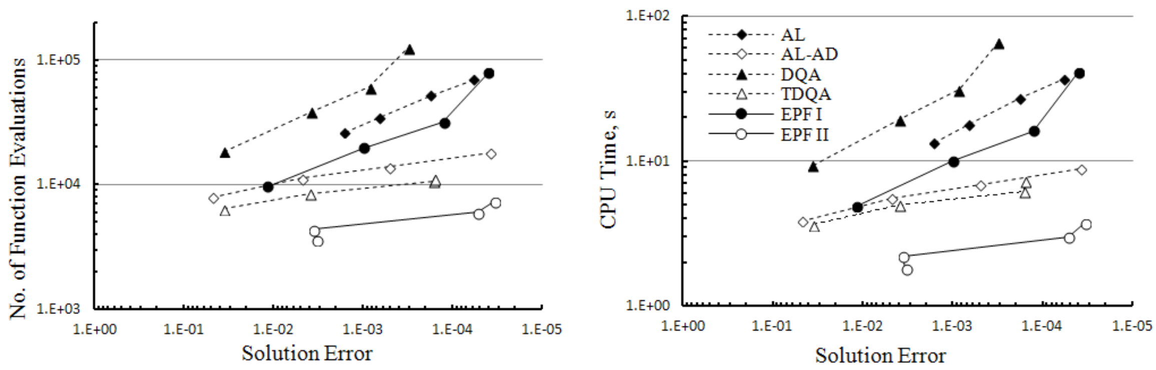

(a) (b)

Figure 4.10 Function evaluations (a) and CPU time (b) versus solution error in Problem 4

In this problem, the EPF II approach offers significant advantage over the other approaches, both with respect to the number of function evaluations and CPU time. EPF II, on average, has 70% less function evaluations than the best among the other approaches. In terms of CPU time, EPF II is at least 105% more efficient than the rest.

Summary and Conclusions

This chapter presented an exponential penalty function (EPF) formulation based on method of multipliers for solution of hierarchically decomposed optimization problems within the analytical target cascading (ATC) framework. The EPF formulation was combined with double-loop (EPF I) and single-loop (EPF II) coordination strategies and two penalty parameter updating schemes. Four benchmark (convex and non-convex) optimization problems were solved using the proposed approaches with different termination tolerance, τ values. These problems were all nonlinear but diverse in terms of the number of design variables and associated side constraints, number of design constraints, and inclusion of inequality and equality constraints. Performance metrics included the number of function evaluations and CPU time. The results were compared with those obtained using four other techniques (i.e., AL, AL-AD, DQA, TDQA) presented in the literature. Other characteristics, such as sensitivity to the penalty parameter updating methodology and alternative problem decompositions were also investigated.

The results showed that when a convex programming problem was decomposed into a multilevel system but solved as an all-in-one (AIO) optimization problem, EPF was less computationally efficient than AL by using 53% more iterations and 47% more function evaluations. However, when the same problem was solved as a decomposed multilevel system using ATC, the single-loop EPF II approach was more efficient than all the other approaches by requiring 23% fewer function evaluations than AL-AD and 88% less than DQA for $\tau = 10^{-2}$. For smaller τ values, the difference was even greater. For the non-convex benchmark problems, EPF II approach required on average 40% to 70% fewer function evaluations than all the rest in solving the decomposed multilevel systems. Generally, EPF I had better performance than the other double-loop methods (AL and DQA), whereas EPF II was found to be more efficient than TDQA and AL-AD.

The proposed approach overcomes the convergence difficulties and ill conditioning that exist in some of the other approaches. Also, while an iterative formulation was employed in AL to update the weight factor, the EPF-based calculations were done using a fixed weight factor.

In regard to the penalty parameters, both dependent and independent approaches were examined, and the results indicated that for the same level of accuracy, the number of function evaluations is generally reduced when the penalty parameters are kept independent of the multipliers. Moreover, updating the penalty parameters during the solution process provides greater computational efficiency than keeping them fixed.

CHAPTER V

HIERARCHICAL ANALYSIS AND OPTIMIZATION OF NANO-ENHANCED COMPOSITE SANDWICH PLATES

Advances in nanoscale materials (e.g., carbon nanotube) have led to the creation of multiscale composite materials with enhanced properties that can be designed for specific applications. Through proper tailoring of the constituents, it is possible to greatly enhance both the stiffness and strength characteristics of the composite materials. In the case of hybrid multiscale composite materials, where conventional reinforcing fibers are combined with a nano-enhanced matrix, the nanoreinforcements can improve the interfacial shear strength (ISS) properties between the conventional fibers and the nano-enhanced matrix (Thostenson et al., 2002; Garg et al., 2008). In addition, nano-enhancements may improve the overall mechanical properties of the hybrid composite material (Chisholm et al., 2005; Gojny et al., 2005; Zhou et al., 2008).

The hierarchical nature of the nano-enhanced composite materials and the structural components built using such materials provide an opportunity to expand the design problem by considering the mechanical attributes of interest at different length scales.

In this chapter, recent advances in optimization of decomposed multilevel systems (DorMohammadi and Rais-Rohani 2012; 2013) presented in Chapters 3 and 4 are applied to design of composite structures. The particular example considered is that of a simply-supported rectangular sandwich plate, where the thin-walled honeycomb core is supported by two identical laminated face sheets with multiple unidirectional layers that consist of continuous fibers at different orientation angles and CNF-enhanced polymer matrix. The overall hierarchy is shown in figure 5.1. A key element in this hierarchy is the modeling of the three-dimensional interphase that surround the CNF inside the matrix as well as the waviness observed in the CNF. These elements are included in both the analysis and design optimization of the composite sandwich plate.

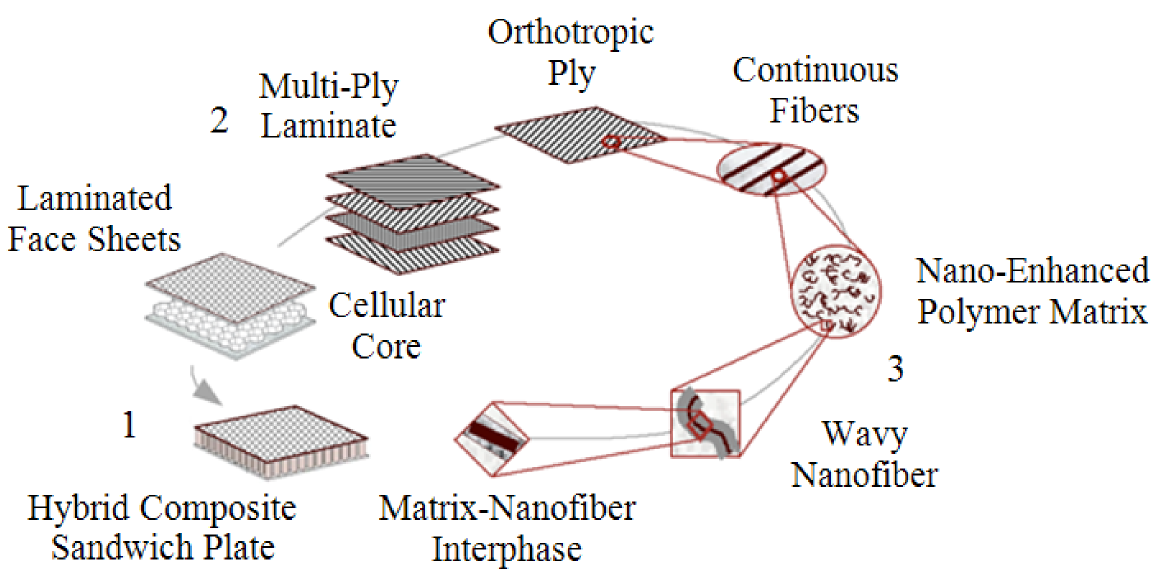

Figure 5.1 Decomposed hierarchy of nano-enhanced composite sandwich plate (Courtesy of M. Rais-Rohani)

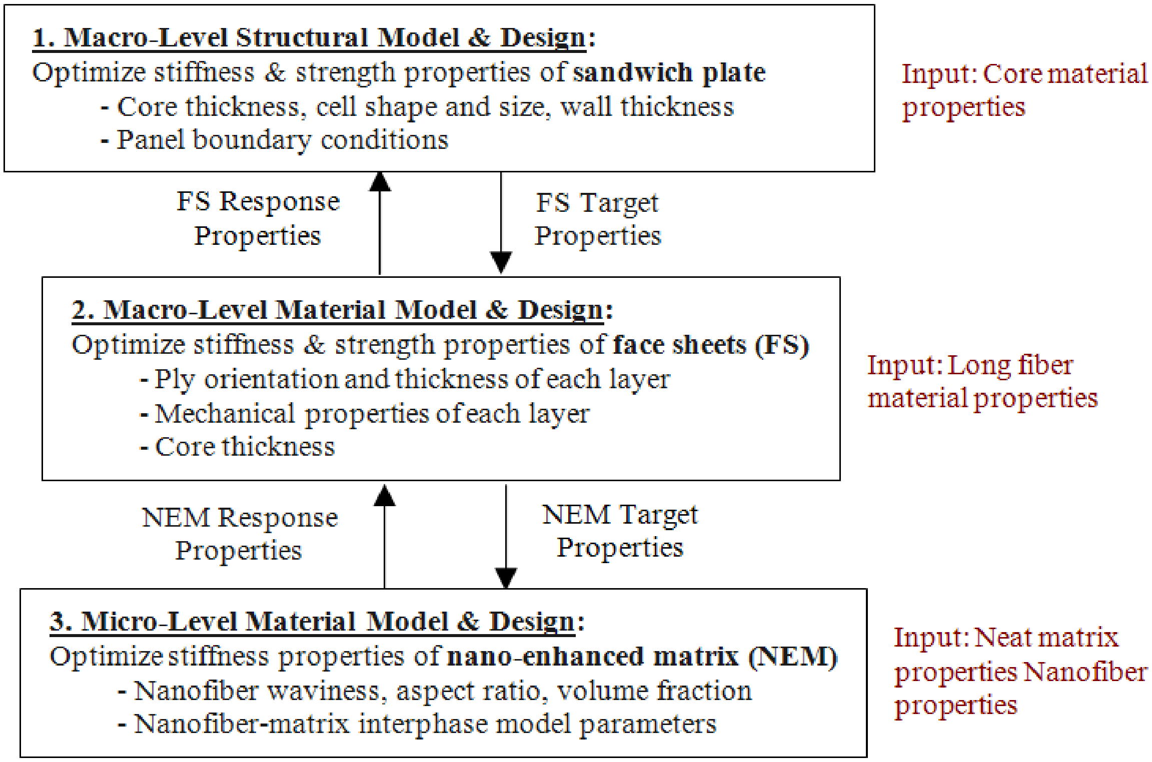

Figure 5.2 Decomposed multilevel optimization framework for the nano-enhanced composite sandwich plate (Courtesy of M. Rais-Rohani)

Following the decomposition strategy presented in Chapters 2 and 4, the multilevel sandwich plate optimization problem follows the arrangement shown in figure 5.2. At the bottom level in element 33, the enhanced matrix properties are optimized based on the neat matrix and CNF properties. The local design variable is principally the volume fraction of the randomly distributed CNFs given the interphase properties and waviness characteristics. The enhanced matrix properties calculated at this level are treated as input to the mid-level element 22 where the macro-level material modeling and design are performed. Key design variables in this level are the thickness and orientation angle of the individual plies that make up the face sheets of the sandwich plate. At this level the target value(s) for the bottom level are defined such that together with the local design variables, the face sheet properties are optimized. Similarly, the capabilities at the mid-level are passed up to the top-level element 11 where the overall system requirement are met while minimizing the weight or any other performance characteristic of the plate. Specific details of this problem are described later in discussion of the optimization problem.

Multilevel Composite Sandwich Plate Analysis

Sandwich plates appear in many engineering systems including automotive and aerospace structures. The plate consists of laminated composite face sheets (with symmetric or unsymmetric ply patterns) and a cellular core as shown in figure 5.1. Besides the conventional continuous (e.g., carbon) fibers, each unidirectional face-sheet ply is further stiffened by inclusion of carbon nanofibers (CNFs) mixed with the neat polymer matrix (e.g., vinyl ester, epoxy). The resulting multiscale composite material in the face sheets can be designed by controlling not only the fiber orientation and thickness of the individual plies but also the properties and composition of the constituent materials (e.g., volume fractions of fibers and CNFs, mean aspect ratio of CNFs, etc.).

Micro-level material model

Mori-Tanaka homogenization based on Eshelby's ellipsoidal inclusion model is often used for micromechanical approximation of stiffness properties based on mean field theory. In this approach, the prevailing assumptions include weak interaction among the inclusions (inhomogeneities) and perfect interface between inhomogeneity and the surrounding matrix (no interphase). Ellipsoidal model can be manipulated to produce various shapes (e.g., elliptic or circular platelets, spherical particles, cylindrical fibers) including voids. Due to problems associated with agglomeration of the inhomogeneities, Mori-Tanaka is used for dilute to semi-dilute matrix-inclusion mixture with volume fraction below 30%. Under these assumptions, it is possible to analyze the effect of CNF inclusions on the enhanced matrix properties. For example, Rouhi et al. (2010) used CNF-reinforced vinyl-ester $(E_0 = 3.5\ GPa,\ \nu_0 = 0.3,\ E_1 = 450\ GPa,$ and $\nu_1 = 0.3)$ with randomly oriented/distributed ellipsoidal CNF to examine the effect of CNF volume fraction (V_{CNF}) and aspect ratio (AR) on effective modulus (E_{EM}) of the enhanced matrix as shown in figure 5.3.

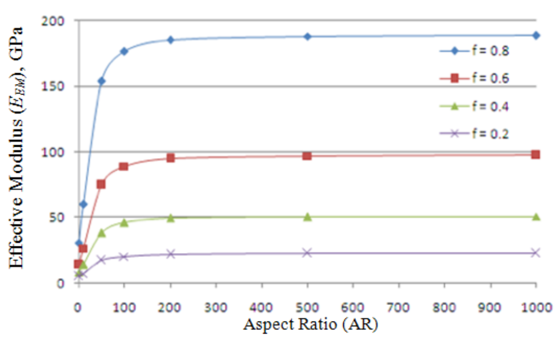

(a)

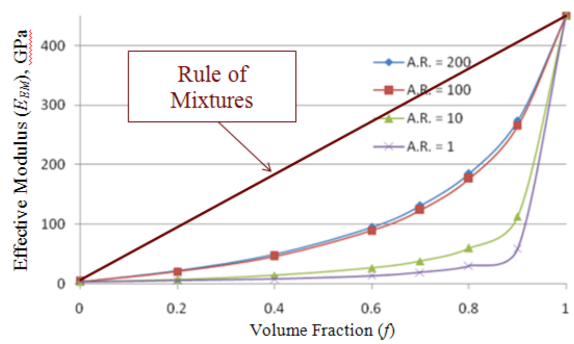

(b)

Figure 5.3 Effect of CNF on enhanced matrix properties as a function of (a) aspect ratio and (b) volume fraction (Rouhi et al. 2010)

Following the procedure presented by Rouhi et al. (2010) and Rouhi (2011), the effect of three-dimensional inhomogeneous interphase on enhanced matrix properties is modeled using the multi-inclusion approach (Nemat-Nasser and Hori 1993). In this case, the interphase is treated as a functionally graded (piecewise homogeneous) material whose effective properties can be calculated using the multi-inclusion (*MI*) model.

Using the functionally graded representation of the interphase as shown in figure 5.4, each elastic property (e.g., Young's modulus, Poisson's ratio) from the surface of the inclusion (x = 0) to the outermost layer of the interphase is approximated as (Rouhi 2011)

$$P = P_{in} + (P_{out} - P_{in})\left(\frac{x}{L}\right)^n \approx P_{in} + (P_{out} - P_{in})\left(\frac{\alpha-1}{N}\right)^n \tag{5.1}$$

where P represents the interphase property, n is the interphase variation parameter, with α varying in the range of 1 to N+1.

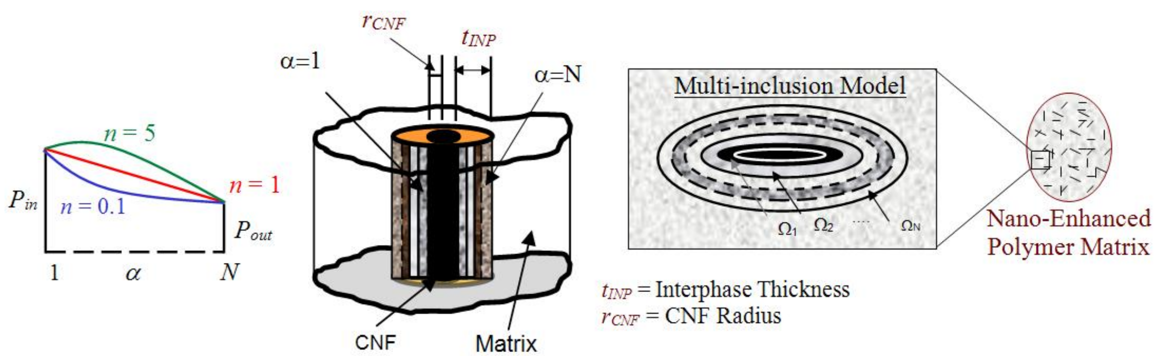

Figure 5.4 CNF-interphase modeled as multi-inclusion with functionally graded properties (Rouhi and Rais-Rohani, 2013)

For example, using CNF-reinforced vinyl-ester ($E_0 = 3.5\ GPa$, $\nu_0 = 0.3$, $E_1 = 450\ GPa$, and $\nu_1 = 0.3$) with randomly oriented/distributed ellipsoidal CNF at *AR* = 100 and $f_1 = 0.01$ and assuming a homogeneous interphase (N = 1), variation of effective modulus (E_{EM}) can be seen in figure 5.5(a) (Rouhi and Rais-Rohani 2013). The no interphase case is denoted by No-INP, whereas the other two cases consider an interphase with modulus higher (i.e., High-INP, $E_{INP} = 100\ GPa$ or $\sim 29E_0$) or lower (i.e., Low-INP, $E_{INP} = 2\ GPa$ or $\sim 0.6E_0$) than that of the matrix. ITR represents the ratio of interphase thickness to CNF radius $^{t_{INP}}/_{r_{CNF}}$. As indicated in figure 5.5(a), for the High-INP case, E_{EM} can improve by as much as 15% while for the Low-INP case, it reduces by 1.4%.

Using the same CNF-reinforced vinyl-ester material properties but with $f_1 = 0.038$ and treating the interphase as inhomogeneous (piecewise homogeneous) would result in the E_{EM} variation as shown in figure 5.5(b) (Rouhi and Rais-Rohani 2013). In this case, the interphase is divided into 20 separate regions (Ω_1 to Ω_{20}) such that the effective volume fraction of the interphase is kept constant while the interphase variation parameter *n* is allowed to vary from 0.1 to 5 (see figure 5.4). E-Ratio represents the ratio of moduli in interphase region 1 to that in region *N* = 20. It is worth noting that ITR is not constant from one case to the other because of the intent to keep the effective volume fraction of the interphase fixed. Based on the results shown in figure 5.5(b) it can be concluded that the overall interphase modulus is more important than its distribution.

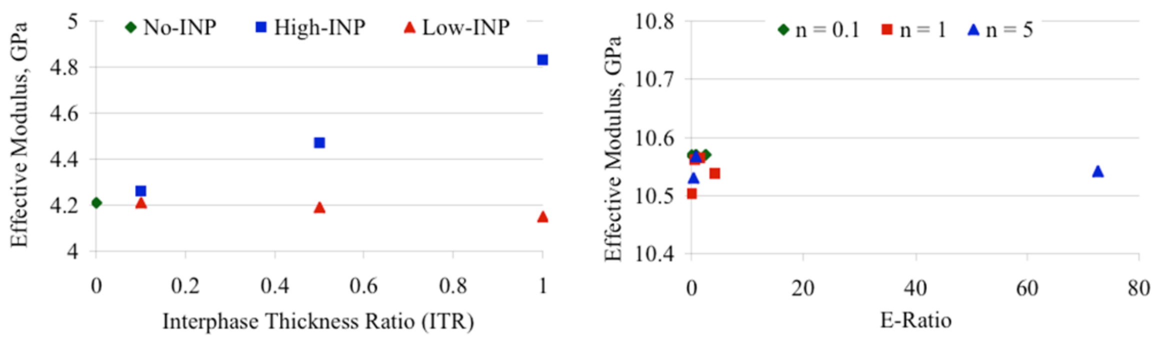

Figure 5.5 Variation of effective modulus for (a) homogeneous and (b) non-homogeneous interphase (Rouhi and Rais-Rohani, 2013)

For modeling the effect of CNF waviness on enhanced matrix properties, the approach taken by Fisher (2002) is used such that the wavy CNF is assumed to follow a sine wave with specified amplitude and wavelength. Using the strain energy formulation and Castigliano's second theorem, the equivalent modulus of straight ellipsoidal CNF is calculated and used in the micromechanical analysis.

The final outcome of this analysis is that, given the CNF material properties, aspect ratio, volume fraction, and waviness together with the interphase model and neat matrix properties, the effective modulus of the nano-enhanced matrix can be calculated for use in evaluation of ply-level properties. For micromechanical material model, a MATLAB code developed by Rouhi (2011) is adopted to calculate the stiffness and strength properties of the nano-enhanced matrix as described later.

Macro-level material model

For a lamina consisting of continuous fibers and nano-enhanced polymer matrix of known volume fractions, the self-consistent field model or the variational bounding method may be used for a more accurate prediction of the transverse modulus (Daniel and Ishai 1994); however, here the simplified mechanics of materials approach through *rule of mixtures* is applied for finding all the in-plane elastic properties (i.e., $E_1, E_2, G_{12}, \nu_{12}$) of a lamina, where the fiber can be anisotropic but the nano-enhanced matrix is assumed isotropic with homogenized properties. With the ply properties of a unidirectional lamina known, the transformed elastic constants at any orientation angle can be found and integrated over the thickness direction to find either the macroscopic properties of the resulting laminate. Furthermore, through the application of classical lamination theory and Kirchhoff hypothesis together with Hooke's law and equilibrium equations, the force-deformation and moment-deformation relationships can be found, which in a combined form relate the in-plane resultant forces (**N**) and moments (**M**) to the mid-plane strains ($\boldsymbol{\varepsilon}$) and curvatures ($\boldsymbol{\kappa}$) as

$$\begin{Bmatrix} \boldsymbol{N} \\ \boldsymbol{M} \end{Bmatrix} = \begin{bmatrix} A & B \\ B & D \end{bmatrix} \begin{Bmatrix} \boldsymbol{\varepsilon} \\ \boldsymbol{\kappa} \end{Bmatrix} \tag{5.2}$$

where the extensional, coupling, and bending stiffness matrices (i.e., *A*, *B*, *D*) are found as

$$A_{ij} = \sum_{k=1}^{N_p} \bar{Q}_{ij}^k (z_k - z_{k-1}) \tag{5.3}$$

$$B_{ij} = \frac{1}{2} \sum_{k=1}^{N_p} \bar{Q}_{ij}^k (z_k^2 - z_{k-1}^2)$$

$$D_{ij} = \frac{1}{3} \sum_{k=1}^{N_p} \bar{Q}_{ij}^k (z_k^3 - z_{k-1}^3)$$

In equations (5.3), $\bar{Q}_{ij}^k$ represents the transformed stiffness matrix of the kth lamina with z measuring the distance through thickness from the mid-plane surface.

Macro-level structural model

The geometric layout and structural parameters of a rectangular sandwich plate are shown in figure 5.6. The parameters consist of the planform dimensions a and b, ply thickness (t_i) and orientation angle (θ_i), face sheet thickness (t_f), core cell size (S), core foil thickness (t_c), and overall core thickness (h_c).

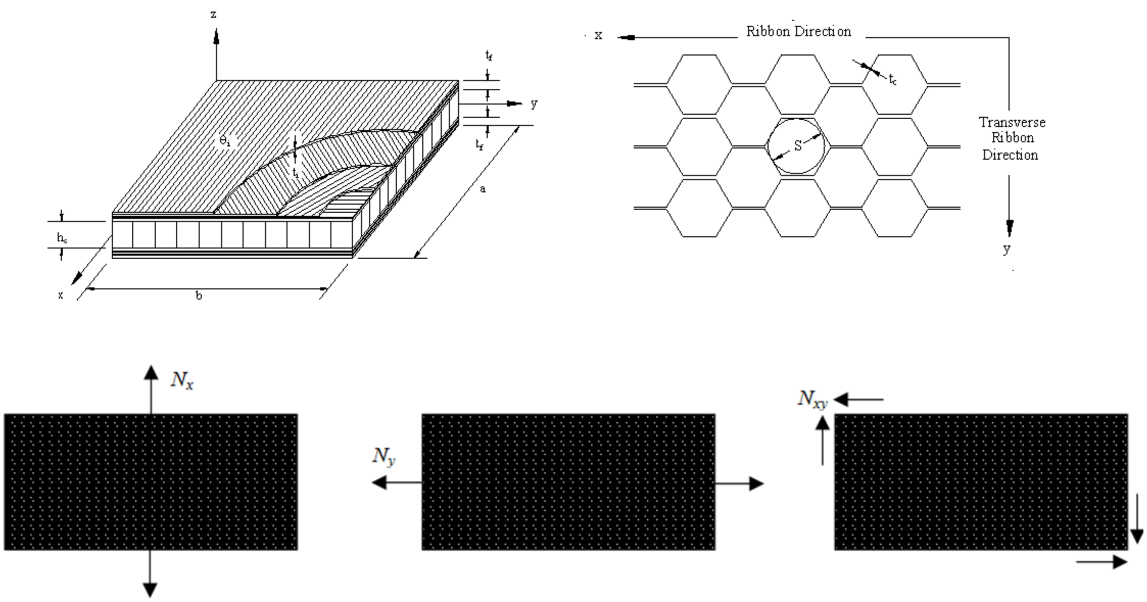

Figure 5.6 General layout of the sandwich plate with laminated face sheets and honeycomb core (Clements 1997)

The sandwich plate analysis is based on the general small-deflection theory for rectangular orthotropic sandwich plates developed by Libove and Batdorf (1948), and subsequently extended by Rao (1985) for buckling analysis of simply-supported sandwich plates with anisotropic face sheets. In this theory, the plate's curvatures are expressed in terms of lateral deflection of the plate and transverse shear strains in the core. While the bending stiffness is provided mainly by the face sheets, the transverse shear stiffness is due to the core, which is assumed to have infinite transverse normal rigidity with insignificant its in-plane rigidities compared to those of the face sheets. Hence, together with equation (5.2), the transverse shear forces are found as

$$\begin{Bmatrix} Q_x \\ Q_y \end{Bmatrix} = \begin{bmatrix} S_x & 0 \\ 0 & S_y \end{bmatrix} \begin{Bmatrix} \gamma_{xy} \\ \gamma_{yz} \end{Bmatrix} \tag{5.3}$$

where transverse shear rigidities are defined as $S_x = h_c G_{xz}$ and $S_y = h_c G_{yz}$. According to the theory used, the core's out-of-plane shear moduli contribute to the transverse shear rigidity while only the face sheets contribute to the *A*, *B*, and *D* matrices.

Through the application of Rayleigh-Ritz method, the strain energy stored in the face sheets and the core, along with the potential energy associated with the external in-plane reaction forces are calculated for the entire plate. Using the principle of minimum total potential energy, the resulting eigenvalue problem is solved for the in-plane buckling loads are found as described by Rais-Rohani and Marcellier (1999) and Clements (1997). Once the resultant buckling force components $(N_{x_{cr}}, N_{y_{cr}}, N_{xy_{cr}})$ are found, the corresponding buckling stresses are found as

$$\sigma_{x_{cr}} = \frac{N_{x_{cr}}}{2t_f}; \;\; \sigma_{y_{cr}} = \frac{N_{y_{cr}}}{2t_f}; \;\; \tau_{xy_{cr}} = \frac{N_{xy_{cr}}}{2t_f} \tag{5.4}$$

The second mode of instability of sandwich panels is shear crimping, which is considered a degenerate case of plate buckling. This core dominated instability is caused by excessively low core shear modulus resulting in localized buckling of the core. The shear crimping stress components are found as (Bruhn 1973; Vinson and Sierakowski 1986)

$$\sigma_{x_{cr}}^{sc} = \left(\frac{2}{3}\right)\frac{t_c h_c G_c}{S\,t_f};\;\; \sigma_{y_{cr}}^{sc} = \left(\frac{4}{15}\right)\frac{t_c h_c G_c}{S\,t_f};\;\; \tau_{xy_{cr}}^{sc} = \sqrt{\frac{8}{45}}\frac{t_c h_c G_c}{S\,t_f} \tag{5.5}$$

The honeycomb core ribbon direction is responsible for the difference in the coefficients of the normal shear crimping stresses. Vinson and Sierakowski (1986) define four parameters to help make a distinction between the likelihood of global buckling and shear crimping (local instability). Those parameters are considered in this analysis to identify the principal instability mode.

For a sandwich plate with a cellular core, another mode of instability is that associated with intracell buckling, otherwise known as face sheet dimpling. This instability occurs when the face sheet becomes too thin relative to the cell size causing the local buckling of the face sheet inside the core cell cavity.

$$\sigma_{cr}^{ib} = \tau_{cr}^{ib} = \left(\frac{2\sqrt{\bar{E}_x\bar{E}_y}}{1-\bar{\upsilon}_{xy}\,\bar{\upsilon}_{yx}}\right)\left(\frac{t_f}{S}\right)^2 \tag{5.6}$$

where the in-plane elastic properties denoted as $\bar{\;}$ represent the effective laminate properties that are functions of only the *A* matrix and face sheet thickness (Daniel and Ishai 1994).

The last sandwich failure mode considered is that of face sheet wrinkling. This instability occurs when the face sheets are too thin relative to the core taking a similar form of instability as a thin plate on an elastic foundation. It is calculated as (Vinson and Sierakowski 1986)

$$\sigma_{cr}^{w} = \tau_{cr}^{w} = \sqrt{\frac{16 t_f t_c E_c\sqrt{\bar{E}_x\bar{E}_y}}{9 h_c S(1-\bar{\upsilon}_{xy}\,\bar{\upsilon}_{yx})}} \tag{5.7}$$

where E_c represents the core's Young's modulus in the plate thickness direction.

Multilevel Material-Product Optimization Problem

The sandwich plate optimization problem decomposed according to the three-level hierarchy in figure 5.2 consists of three separate elements: micro-level material design at the bottom level, macro-level material design in the middle, and structural-level component (i.e., sandwich plate) design at the top.

At the micro-level material design (element 33), target and response variables are the mechanical properties, i.e., Young's modulus (E_{em}) and Poisson's ratio (ν_{em}) of the nano-enhanced matrix with volume fraction of CNF (V_{CNF}) as the only local design variable. Previous studies have shown that addition of small amount of CNF (V_{CNF} < 3%) to a polymer matrix can enhance its mechanical properties without compromising manufacturability of the resulting composite material due to excessive viscosity. Therefore, the objective function of this element is the inconsistency between enhanced matrix properties and their target values from the macro-level element above. The element optimization problem based on the EFP formulation is expressed as

$$\min_{\bar{x}_{33}} \quad \left\{\frac{\boldsymbol{\lambda}_{33}}{\boldsymbol{a}_{33}}\left(e^{\boldsymbol{a}_{33}\,(\boldsymbol{t}_{33}-\boldsymbol{r}_{33})}-1\right)+\frac{\boldsymbol{\gamma}_{33}}{\boldsymbol{b}_{33}}\left(e^{\boldsymbol{b}_{33}\,(\boldsymbol{r}_{33}-\boldsymbol{t}_{33})}-1\right)\right\} \tag{5.8}$$

$$s.t. \quad 0 \le x_{33} \le 0.03$$

where,

$$\boldsymbol{t}_{33} = (E_{em}^T, \nu_{em}^T);\ \boldsymbol{r}_{33} = f_{M-T}(x_{33}) = (E_{em}^R, \nu_{em}^R);\ \ \bar{x}_{33} = (x_{33});\ x_{33} = V_{CNF}$$

The superscripts *T* and *R* denote target and response, respectively.

At the macro-level material design (element 22), macroscopic properties of the composite material include both the nano-enhanced matrix and continuous fiber reinforcements. This element design is mostly aimed at the face sheets including their geometric and material properties. The rule of mixtures is used to determine the mechanical properties of the nano-enhanced orthotropic ply ($E_1, E_2, G_{12}, \nu_{12}$).

Assuming identical face sheets, the macro-level design problem has a composite objective function consisting of f_{22} and inconsistencies between the targets and responses associated with both the top and bottom elements in levels 1 and 3, respectively. The f_{22} term consists of the normalized weight of each face sheet (W_{fs}), normalized Young's modulus of the nano-enhanced matrix (E_{em}), and volume fraction of the continuous fibers (V_f). Non-dimensionalization of the weight and modulus terms ensures proper scaling of the different objectives. For both the weight and Young's modulus, separate minimum and maximum values are defined. The term with the normalized E_{em} and V_f serves as surrogate for the upper bound on manufacturing cost of the nano-enhanced laminated face sheets, which is an important consideration. The coefficients w_1 through w_3 are the weight factors signifying the importance of weight, material enhancement and cost.

There are two sets of targets and responses in this element; $\boldsymbol{t}_{33}$ and $\boldsymbol{r}_{33}$ include Young's modulus and Poisson's ratio of the nano-enhanced matrix (E_{em}, ν_{em}), whereas $\boldsymbol{t}_{22}$ and $\boldsymbol{r}_{22}$ consist of the stiffness properties of the face sheets, together with core thickness and face sheet thickness. The local design variables include volume fraction (V_f) of the continuous fibers, as well as the orientation angle (θ_i) and thickness (t_i) of each ply in the laminate sub-stack. Besides the local design variables, the decision variable vector $\bar{x}_{22}$ also includes the stiffness matrices ($\boldsymbol{A}$, $\boldsymbol{B}$, $\boldsymbol{D}$), enhanced matrix properties (E_{em}, ν_{em}), total face sheet thickness (t_f), and core thickness (h_c). The side constraints in this element follow manufacturing limitations. It should be noted that due to matrix symmetry, each stiffness matrix consists of six separate terms. Similar to the micro-level material problem, the element optimization problem at the macro-level is formulated as

$$\text{Min}_{\bar{x}_{22}}\, f_{22} + \left\{\frac{\boldsymbol{\lambda}_{22}}{\boldsymbol{a}_{22}}\left(e^{\boldsymbol{a}_{22}\,(\boldsymbol{t}_{22}-\boldsymbol{r}_{22})} - 1\right) + \frac{\boldsymbol{\gamma}_{22}}{\boldsymbol{b}_{22}}\left(e^{\boldsymbol{b}_{22}\,(\boldsymbol{r}_{22}-\boldsymbol{t}_{22})} - 1\right)\right\} +$$

$$\left\{\frac{\boldsymbol{\lambda}_{33}}{\boldsymbol{a}_{33}}\left(e^{\boldsymbol{a}_{33}\,(\boldsymbol{t}_{33}-\boldsymbol{r}_{33})} - 1\right) + \frac{\boldsymbol{\gamma}_{33}}{\boldsymbol{b}_{33}}\left(e^{\boldsymbol{b}_{33}\,(\boldsymbol{r}_{33}-\boldsymbol{t}_{33})} - 1\right)\right\} \tag{5.9}$$

$$s.t. \quad 0.25 \le V_f \le 0.75;\; 0.006 \le t_i \le 0.6 \text{ in};\; -90° \le \theta_i \le 90°;\;\; 0.1 \le h_c \le 5.0 \text{ in}$$

where

$$f_{22} = \left\{w_1\left(\frac{W_{fs}-W_{fs}^{min}}{W_{fs}^{max}-W_{fs}^{min}}\right) + w_2\left(\frac{E_{em}^{T}-E_{em}^{min}}{E_{em}^{max}-E_{em}^{min}}\right) + w_3 V_f\right\}$$

$$\boldsymbol{t}_{22} = \left(\boldsymbol{A}^T, \boldsymbol{B}^T, \boldsymbol{D}^T, t_f^T, h_c^T\right); \boldsymbol{r}_{22} = \left(\boldsymbol{A}^R, \boldsymbol{B}^R, \boldsymbol{D}^R, t_f^R, h_c^R\right)$$

$$\boldsymbol{A} = f_A(\boldsymbol{x}_{22}); \boldsymbol{B} = f_B(\boldsymbol{x}_{22}); \boldsymbol{D} = f_D(\boldsymbol{x}_{22}); t_f = 4\sum t_i$$

$$\boldsymbol{t}_{33} = (E_{em}^T, \nu_{em}^T); \boldsymbol{r}_{33} = (E_{em}^R, \nu_{em}^R); \boldsymbol{x}_{22} = \left(V_f, t_i, \theta_i\right); \bar{x}_{22} = (h_c^R, \boldsymbol{t}_{33}, \boldsymbol{x}_{22})$$

The total plate thickness is $2t_f + h_c$. The core material properties (E_c, G_c, ν_c), and panel dimensions are the parameters provided as input to this element problem and are held fixed.

At the structural-level design (element 11), the stiffness and strength properties of a rectangular sandwich plate of specified planform dimensions and boundary conditions under a single or combined in-plane load are optimized. For buckling consideration, the applied loads in the x and y directions are compressive (i.e., $-N_x$ and $-N_y$). In this element, the face sheet is treated as a single layer of thickness t_f and stiffness properties given by A, B, and D matrices. The design constraints consist of global buckling (g_{cr}), shear crimping (g_{sc}), intracell buckling (g_{ib}), and face sheet wrinkling (g_w) with the corresponding analyses performed using a sandwich plate design and analysis tool developed through previous research and modified for the product-material problem in figure 5.2. The local design variables for this optimization problem are the honeycomb core cell size (S) and cell wall or foil thickness (t_c). With the overall weight of the sandwich plate (W_{SP}) together with target-response inconsistencies treated as the objective function, the element optimization problem is given as

$$\min_{\bar{x}_{11}} \quad f_{11} + \left\{\frac{\boldsymbol{\lambda}_{22}}{\boldsymbol{a}_{22}}\left(e^{\boldsymbol{a}_{22}\,(\boldsymbol{t}_{22}-\boldsymbol{r}_{22})} - 1\right) + \frac{\boldsymbol{\gamma}_{22}}{\boldsymbol{b}_{22}}\left(e^{\boldsymbol{b}_{22}\,(\boldsymbol{r}_{22}-\boldsymbol{t}_{22})} - 1\right)\right\} \tag{5.10}$$

$s.t. \quad g_{cr} \geq 0;\ g_{sc} \geq 0;\ g_{ib} \geq 0;\ g_w \geq 0;\ 0.0625 \leq S \leq 2.0$ in; $0.0007 \leq t_c \leq$ 0.01 in

where

$$f_{11} = W_{SP}$$

$$\boldsymbol{t}_{22} = \left(\boldsymbol{A}^T, \boldsymbol{B}^T, \boldsymbol{D}^T, t_f^T, h_c^T\right); \boldsymbol{r}_{22} = \left(\boldsymbol{A}^R, \boldsymbol{B}^R, \boldsymbol{D}^R, t_f^R, h_c^R\right);\ \boldsymbol{x}_{11} = (S, t_c);\ \bar{x}_{11} = (\boldsymbol{t}_{22}, \boldsymbol{x}_{11})$$

All the individual computer tools were modified to fit the description of the material-product design problem in figure 5.2. The functionality of each tool based on the individual input parameters has been tested and verified.

Discussion of Results

Based on results from the prior studies (Rouhi et al., 2010; Rouhi 2011), the CNF waviness parameters ($W_\lambda = 150$ μm, $W_a = 50$ μm) along with interphase thickness ratio (ITR = 0.5) and interphase variation parameter ($n = 1$) are all held fixed. Different combinations of loading conditions, plate aspect ratio, and material systems were examined with summary of the results presented herein.

The properties used for the various materials are as follows: CNF ($E_{CNF} = 65.27 \times 10^6\ psi$, $\nu_{CNF} = 0.3$); continuous carbon fiber ($E_f = 27 \times 10^6\ psi$, $\nu_f = 0.3$); vinyl-ester matrix ($E_m = 0.507 \times 10^6\ psi$, $\nu_m = 0.3$); and Hexcel 2024 aluminum alloy honeycomb core ($E_c = 10 \times 10^6\ psi$, $\nu_c = 0.3$).

All the plate examples have the same number of face sheet plies (i.e., 32). The laminate lay-up follows two stacks of eight plies on either side of the face sheet mid-plane to form a symmetric face sheet. The upper and lower face sheets are identical in every aspect. There are 21 design variables as shown in Table 5.1. Given the non-convex nature of the design problem, each optimization problem is solved three different times using alternative initial design points. The solution reported in each case is the best among the three found for each set. All the multilevel optimization problems are solved using the coordination scheme II of EPF approach.

The results in Table 5.1 are for a square sandwich plate under bi-axial compression with the face-sheet material being CNF-enhanced carbon-vinyl ester composite. In this case, $w_1 = w_2 = w_3 = 1.0$; it is important to note that although the plate weight and nano-enhanced Young's modulus are normalized, the difference in the max and min values can still create some disparity in the two normalized terms. This is reflected in the value of f_{22} shown in Table 5.1 as well as the subsequent tables. Given the low effective density of the honeycomb core, the optimum sandwich plate is one with relatively large core thickness and fairly thin face sheets. The dominance of the large core thickness reduces the involvement of both CNF and carbon fiber reinforcement as reflected by their optimum volume fractions. The ply lay-up favors a cross-ply laminate with more zero than ninety degree plies. The difference in the number of plies in each direction is due to the difference in the core properties in the two principal directions as noted previously. To eliminate the possibility of intracell buckling given the small face sheet thickness, the core cell size is pushed to its lower bound while the foil thickness has reached its upper bound. For manufacturability considerations, a simplified form of the optimum design is provided in the last column of each table.

To examine the influence of the weight factors in the objective function on the optimum design, different combinations are considered. The results in Table 5.2 are for the same material system, loading conditions, and plate dimensions as those in Table 5.1. However, in this case, $w_1 = w_2 = 10, w_3 = 1$; The difference in the selected weight factors affects the value of f_{22}, but it does not have any significant influence on the optimum design point, which is not surprising given the dominance of the core thickness.

Table 5.1 Sandwich plate properties for $a/b = 1$, $N_x = N_y$ and $w_1 = w_2 = w_3 = 1$

Design Variables	Lower Bound	Initial Design	Upper Bound	Optimum Design	Optimum Simplified
V_{CNF}	0.0	0.01	0.03	0.0001	0.0001
V_f	0.25	0.25	0.75	0.25	0.25
t_1, in	0.006	0.1515	0.6	0.0138	0.0150
t_2, in	0.006	0.1515	0.6	0.0215	0.0225
t_3, in	0.006	0.1515	0.6	0.0411	0.0450
t_4, in	0.006	0.1515	0.6	0.0064	0.0075
t_5, in	0.006	0.1515	0.6	0.0130	0.0150
t_6, in	0.006	0.1515	0.6	0.0176	0.0225
t_7, in	0.006	0.1515	0.6	0.0127	0.0150
t_8, in	0.006	0.1515	0.6	0.0140	0.0150
$\theta_1{}^\circ$	-90	0.0	90	-1.0469	0.0
$\theta_2{}^\circ$	-90	45.0	90	-0.4847	0.0
$\theta_3{}^\circ$	-90	-45.0	90	-90.0	90.0
$\theta_4{}^\circ$	-90	90.0	90	-0.4600	0.0
$\theta_5{}^\circ$	-90	90.0	90	-0.4036	0.0
$\theta_6{}^\circ$	-90	-45.0	90	-90.0	90.0
$\theta_7{}^\circ$	-90	45.0	90	-0.1759	0.0
$\theta_8{}^\circ$	-90	0.0	90	-0.1733	0.0
h_c, in	0.1	1.275	5.0	3.8889	3.9
S, in	0.0625	1.265	2.0	0.0625	0.06
t_c, in	0.0007	0.00535	0.01	0.01	0.01
Weight, lb	2.024	50.5	200.2	12.73	13.48
$f_{22} \times 1000$	250	828.36	2750	304.21	311.14

Note: CNF-enhanced carbon-vinyl ester sandwich plate with $a = b = 12\ in$ and $N_x = N_y = -3.1 \times 10^6\ lb$, $f_{22} = \left\{\left(\frac{W_{fs} - W_{fs}^{min}}{W_{fs}^{max} - W_{fs}^{min}}\right) + \left(\frac{E_{em}^{T} - E_{em}^{min}}{E_{em}^{max} - E_{em}^{min}}\right) + V_f\right\}$

A significant change in the weight factors is used next with the results for $w_1 = 1000, w_2 = 0.1, w_3 = 1$ as shown in Table 5.3. To focus on this effect, the other problem parameters are held fixed. Although the optimum core thickness is the same as those in Tables 1 and 2, we note a significant change in both the CNF and continuous carbon fiber volume fractions, with the latter moving closer to its upper bound. The larger emphasis on weight has reduced the optimum thickness of each face sheet ply with compensation through higher carbon volume faction and to a lesser extent increase in optimum volume fraction of CNFs. As the loading condition and plate aspect ratio has not changed, it appears that the preferred stacking sequence and ply orientation angles remain unchanged as compared to the previous two cases. The optimum plate in Table 5.3 is about 12% lighter than those shown in Tables 1 and 2.

For comparison purposes, one case was tested using both the multilevel approach as well as the all-at-once (AAO) formulation where all the design variables, constraints, and objectives are defined in a single optimization problem. The results in Table 5.4 are for the AAO problem with a slightly different weight factors than those in Tables 5.1 through 5.3. The major finding is that while each of the multilevel optimization problems took nearly 6 CPU hours[a] to complete, the AAO problem took nearly 5 CPU days. This clearly shows the advantage of multilevel approach in practical material-product design optimization problems where the cost of analysis is highly dependent on the computational time associated with each function evaluation. Another important distinction is the difference in the ply angles with two at -67 degrees as opposed to 90 degrees found in the multilevel problems for the same loading condition.

[a]OS: XP SP3; Processor: Intel Core 2 Duo CPU E8400 @ 3 GHz and 4.0 GB RAM.

In gradient-based optimization methods, it is necessary to calculate the gradients of the objective and constraint functions to find the search vector at each design point. Optimization software commonly use forward finite difference scheme to determine the gradient of the objective and constraint functions as

$$S'(x) = \frac{S(x+\Delta x)-S(x)}{\Delta x} \tag{5.11}$$

where S is an arbitrary function, $S'(x)$ is the derivative of S respect to x, and Δx is a small increment in x.

For the sandwich plate design, the AAO optimization problem is described as

$$\min_{x_1,\ldots,x_{21}} f \tag{5.12}$$

$$s.t. \quad g_{cr} \geq 0;\ g_{sc} \geq 0;\ g_{ib} \geq 0;\ g_w \geq 0$$

where the f term consists of the normalized weight of the sandwich plate (W), volume fraction of the continuous fibers (V_f), and volume fraction of nano-enhanced matrix CNF (V_{CNF}). W is evaluated by Fortran code. To evaluate the constraint functions, optimizer calls both Fortran and MATLAB codes. While the MATLAB code is the most computationally expensive code in our problem, it governs the overall computational cost of the optimization problem. Assuming M_C and F_C are the computational costs for executing the MATLAB and Fortran codes, respectively, for AAO optimization, the computational cost for each iteration is approximately $22 \times \mathrm{M}_C$ as $\mathrm{M}_C \gg \mathrm{F}_C$.

In ATC, the optimization problem is decomposed into multiple elements. The element optimization problems based on the EFP formulation are expressed as

$$\boldsymbol{P}_{33}: \tag{5.13}$$

$$\min_{\bar{x}_{33}} \quad \left\{\frac{\boldsymbol{\lambda}_{33}}{\boldsymbol{a}_{33}}\left(e^{\boldsymbol{a}_{33}\,(\boldsymbol{t}_{33}-\boldsymbol{r}_{33})}-1\right)+\frac{\boldsymbol{\gamma}_{33}}{\boldsymbol{b}_{33}}\left(e^{\boldsymbol{b}_{33}\,(\boldsymbol{r}_{33}-\boldsymbol{t}_{33})}-1\right)\right\};\ \text{s.t.} \quad 0 \le x_{33} \le 0.03$$

$$\boldsymbol{t}_{33} = (E_{em}^{T}, \nu_{em}^{T});\ \boldsymbol{r}_{33} = f_{M-T}(x_{33}) = (E_{em}^{R}, \nu_{em}^{R});\ \ \bar{x}_{33} = (x_{33});\ x_{33} = V_{CNF}$$

$$\boldsymbol{P}_{22}: \tag{5.14}$$

$$\mathrm{Min}_{\bar{x}_{22}}\, f_{22} + \left\{\frac{\boldsymbol{\lambda}_{22}}{\boldsymbol{a}_{22}}\left(e^{\boldsymbol{a}_{22}\,(\boldsymbol{t}_{22}-\boldsymbol{r}_{22})}-1\right)+\frac{\boldsymbol{\gamma}_{22}}{\boldsymbol{b}_{22}}\left(e^{\boldsymbol{b}_{22}\,(\boldsymbol{r}_{22}-\boldsymbol{t}_{22})}-1\right)\right\} +$$

$$\left\{\frac{\boldsymbol{\lambda}_{33}}{\boldsymbol{a}_{33}}\left(e^{\boldsymbol{a}_{33}\,(\boldsymbol{t}_{33}-\boldsymbol{r}_{33})}-1\right)+\frac{\boldsymbol{\gamma}_{33}}{\boldsymbol{b}_{33}}\left(e^{\boldsymbol{b}_{33}\,(\boldsymbol{r}_{33}-\boldsymbol{t}_{33})}-1\right)\right\}$$

$$s.t.\ \ 0.25 \le V_f \le 0.75;\ 0.006 \le t_i \le 0.6 \text{ in};\ -90° \le \theta_i \le 90°;\ \ 0.1 \le h_c \le 5.0 \text{ in}$$

$$f_{22} = \left\{w_1\left[\left(\frac{W_{fs}-W_{fs}^{min}}{W_{fs}^{max}-W_{fs}^{min}}\right)\right] + \left[w_2\left(\frac{E_{em}^{T}-E_{em}^{min}}{E_{em}^{max}-E_{em}^{min}}\right) + w_3 V_f\right]\right\}$$

$$\boldsymbol{t}_{22} = \left(\boldsymbol{A}^T, \boldsymbol{B}^T, \boldsymbol{D}^T, t_f^T, h_c^T\right); \boldsymbol{r}_{22} = \left(\boldsymbol{A}^R, \boldsymbol{B}^R, \boldsymbol{D}^R, t_f^R, h_c^R\right)$$

$$\boldsymbol{A} = f_A(\boldsymbol{x}_{22}); \boldsymbol{B} = f_B(\boldsymbol{x}_{22}); \boldsymbol{D} = f_D(\boldsymbol{x}_{22}); t_f = 4\sum t_i$$

$$\boldsymbol{t}_{33} = (E_{em}^{T}, \nu_{em}^{T}); \boldsymbol{r}_{33} = (E_{em}^{R}, \nu_{em}^{R}); \boldsymbol{x}_{22} = \left(V_f, t_i, \theta_i\right); \bar{x}_{22} = (h_c^R, \boldsymbol{t}_{33}, \boldsymbol{x}_{22})$$

$$\boldsymbol{P}_{11}: \tag{5.15}$$

$$\min_{\bar{x}_{11}} \quad f_{11} + \left\{\frac{\boldsymbol{\lambda}_{22}}{\boldsymbol{a}_{22}}\left(e^{\boldsymbol{a}_{22}\,(\boldsymbol{t}_{22}-\boldsymbol{r}_{22})}-1\right)+\frac{\boldsymbol{\gamma}_{22}}{\boldsymbol{b}_{22}}\left(e^{\boldsymbol{b}_{22}\,(\boldsymbol{r}_{22}-\boldsymbol{t}_{22})}-1\right)\right\}$$

$s.t.$ $\quad g_{cr} \ge 0;\ g_{sc} \ge 0;\ g_{ib} \ge 0;\ g_w \ge 0;\ 0.0625 \le S \le 2.0$ in; $0.0007 \le t_c \le$ 0.01 in

$$f_{11} = W_{SP}$$

$$\boldsymbol{t}_{22} = \left(\boldsymbol{A}^T, \boldsymbol{B}^T, \boldsymbol{D}^T, t_f^T, h_c^T\right); \boldsymbol{r}_{22} = \left(\boldsymbol{A}^R, \boldsymbol{B}^R, \boldsymbol{D}^R, t_f^R, h_c^R\right);\ \boldsymbol{x}_{11} = (S, t_c);\ \bar{x}_{11} = (\boldsymbol{t}_{22}, \boldsymbol{x}_{11})$$

The computational costs for evaluation of functional derivatives in elements 11, 22, and 33 are equal to $(N_{11}+1)\times \mathrm{F}_C$, $(N_{22}+1)\times \mathrm{F}_C$, and M_C, respectively, where $N_{11} = 16$ and $N_{22} = 17$ are number of design variables in elements 11 and 22.

Therefore, the computational cost for one iteration of ATC is equal to $(N_{11}+1)\times \mathrm{F}_C +$ $(N_{22}+1)\times \mathrm{F}_C + \mathrm{M}_C$ which is much less than $22 \times \mathrm{M}_C$ for AAO optimization.

Table 5.2 Sandwich plate properties for $a/b = 1$, $N_x = N_y$ and $w_1 = w_2 = 10, w_3 = 1$

Design Variables	Lower Bound	Initial Design	Upper Bound	Optimum Design	Optimum Simplified
V_{CNF}	0.0	0.01	0.03	0.0001	0.0001
V_f	0.25	0.25	0.75	0.25	0.25
t_1, in	0.006	0.1515	0.6	0.0129	0.0150
t_2, in	0.006	0.1515	0.6	0.0236	0.0225
t_3, in	0.006	0.1515	0.6	0.0368	0.0375
t_4, in	0.006	0.1515	0.6	0.0085	0.0150
t_5, in	0.006	0.1515	0.6	0.0108	0.0150
t_6, in	0.006	0.1515	0.6	0.0222	0.0225
t_7, in	0.006	0.1515	0.6	0.0124	0.0150
t_8, in	0.006	0.1515	0.6	0.0129	0.0150
θ_1 °	-90	0.0	90	-0.6066	0.0
θ_2 °	-90	45.0	90	-0.2870	0.0
θ_3 °	-90	-45.0	90	-90.0	90.0
θ_4 °	-90	90.0	90	-0.2870	0.0
θ_5 °	-90	90.0	90	-0.2595	0.0
θ_6 °	-90	-45.0	90	-89.9430	90.0
θ_7 °	-90	45.0	90	-0.1166	0.0
θ_8 °	-90	0.0	90	-0.1091	0.0
h_c, in	0.1	1.275	5.0	3.8886	3.9
S, in	0.0625	1.265	2.0	0.0625	0.06
t_c, in	0.0007	0.00535	0.01	0.01	0.01
Weight, lb	2.024	50.5	200.2	12.73	13.48
$f_{22} \times 1000$	250	6033.68	20750	792.14	861.44

Note: CNF-enhanced carbon-vinyl ester sandwich plate with $a = b = 12\ in$ and $N_x = N_y = -3.1 \times 10^6\ lb$, $f_{22} = \left\{10\left(\frac{W_{fs} - W_{fs}^{min}}{W_{fs}^{max} - W_{fs}^{min}}\right) + 10\left(\frac{E_{em}^{T} - E_{em}^{min}}{E_{em}^{max} - E_{em}^{min}}\right) + V_f\right\}$

Table 5.3 Sandwich plate properties for $a/b = 1$, $N_x = N_y$ and $w_1 = 1000, w_2 = 0.1, w_3 = 1$

Design Variables	Lower Bound	Initial Design	Upper Bound	Optimum Design	Optimum Simplified
V_{CNF}	0.0	0.01	0.03	0.0047	0.005
V_f	0.25	0.25	0.75	0.6671	0.70
t_1, in	0.006	0.1515	0.6	0.0148	0.0150
t_2, in	0.006	0.1515	0.6	0.0139	0.0150
t_3, in	0.006	0.1515	0.6	0.0269	0.0300
t_4, in	0.006	0.1515	0.6	0.0060	0.0075
t_5, in	0.006	0.1515	0.6	0.0060	0.0075
t_6, in	0.006	0.1515	0.6	0.0146	0.0150
t_7, in	0.006	0.1515	0.6	0.0142	0.0150
t_8, in	0.006	0.1515	0.6	0.0066	0.0075
θ_1°	-90	0.0	90	-0.0967	0.0
θ_2°	-90	45.0	90	0.4882	0.0
θ_3°	-90	-45.0	90	-90.0	90
θ_4°	-90	90.0	90	-0.1164	0.0
θ_5°	-90	90.0	90	4.1346	0.0
θ_6°	-90	-45.0	90	-90.0	90
θ_7°	-90	45.0	90	0.0600	0.0
θ_8°	-90	0.0	90	-0.1366	0.0
h_c, in	0.1	1.275	5.0	3.8852	3.9
S, in	0.0625	1.265	2.0	0.0625	0.06
t_c, in	0.0007	0.00535	0.01	0.01	0.01
Weight, lb	2.024	50.5	200.2	11.19	11.61
f_{22}	0.25	244.89	1000.85	47.98	49.09

Note: CNF-enhanced carbon-vinyl ester sandwich plate with $a = b = 12\ in$ and $N_x = N_y = -3.1 \times 10^6\ lb$, $f_{22} = \left\{1000\left(\frac{W_{fs}-W_{fs}^{min}}{W_{fs}^{max}-W_{fs}^{min}}\right) + 0.1\left(\frac{E_{em}^{T}-E_{em}^{min}}{E_{em}^{max}-E_{em}^{min}}\right) + V_f\right\}$

Table 5.4 Comparison of initial and AAO optimum designs for $a/b = 1$ and $N_x = N_y$

Design Variables	Lower Bound	Initial Design	Upper Bound	Optimum Design	Optimum Simplified
V_{CNF}	0.0	0.01	0.30	0.0371	0.04
V_f	0.25	0.25	0.75	0.25	0.25
t_1, in	0.006	0.1515	0.6	0.0094	0.0150
t_2, in	0.006	0.1515	0.6	0.0094	0.0150
t_3, in	0.006	0.1515	0.6	0.0165	0.0225
t_4, in	0.006	0.1515	0.6	0.0094	0.0150
t_5, in	0.006	0.1515	0.6	0.0094	0.0150
t_6, in	0.006	0.1515	0.6	0.0332	0.0300
t_7, in	0.006	0.1515	0.6	0.0131	0.0150
t_8, in	0.006	0.1515	0.6	0.0437	0.0450
$\theta_1{}^\circ$	-90	0.0	90	-0.1276	0.0
$\theta_2{}^\circ$	-90	45.0	90	-0.0190	0.0
$\theta_3{}^\circ$	-90	-45.0	90	-67.32	-67.0
$\theta_4{}^\circ$	-90	90.0	90	-0.2109	0.0
$\theta_5{}^\circ$	-90	90.0	90	-0.2109	0.0
$\theta_6{}^\circ$	-90	-45.0	90	-67.32	-67.0
$\theta_7{}^\circ$	-90	45.0	90	-0.1238	0.0
$\theta_8{}^\circ$	-90	0.0	90	-0.0548	0.0
h_c, in	0.1	1.275	5.0	4.2993	4.3
S, in	0.0625	1.265	2.5	0.0625	0.0625
t_c, in	0.0007	0.00535	0.01	0.0091	0.009
Weight, lb	2.024	50.5	200.2	12.91	14.05
$f_{22} \times 1000$	2.5	247.44	1008.5	57.73	64.52

Note: CNF-enhanced carbon-vinyl ester sandwich plate with $a = b = 12\ in$ and $N_x = N_y = -3.1 \times 10^6\ lb$, $f_{22} = \left\{1000\left(\frac{W_{fs}-W_{fs}^{min}}{W_{fs}^{max}-W_{fs}^{min}}\right) + \left(\frac{E_{em}^{T}-E_{em}^{min}}{E_{em}^{max}-E_{em}^{min}}\right) + 10V_f\right\}$

In Table 5.5 the results for a square sandwich plate under uniaxial compression in the x direction are shown. The optimum design yields a cross-ply laminated face sheet with equal number of zero- and ninety-degree plies with different thicknesses. Given the load magnitude and direction, both CNF and carbon fiber volume fractions are at or near their lower bounds due to sensitivity of the objective function to these two design variables.

The results in Table 5.6 are for a square sandwich plate under uni-axial compression in the y direction. Although the load magnitude is the same as that in Table 5.5, the core thickness has increased by over 50%. The core is orthotropic due to different properties in the x (the ribbon direction) and y (the perpendicular) directions; thus, the transverse shear stiffnesses of the core are different in the x and y directions. Under uniaxial compression in the y direction, the weight of the plate is higher than the weight of the sandwich plate under uniaxial compression in the x direction since the transverse shear stiffness in the x direction is higher than the transverse shear stiffness in the y direction (Harris 1995). There is not much difference in the face sheet ply patterns between Table 5.5 and 6, although there are some differences in the ply thicknesses. The overall plate thickness in Table 5.6 is about 32% higher than that in Table 5.5.

The optimum design for a square sandwich plate under pure in-plane shear loading is presented in Table 5.7. The load magnitude is the same as those in Tables 5.5 and 5.6; also, as in the previous two cases, the CNF and carbon fiber volume fractions are at their respective lower bounds. This, of course, has to do with the magnitude of the applied load. By increasing the load, one or both volume fractions will increase to enhance the plate stiffness. There is very little difference between the core thickness in this case and that in Table 5.5 with the overall weight being slightly higher.

The results in Tables 5.5 through 5.7 indicate that although the loading direction affects the sizing variables such as ply or core thickness, it does not alter the preferred ply orientation angles or the volume fractions of the reinforcing materials. For the remaining tables, $f_{22} = \left\{1000\left(\frac{W_{fs}-W_{fs}^{min}}{W_{fs}^{max}-W_{fs}^{min}}\right) + 100\left(\frac{E_{em}^{T}-E_{em}^{min}}{E_{em}^{max}-E_{em}^{min}}\right) + 100V_f\right\}$.

Table 5.5 Comparison of initial and optimum designs for $a/b = 1$ and N_x

Design Variables	Lower Bound	Initial Design	Upper Bound	Optimum Design	Optimum Simplified
V_{CNF}	0.0	0.01	0.03	0.0001	0.0001
V_f	0.25	0.25	0.75	0.25	0.25
t_1, in	0.006	0.1515	0.6	0.0139	0.0150
t_2, in	0.006	0.1515	0.6	0.0072	0.0075
t_3, in	0.006	0.1515	0.6	0.0060	0.0075
t_4, in	0.006	0.1515	0.6	0.0065	0.0075
t_5, in	0.006	0.1515	0.6	0.0065	0.0075
t_6, in	0.006	0.1515	0.6	0.0068	0.0075
t_7, in	0.006	0.1515	0.6	0.0103	0.0150
t_8, in	0.006	0.1515	0.6	0.0103	0.0150
θ_1 °	-90	0.0	90	-1.2966	0.0
θ_2 °	-90	45.0	90	89.0428	90
θ_3 °	-90	-45.0	90	-88.8615	90
θ_4 °	-90	90.0	90	2.3553	0.0
θ_5 °	-90	90.0	90	2.3553	0.0
θ_6 °	-90	-45.0	90	-88.8615	90
θ_7 °	-90	45.0	90	89.0428	90
θ_8 °	-90	0.0	90	-1.2966	0.0
h_c, in	0.1	1.275	5.0	1.0888	1.10
S, in	0.0625	1.265	2.0	0.0625	0.06
t_c, in	0.0007	0.00535	0.01	0.0083	0.01
Weight, lb	2.024	50.5	200.2	4.42	5.38
f_{22}	25	302.99	1175	37.46	42.27

Note: CNF-enhanced carbon-vinyl ester sandwich plate with $a = b = 12\ in$ and $N_x = -1.8 \times 10^6\ lb$

Table 5.6 Comparison of initial and optimum designs for $a/b = 1$ and N_y

Design Variables	Lower Bound	Initial Design	Upper Bound	Optimum Design	Optimum Simplified
V_{CNF}	0.0	0.01	0.03	0.0001	0.0001
V_f	0.25	0.25	0.75	0.25	0.25
t_1, in	0.006	0.1515	0.6	0.0098	0.0150
t_2, in	0.006	0.1515	0.6	0.0066	0.0075
t_3, in	0.006	0.1515	0.6	0.0128	0.0150
t_4, in	0.006	0.1515	0.6	0.0093	0.0150
t_5, in	0.006	0.1515	0.6	0.0065	0.0075
t_6, in	0.006	0.1515	0.6	0.0094	0.0150
t_7, in	0.006	0.1515	0.6	0.0081	0.0075
t_8, in	0.006	0.1515	0.6	0.0099	0.0150
$\theta_1{}^\circ$	-90	0.0	90	-0.0875	0.0
$\theta_2{}^\circ$	-90	45.0	90	88,2174	90
$\theta_3{}^\circ$	-90	-45.0	90	-88.7213	90
$\theta_4{}^\circ$	-90	90.0	90	0.9704	0.0
$\theta_5{}^\circ$	-90	90.0	90	6.6224	0.0
$\theta_6{}^\circ$	-90	-45.0	90	-88.8194	90
$\theta_7{}^\circ$	-90	45.0	90	88.2174	90
$\theta_8{}^\circ$	-90	0.0	90	-0.0750	0.0
h_c, in	0.1	1.275	5.0	1.5989	1.60
S, in	0.0625	1.265	2.0	0.0625	0.06
t_c, in	0.0007	0.00535	0.01	0.01	0.01
Weight, lb	2.024	50.5	200.2	5.85	6.89
f_{22}	25	302.99	1175	44.70	49.90

Note: CNF-enhanced carbon-vinyl ester sandwich plate with $a = b = 12\ in$ and $N_y = -1.8 \times 10^6\ lb$

Table 5.7 Comparison of initial and optimum designs for $a/b = 1$ and N_{xy}

Design Variables	Lower Bound	Initial Design	Upper Bound	Optimum Design	Optimum Simplified
V_{CNF}	0.0	0.01	0.03	0.0001	0.0001
V_f	0.25	0.25	0.75	0.25	0.25
t_1, in	0.006	0.1515	0.6	0.0086	0.0150
t_2, in	0.006	0.1515	0.6	0.0073	0.0075
t_3, in	0.006	0.1515	0.6	0.0080	0.0075
t_4, in	0.006	0.1515	0.6	0.0113	0.0150
t_5, in	0.006	0.1515	0.6	0.0060	0.0075
t_6, in	0.006	0.1515	0.6	0.0076	0.0075
t_7, in	0.006	0.1515	0.6	0.0065	0.0075
t_8, in	0.006	0.1515	0.6	0.0078	0.0075
θ_1 °	-90	0.0	90	-0.0816	0.0
θ_2 °	-90	45.0	90	86.1665	90
θ_3 °	-90	-45.0	90	-86.0826	90
θ_4 °	-90	90.0	90	0.1777	0.0
θ_5 °	-90	90.0	90	3.3875	0.0
θ_6 °	-90	-45.0	90	-86.0826	90
θ_7 °	-90	45.0	90	86.1665	90
θ_8 °	-90	0.0	90	0.0400	0.0
h_c, in	0.1	1.275	5.0	1.0536	1.10
S, in	0.0625	1.265	2.0	0.0625	0.06
t_c, in	0.0007	0.00535	0.01	0.01	0.01
Weight, lb	2.024	50.5	200.2	4.50	5.07
f_{22}	25	302.99	1175	37.82	40.70

Note: CNF-enhanced carbon-vinyl ester sandwich plate with $a = b = 12\ in$ and $N_{xy} = 1.8 \times 10^6\ lb$

Table 5.8 Comparison of initial and optimum designs for $a/b = 1$ and $N_x = N_y$

Design Variables	Lower Bound	Initial Design	Upper Bound	Optimum Design	Optimum Simplified
V_{CNF}	0.0	0.01	0.03	0.001	0.001
V_f	0.25	0.25	0.75	0.25	0.25
t_1, in	0.006	0.1515	0.6	0.0070	0.0075
t_2, in	0.006	0.1515	0.6	0.0087	0.0075
t_3, in	0.006	0.1515	0.6	0.0089	0.0075
t_4, in	0.006	0.1515	0.6	0.0200	0.0225
t_5, in	0.006	0.1515	0.6	0.0119	0.015
t_6, in	0.006	0.1515	0.6	0.0089	0.0075
t_7, in	0.006	0.1515	0.6	0.0092	0.0075
t_8, in	0.006	0.1515	0.6	0.0070	0.0075
θ_1 °	-90	0.0	90	-0.1343	0
θ_2 °	-90	45.0	90	-0.0625	0
θ_3 °	-90	-45.0	90	-87.0870	-90
θ_4 °	-90	90.0	90	86.5823	90
θ_5 °	-90	90.0	90	-0.0925	0
θ_6 °	-90	-45.0	90	-86.6493	-90
θ_7 °	-90	45.0	90	-0.0625	0
θ_8 °	-90	0.0	90	-0.1239	0
h_c, in	0.1	1.275	5.0	2.2918	2.3
S, in	0.0625	1.265	2.0	0.0625	0.06
t_c, in	0.0007	0.00535	0.01	0.0100	0.01
Weight, lb	4.048	101	400.4	7.4670	7.518
f_{22}	25	302.99	1175	52.5628	52.8211

CNF-enhanced carbon-vinyl ester sandwich plate with $a = b = 12\ in$ and $N_x = N_y = -1.8 \times 10^6\ lb$

Table 5.9 Comparison of initial and optimum designs for $a/b = 1$ and $N_x = N_y = N_{xy}$

Design Variables	Lower Bound	Initial Design	Upper Bound	Optimum Design	Optimum Simplified
V_{CNF}	0.0	0.01	0.03	0.001	0.001
V_f	0.25	0.25	0.75	0.25	0.25
t_1, in	0.006	0.1515	0.6	0.0204	0.0225
t_2, in	0.006	0.1515	0.6	0.0205	0.0225
t_3, in	0.006	0.1515	0.6	0.0137	0.0150
t_4, in	0.006	0.1515	0.6	0.0060	0.0075
t_5, in	0.006	0.1515	0.6	0.0089	0.0075
t_6, in	0.006	0.1515	0.6	0.0357	0.03
t_7, in	0.006	0.1515	0.6	0.0060	0.0075
t_8, in	0.006	0.1515	0.6	0.0060	0.0075
$\theta_1{}^\circ$	-90	0.0	90	-0.1320	0
$\theta_2{}^\circ$	-90	45.0	90	-0.0877	0
$\theta_3{}^\circ$	-90	-45.0	90	-90.0000	-90
$\theta_4{}^\circ$	-90	90.0	90	-0.0675	0
$\theta_5{}^\circ$	-90	90.0	90	89.6135	90
$\theta_6{}^\circ$	-90	-45.0	90	-90.0000	-90
$\theta_7{}^\circ$	-90	45.0	90	0.5884	0
$\theta_8{}^\circ$	-90	0.0	90	-0.0877	0
h_c, in	0.1	1.275	5.0	2.5988	2.6
S, in	0.0625	1.265	2.0	0.0625	0.06
t_c, in	0.0007	0.00535	0.01	0.0100	0.01
Weight, lb	4.048	101	400.4	9.4850	9.607
f_{22}	25	302.99	1175	62.7818	63.3996

Note: CNF-enhanced carbon-vinyl ester sandwich plate with $a = b = 12\ in$ and $N_x = N_y = -N_{xy} = -1.8 \times 10^6\ lb$

Table 5.10 Comparison of initial and optimum designs for $a/b = 2$ and N_x

Design Variables	Lower Bound	Initial Design	Upper Bound	Optimum Design	Optimum Simplified
V_{CNF}	0.0	0.01	0.03	0.001	0.001
V_f	0.25	0.25	0.75	0.25	0.25
t_1, in	0.006	0.1515	0.6	0.0100	0.0150
t_2, in	0.006	0.1515	0.6	0.0060	0.0075
t_3, in	0.006	0.1515	0.6	0.0121	0.0150
t_4, in	0.006	0.1515	0.6	0.0060	0.0075
t_5, in	0.006	0.1515	0.6	0.0060	0.0075
t_6, in	0.006	0.1515	0.6	0.0134	0.0150
t_7, in	0.006	0.1515	0.6	0.0060	0.0075
t_8, in	0.006	0.1515	0.6	0.0060	0.0075
$\theta_1\,^\circ$	-90	0.0	90	-0.3040	0
$\theta_2\,^\circ$	-90	45.0	90	-0.0350	0
$\theta_3\,^\circ$	-90	-45.0	90	-90.0000	-90
$\theta_4\,^\circ$	-90	90.0	90	-0.0550	0
$\theta_5\,^\circ$	-90	90.0	90	-0.0700	0
$\theta_6\,^\circ$	-90	-45.0	90	-90.0000	-90
$\theta_7\,^\circ$	-90	45.0	90	-0.0750	0
$\theta_8\,^\circ$	-90	0.0	90	-0.5055	0
h_c, in	0.1	1.275	5.0	1.0561	1.1
S, in	0.0625	1.265	2.0	0.2682	0.27
t_c, in	0.0007	0.00535	0.01	0.0099	0.01
Weight, lb	4.048	101	400.4	8.8380	10.4
f_{22}	25	302.99	1175	59.4902	67.4152

Note: CNF-enhanced carbon-vinyl ester sandwich plate with $a = 24, b = 12\ in$ and $N_x = -1.8 \times 10^6\ lb$

Table 5.11 Comparison of initial and optimum designs for $a/b = 2$ and N_y

Design Variables	Lower Bound	Initial Design	Upper Bound	Optimum Design	Optimum Simplified
V_{CNF}	0.0	0.01	0.03	0.001	0.001
V_f	0.25	0.25	0.75	0.25	0.25
t_1, in	0.006	0.1515	0.6	0.0060	0.0075
t_2, in	0.006	0.1515	0.6	0.0088	0.0075
t_3, in	0.006	0.1515	0.6	0.0270	0.03
t_4, in	0.006	0.1515	0.6	0.0060	0.0075
t_5, in	0.006	0.1515	0.6	0.0067	0.0075
t_6, in	0.006	0.1515	0.6	0.0110	0.0150
t_7, in	0.006	0.1515	0.6	0.0060	0.0075
t_8, in	0.006	0.1515	0.6	0.0060	0.0075
θ_1°	-90	0.0	90	-0.7166	0
θ_2°	-90	45.0	90	-0.0987	0
θ_3°	-90	-45.0	90	-90.0000	-90
θ_4°	-90	90.0	90	-0.0987	0
θ_5°	-90	90.0	90	-0.0987	0
θ_6°	-90	-45.0	90	-90.0000	-90
θ_7°	-90	45.0	90	-0.0987	0
θ_8°	-90	0.0	90	-0.5589	0
h_c, in	0.1	1.275	5.0	1.8558	1.9
S, in	0.0625	1.265	2.0	0.0625	0.06
t_c, in	0.0007	0.00535	0.01	0.0094	0.01
Weight, lb	4.048	101	400.4	12.6700	14.23
f_{22}	25	302.99	1175	78.7584	86.8100

Note: CNF-enhanced carbon-vinyl ester sandwich plate with $a = 24, b = 12\ in$ and $N_y = -3.6 \times 10^6\ lb$

Table 5.12 Comparison of initial and optimum designs for $a/b = 2$ and N_{xy}

Design Variables	Lower Bound	Initial Design	Upper Bound	Optimum Design	Optimum Simplified
V_{CNF}	0.0	0.01	0.03	0.001	0.001
V_f	0.25	0.25	0.75	0.25	0.25
t_1, in	0.006	0.1515	0.6	0.0060	0.0075
t_2, in	0.006	0.1515	0.6	0.0060	0.0075
t_3, in	0.006	0.1515	0.6	0.0164	0.0150
t_4, in	0.006	0.1515	0.6	0.0060	0.0075
t_5, in	0.006	0.1515	0.6	0.0060	0.0075
t_6, in	0.006	0.1515	0.6	0.0125	0.0150
t_7, in	0.006	0.1515	0.6	0.0060	0.0075
t_8, in	0.006	0.1515	0.6	0.0060	0.0075
$\theta_1 {}^\circ$	-90	0.0	90	0.0000	0
$\theta_2 {}^\circ$	-90	45.0	90	-0.0200	0
$\theta_3 {}^\circ$	-90	-45.0	90	-90.0000	-90
$\theta_4 {}^\circ$	-90	90.0	90	-0.0200	0
$\theta_5 {}^\circ$	-90	90.0	90	-0.0200	0
$\theta_6 {}^\circ$	-90	-45.0	90	-90.0000	-90
$\theta_7 {}^\circ$	-90	45.0	90	-0.0200	0
$\theta_8 {}^\circ$	-90	0.0	90	0.0000	0
h_c, in	0.1	1.275	5.0	1.1509	1.2
S, in	0.0625	1.265	2.0	0.0625	0.06
t_c, in	0.0007	0.00535	0.01	0.0100	0.01
Weight, lb	4.048	101	400.4	9.4830	10.49
f_{22}	25	302.99	1175	62.7717	67.8710

Note: CNF-enhanced carbon-vinyl ester sandwich plate with $a = 24, b = 12\ in$ and $N_{xy} = 3.6 \times 10^6\ lb$

Table 5.13 Comparison of initial and optimum designs for $a/b = 2$ and N_x, N_y

Design Variables	Lower Bound	Initial Design	Upper Bound	Optimum Design	Optimum Simplified
V_{CNF}	0.0	0.01	0.03	0.001	0.001
V_f	0.25	0.25	0.75	0.25	0.25
t_1, in	0.006	0.1515	0.6	0.0086	0.0075
t_2, in	0.006	0.1515	0.6	0.0086	0.0075
t_3, in	0.006	0.1515	0.6	0.0300	0.03
t_4, in	0.006	0.1515	0.6	0.0086	0.0075
t_5, in	0.006	0.1515	0.6	0.0079	0.0075
t_6, in	0.006	0.1515	0.6	0.0077	0.0075
t_7, in	0.006	0.1515	0.6	0.0060	0.0075
t_8, in	0.006	0.1515	0.6	0.0060	0.0075
θ_1°	-90	0.0	90	-0.0938	0
θ_2°	-90	45.0	90	-0.0750	0
θ_3°	-90	-45.0	90	-90.0000	-90
θ_4°	-90	90.0	90	-0.0750	0
θ_5°	-90	90.0	90	-0.0750	0
θ_6°	-90	-45.0	90	-90.0000	-90
θ_7°	-90	45.0	90	-0.0750	0
θ_8°	-90	0.0	90	-0.0938	0
h_c, in	0.1	1.275	5.0	2.4501	2.5
S, in	0.0625	1.265	2.0	0.0625	0.06
t_c, in	0.0007	0.00535	0.01	0.0100	0.01
Weight, lb	4.048	101	400.4	15.6400	15.75
f_{22}	25	302.99	1175	93.9502	94.5071

Note: CNF-enhanced carbon-vinyl ester sandwich plate with $a = 24, b = 12\ in$ and $N_x = -1.8 \times 10^6\ lb, N_y = -3.6 \times 10^6\ lb$

Table 5.14 Comparison of initial and optimum designs for $a/b = 2$ and N_x, N_y, N_{xy}

Design Variables	Lower Bound	Initial Design	Upper Bound	Optimum Design	Optimum Simplified
V_{CNF}	0.0	0.01	0.03	0.001	0.001
V_f	0.25	0.25	0.75	0.25	0.25
t_1, in	0.006	0.1515	0.6	0.0201	0.0225
t_2, in	0.006	0.1515	0.6	0.0063	0.0075
t_3, in	0.006	0.1515	0.6	0.0336	0.03
t_4, in	0.006	0.1515	0.6	0.0070	0.0075
t_5, in	0.006	0.1515	0.6	0.0070	0.0075
t_6, in	0.006	0.1515	0.6	0.0124	0.0150
t_7, in	0.006	0.1515	0.6	0.0219	0.0225
t_8, in	0.006	0.1515	0.6	0.0114	0.0150
θ_1 °	-90	0.0	90	-0.0841	0
θ_2 °	-90	45.0	90	0.9116	0
θ_3 °	-90	-45.0	90	-88.1505	-90
θ_4 °	-90	90.0	90	81.6309	81
θ_5 °	-90	90.0	90	81.6309	81
θ_6 °	-90	-45.0	90	-85.6879	-85
θ_7 °	-90	45.0	90	-0.0741	0
θ_8 °	-90	0.0	90	-0.0841	0
h_c, in	0.1	1.275	5.0	2.7668	2.8
S, in	0.0625	1.265	2.0	0.0625	0.06
t_c, in	0.0007	0.00535	0.01	0.0100	0.01
Weight, lb	4.048	101	400.4	19.7900	20.55
f_{22}	25	302.99	1175	114.9654	118.8139

Note: CNF-enhanced carbon-vinyl ester sandwich plate with $a = 24, b = 12\ in$ and $N_x = -1.8 \times 10^6\ lb, N_y = -N_{xy} = -3.6 \times 10^6\ lb$

Table 5.15 Comparison of initial and optimum designs for $a/b = 5$ and N_x

Design Variables	Lower Bound	Initial Design	Upper Bound	Optimum Design	Optimum Simplified
V_{CNF}	0.0	0.01	0.03	0.001	0.001
V_f	0.25	0.25	0.75	0.25	0.25
t_1, in	0.006	0.1515	0.6	0.0060	0.0075
t_2, in	0.006	0.1515	0.6	0.0060	0.0075
t_3, in	0.006	0.1515	0.6	0.0060	0.0075
t_4, in	0.006	0.1515	0.6	0.0060	0.0075
t_5, in	0.006	0.1515	0.6	0.0060	0.0075
t_6, in	0.006	0.1515	0.6	0.0226	0.0225
t_7, in	0.006	0.1515	0.6	0.0060	0.0075
t_8, in	0.006	0.1515	0.6	0.0060	0.0075
θ_1°	-90	0.0	90	-0.3098	0
θ_2°	-90	45.0	90	-0.0564	0
θ_3°	-90	-45.0	90	-90.0000	-90
θ_4°	-90	90.0	90	-0.0450	0
θ_5°	-90	90.0	90	-0.1163	0
θ_6°	-90	-45.0	90	-90.0000	-90
θ_7°	-90	45.0	90	-0.0362	0
θ_8°	-90	0.0	90	-2.1642	0
h_c, in	0.1	1.275	5.0	1.0097	1.0
S, in	0.0625	1.265	2.0	0.0625	0.06
t_c, in	0.0007	0.00535	0.01	0.0089	0.01
Weight, lb	4.048	101	400.4	21.4100	24.46
f_{22}	25	302.99	1175	123.1689	138.6138

Note: CNF-enhanced carbon-vinyl ester sandwich plate with $a = 60, b = 12\ in$ and $N_x = -1.8 \times 10^6\ lb$

Table 5.16 Comparison of initial and optimum designs for $a/b = 5$ and N_y

Design Variables	Lower Bound	Initial Design	Upper Bound	Optimum Design	Optimum Simplified
V_{CNF}	0.0	0.01	0.03	0.001	0.001
V_f	0.25	0.25	0.75	0.25	0.25
t_1, in	0.006	0.1515	0.6	0.0121	0.0150
t_2, in	0.006	0.1515	0.6	0.0069	0.0075
t_3, in	0.006	0.1515	0.6	0.0290	0.03
t_4, in	0.006	0.1515	0.6	0.0060	0.0075
t_5, in	0.006	0.1515	0.6	0.0071	0.0075
t_6, in	0.006	0.1515	0.6	0.0180	0.0150
t_7, in	0.006	0.1515	0.6	0.0060	0.0075
t_8, in	0.006	0.1515	0.6	0.0082	0.0075
$\theta_1{}^\circ$	-90	0.0	90	-0.6566	0
$\theta_2{}^\circ$	-90	45.0	90	-0.0556	0
$\theta_3{}^\circ$	-90	-45.0	90	-90.0000	-90
$\theta_4{}^\circ$	-90	90.0	90	-0.0756	0
$\theta_5{}^\circ$	-90	90.0	90	-0.0756	0
$\theta_6{}^\circ$	-90	-45.0	90	-90.0000	-90
$\theta_7{}^\circ$	-90	45.0	90	5.2195	5
$\theta_8{}^\circ$	-90	0.0	90	-0.2434	0
h_c, in	0.1	1.275	5.0	2.5255	2.5
S, in	0.0625	1.265	2.0	0.3256	0.33
t_c, in	0.0007	0.00535	0.01	0.0098	0.01
Weight, lb	4.048	101	400.4	35.8800	36.74
f_{22}	25	302.99	1175	196.4436	200.7985

Note: CNF-enhanced carbon-vinyl ester sandwich plate with $a = 60, b = 12\ in$ and $N_y = -9.0 \times 10^6\ lb$

Table 5.17 Comparison of initial and optimum designs for $a/b = 5$ and N_{xy}

Design Variables	Lower Bound	Initial Design	Upper Bound	Optimum Design	Optimum Simplified
V_{CNF}	0.0	0.01	0.03	0.001	0.001
V_f	0.25	0.25	0.75	0.25	0.25
t_1, in	0.006	0.1515	0.6	0.0060	0.0075
t_2, in	0.006	0.1515	0.6	0.0060	0.0075
t_3, in	0.006	0.1515	0.6	0.0168	0.0150
t_4, in	0.006	0.1515	0.6	0.0060	0.0075
t_5, in	0.006	0.1515	0.6	0.0060	0.0075
t_6, in	0.006	0.1515	0.6	0.0096	0.0075
t_7, in	0.006	0.1515	0.6	0.0060	0.0075
t_8, in	0.006	0.1515	0.6	0.0060	0.0075
$\theta_1{}^\circ$	-90	0.0	90	-2.3040	0
$\theta_2{}^\circ$	-90	45.0	90	-0.1600	0
$\theta_3{}^\circ$	-90	-45.0	90	-90.0000	-90
$\theta_4{}^\circ$	-90	90.0	90	-0.1600	0
$\theta_5{}^\circ$	-90	90.0	90	-0.1600	0
$\theta_6{}^\circ$	-90	-45.0	90	-90.0000	-90
$\theta_7{}^\circ$	-90	45.0	90	-0.1600	0
$\theta_8{}^\circ$	-90	0.0	90	-2.3040	0
h_c, in	0.1	1.275	5.0	1.0187	1.0
S, in	0.0625	1.265	2.0	0.0625	0.06
t_c, in	0.0007	0.00535	0.01	0.0100	0.01
Weight, lb	4.048	101	400.4	22.0200	22.9
f_{22}	25	302.99	1175	126.2579	130.7141

Note: CNF-enhanced carbon-vinyl ester sandwich plate with $a = 60, b = 12\ in$ and $N_{xy} = 9.0 \times 10^6\ lb$

Table 5.18 Comparison of initial and optimum designs for $a/b = 5$ and N_x, N_y

Design Variables	Lower Bound	Initial Design	Upper Bound	Optimum Design	Optimum Simplified
V_{CNF}	0.0	0.01	0.03	0.001	0.001
V_f	0.25	0.25	0.75	0.25	0.25
t_1, in	0.006	0.1515	0.6	0.0071	0.0075
t_2, in	0.006	0.1515	0.6	0.0071	0.0075
t_3, in	0.006	0.1515	0.6	0.0362	0.03
t_4, in	0.006	0.1515	0.6	0.0067	0.0075
t_5, in	0.006	0.1515	0.6	0.0067	0.0075
t_6, in	0.006	0.1515	0.6	0.0066	0.0075
t_7, in	0.006	0.1515	0.6	0.0066	0.0075
t_8, in	0.006	0.1515	0.6	0.0067	0.0075
$\theta_1{}^\circ$	-90	0.0	90	-0.0312	0
$\theta_2{}^\circ$	-90	45.0	90	-0.3375	0
$\theta_3{}^\circ$	-90	-45.0	90	-90.0000	-90
$\theta_4{}^\circ$	-90	90.0	90	-0.3375	0
$\theta_5{}^\circ$	-90	90.0	90	-0.3375	0
$\theta_6{}^\circ$	-90	-45.0	90	-90.0000	-90
$\theta_7{}^\circ$	-90	45.0	90	-0.3375	0
$\theta_8{}^\circ$	-90	0.0	90	-0.4081	0
h_c, in	0.1	1.275	5.0	2.4992	2.5
S, in	0.0625	1.265	2.0	0.0625	0.06
t_c, in	0.0007	0.00535	0.01	0.0100	0.01
Weight, lb	4.048	101	400.4	39.6400	39.37
f_{22}	25	302.99	1175	215.4839	214.1166

Note: CNF-enhanced carbon-vinyl ester sandwich plate with $a = 60, b = 12\ in$ and $N_x = -1.8 \times 10^6\ lb, N_y = -9.0 \times 10^6\ lb$

Table 5.19 Comparison of initial and optimum designs for $a/b = 5$ and N_x, N_y, N_{xy}

Design Variables	Lower Bound	Initial Design	Upper Bound	Optimum Design	Optimum Simplified
V_{CNF}	0.0	0.01	0.03	0.001	0.001
V_f	0.25	0.25	0.75	0.25	0.25
t_1, in	0.006	0.1515	0.6	0.0061	0.0075
t_2, in	0.006	0.1515	0.6	0.0060	0.0075
t_3, in	0.006	0.1515	0.6	0.0311	0.03
t_4, in	0.006	0.1515	0.6	0.0060	0.0075
t_5, in	0.006	0.1515	0.6	0.0100	0.0075
t_6, in	0.006	0.1515	0.6	0.0148	0.0150
t_7, in	0.006	0.1515	0.6	0.0061	0.0075
t_8, in	0.006	0.1515	0.6	0.0060	0.0075
$\theta_1{}^\circ$	-90	0.0	90	-0.8977	0
$\theta_2{}^\circ$	-90	45.0	90	0.0675	0
$\theta_3{}^\circ$	-90	-45.0	90	-90.0000	-90
$\theta_4{}^\circ$	-90	90.0	90	-0.0803	0
$\theta_5{}^\circ$	-90	90.0	90	-0.0675	0
$\theta_6{}^\circ$	-90	-45.0	90	-89.7750	-90
$\theta_7{}^\circ$	-90	45.0	90	-0.0675	0
$\theta_8{}^\circ$	-90	0.0	90	-0.8977	0
h_c, in	0.1	1.275	5.0	2.5031	2.5
S, in	0.0625	1.265	2.0	0.0625	0.06
t_c, in	0.0007	0.00535	0.01	0.0100	0.01
Weight, lb	4.048	101	400.4	40.1500	40.92
f_{22}	25	302.99	1175	218.0660	221.9657

Note: CNF-enhanced carbon-vinyl ester sandwich plate with $a = 60, b = 12\ in$ and $N_x = -1.8 \times 10^6\ lb, N_y = -N_{xy} = -9.0 \times 10^6\ lb$

The results in Tables 5.10 through 5.14 are for a rectangular sandwich plate with dimension in the x direction being twice as long as that in the y direction ($^{a}/_{b} = 2$). The plates are subject to single and combined loading conditions similar to those in Tables 5.5 through 5.9.

In Table 5.10, the ply pattern consists 0 and 90 degree angles. Similar to the sandwich plate in Table 5.5, the plate has roughly a one-inch core with the core cell size at its lower bound.

The ply pattern in Table 5.11 is similar to that in Table 5.6 with layers consisting of 0 and 90 degree angles. As in the case of the square sandwich plate, the change in the loading axis increases the core as well as the honeycomb foil thickness. The overall plate weight in Table 5.11 is about 67% higher than that in Table 5.10, mainly because of thicker core and face sheets. This change in weight is due to different transverse shear stiffness of the core in the x and y directions, which is more obvious in the sandwich plate with higher aspect ratio.

With the exception of one layer in the 8-ply sub-stack, the others are at or near the lower bound thickness for the pure shear case in Table 5.12. The plate weighs about same weight that in Table 5.10. As was the case for the square sandwich plates, the optimum weight for the rectangular plates depends on the loading direction.

As in the previous three cases, the CNF and carbon fiber volume fractions for the rectangular sandwich plates (Tables 5.10 through 5.14) are at their respective lower bounds.

In all of the deterministic multilevel optimization example problems, convergence was reached in approximately 6 CPU hours with the number of inner and outer loops varying slightly from one case to another. The most expensive part of the solution is the micro-level analysis because of consideration of randomly oriented CNFs and the micromechanics approach used. Changes in the weight factors in f_{22} had an impact on the optimization results. The optimum ply angles in the face sheets generally varied between 0 and 90 degrees, with generally more zero than ninety-degree plies. In nearly all the cases, the constraints for global buckling/shear crimping and face sheet wrinkling are active within tolerance 0.001.

In summary, the analytical target cascading with exponential method of multipliers has been adopted to solve two analytical problems and material-product system. The material-product system was decomposed into a three-level hierarchy. In this study, pre-developed simulations and analysis models is used to determine CNF material properties, stiffness matrices (A, B, D) for sandwich plates and face sheets, and various failure modes consist of global buckling (g_{cr}), shear crimping (g_{sc}), intracell buckling (g_{ib}), and face sheet wrinkling (g_w). Thus, sandwich plate design objectives are transformed into individual system design specifications. It is shown that each subsystem with different expertise can work independently to design and optimize the system using appropriate optimization algorithm (possibly similar) for each problem. It can be concluded that the main outcome of the exponential method of multipliers in analytical target cascading framework could be reduction in computational cost by decreasing the number of function calls for the most computationally expensive analysis model.

CHAPTER VI

MULTILEVEL OPTIMIZATION OF NANO-ENHANCED COMPOSITE SANDWICH PLATES UNDER UNCERTAINTY

Uncertainty modeling and reliability analysis

The composite sandwich plate problem presented in Chapter 5 is studied for uncertainty analysis and RBDO. The aleatory uncertainties that exist in the material properties, geometry, and loading conditions are considered in different levels and propagated to the product design problem at the top level. The random variables in the bottom level are the effective (fully dispersed and distributed) volume fraction of the nanofibers, the aspect ratio of the nanofibers, the thickness and properties of the interphase region surrounding the nanofibers inside the matrix, and the waviness of the nanofibers of long aspect ratio. The objective of this study is to show the extended capabilities of ATC framework developed here in solving non-deterministic multilevel material-product optimization problems. For simplicity of implementation, the volume fraction of the nanofibers in the bottom level and the fiber volume fraction in middle level are treated as random variables with known probability distribution function (PDF).

The first two moments of interrelated targets/responses and linking variables are matched in propagating the uncertainty through different levels of hierarchy. To estimate the mean and standard deviation, an approximate method is used for a general function.

Suppose the performance function Y be a general nonlinear function of the random variables $X_i, i = 1, 2, \dots, n$. Mathematically,

$$Y = f(X_1, X_2, \dots, X_n) \tag{6.1}$$

The mean and standard deviation of Y can be calculated using a first-order Taylor series expansion which linearize the performance function as

$$Y = f(x_1^*, x_2^*, \dots, x_n^*) + \sum_{i=1}^{n} (X_i - x_i^*) \frac{\partial f}{\partial X_i}\bigg|_{(x_1^*, x_2^*, \dots, x_n^*)} \tag{6.2}$$

where the x_i^* values (deterministic values) are "design point values" of the random variables X_i, that is, the values about which the function Y is linearized. The choice of the design point values of the random vector $\{X\}$ is very important in structural reliability analysis. (Nowak and Collins 2000)

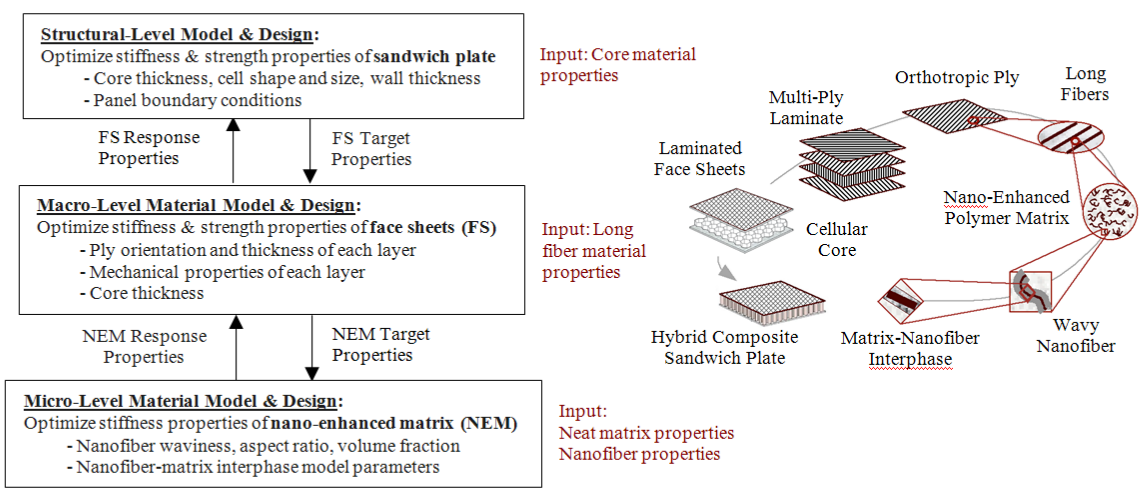

Figure 6.1 Decomposed multilevel hierarchy of the material-product design problem (Courtesy of M. Rais-Rohani)

Three separate computer codes are used in solving the optimization problem in figure 6.1. Besides the micromechanics code developed by Rouhi (2011), a laminate analysis code based on the classical lamination theory will be used to find the effective laminate properties at the middle level and a sandwich analysis code at the top level that is used for evaluating the global buckling and local failure modes associated with thin laminated face sheets and cellular core (Harris 1995). All the analysis codes have been tested individually and are capable of performing the necessary performance analysis. The RBDO formulation SLSV+EPF presented in Chapter 5 is used to solve the probabilistic multilevel optimization problem.

A composite sandwich plate with honeycomb core and laminated face-sheets is to be optimized for minimum weight subject to multiple failure constraints. The hierarchical system with the individual components of the plate structure is shown in figure 6.1.

The problem is decomposed into a material-product design optimization problem. At the bottom level, the modulus of elasticity and Poisson's ratio of the nano-enhanced polymer matrix and associated uncertainties are calculated using the approach developed by Rouhi and Rais-Rohani (2013). The modulus of elasticity and Poisson's ratio are related to volume fraction of nanofibers, elastic modulus of nanofibers, elastic modulus of the interphase at the vicinity of the nanofiber, interphase thickness ratio, as well as the wavelength and amplitude of the wavy nanofibers.

At the middle level, the effective properties of the enhanced matrix are used together with properties of the long fibers to calculate the lamina properties in the principal material directions using the rule of mixtures. Depending on the ply orientation and thickness of the individual layers in the laminate stack, the mechanical properties of the face sheet can be altered.

At the top level, the face sheet properties are combined with those of the core (i.e., cell size, foil thickness, core thickness) to calculate the in-plane properties and weight of the panel. In the system level design optimization problem, the laminate weight is minimized subject to buckling strength and sandwich failure criteria such as face sheet wrinkling, shear crimping and intercell buckling. The necessary stiffness properties of the face sheets are treated as part of the decision variables being optimized with the calculated values sent down to the middle level as response targets. The local design variables at the top level include the geometric properties of the core.

With the face sheet target values specified, the subsystem in the middle searches for the optimum orientation angle and thickness of each ply in the laminated stack. The required values for the effective matrix properties are treated as decision variables. The laminate requirements of product design cascade down from the top level and determine the target for the macro-level material design. Then, requirements for these new targets cascade down to nano-level design to change the nano-enhanced matrix design.

Through an iterative procedure, the capabilities at the lower level are transferred upward while the target values are cascaded downward in repeated solutions of multiple optimization problems. Convergence is reached when the top-level performance targets are met for a minimum-weight sandwich plate.

Uncertainties are introduced at the micro-level and macro-level of the three-level hierarchy. While the objective function in each element of the non-deterministic framework remains the same as that in the deterministic problem shown previously, design variables as well as the target and response variables change as discussed below.

Problem Decomposition

Element 33

$$\min_{\bar{\boldsymbol{x}}_{33}} \quad \left\{\frac{\boldsymbol{\lambda}_{33}}{\boldsymbol{a}_{33}}\left(e^{\boldsymbol{a}_{33}\,(\boldsymbol{t}_{33}-\boldsymbol{r}_{33})}-1\right)+\frac{\boldsymbol{\gamma}_{33}}{\boldsymbol{b}_{33}}\left(e^{\boldsymbol{b}_{33}\,(\boldsymbol{r}_{33}-\boldsymbol{t}_{33})}-1\right)\right\} \tag{6.3}$$

$$s.t. \quad 0 \le x_{33} \le 0.03$$

where

$$\boldsymbol{t}_{33} = \left(\mu_{E_{em}}^{T}, \sigma_{E_{em}}^{T}, \mu_{\nu_{em}}^{T}, \sigma_{\nu_{em}}^{T}\right)$$

$$\boldsymbol{r}_{33} = f_{M-T}(x_{33}) = \left(\mu_{E_{em}}^{R}, \sigma_{E_{em}}^{R}, \mu_{\nu_{em}}^{R}, \sigma_{\nu_{em}}^{R}\right)$$

$$\bar{\boldsymbol{x}}_{33} = (x_{33})$$

$$x_{33} = \mu_{V_{CNF}};\ \sigma_{V_{CNF}} = 0.003$$

Assuming a normal distribution for V_{CNF} and the corresponding responses, chain rule of differentiation is used to estimate the standard deviation of E_{em}, ν_{em} as

$$\sigma_{E_{em}} = \frac{dE_{em}}{dV_{CNF}}\sigma_{V_{CNF}};\ \sigma_{\nu_{em}} = \frac{d\nu_{em}}{dV_{CNF}}\sigma_{V_{CNF}} \tag{6.4}$$

Element 22

$$\mathrm{Min}_{\bar{\boldsymbol{x}}_{22}}\, f_{22} + \left\{\frac{\boldsymbol{\lambda}_{22}}{\boldsymbol{a}_{22}}\left(e^{\boldsymbol{a}_{22}\,(\boldsymbol{t}_{22}-\boldsymbol{r}_{22})}-1\right)+\frac{\boldsymbol{\gamma}_{22}}{\boldsymbol{b}_{22}}\left(e^{\boldsymbol{b}_{22}\,(\boldsymbol{r}_{22}-\boldsymbol{t}_{22})}-1\right)\right\} +$$

$$\left\{\frac{\boldsymbol{\lambda}_{33}}{\boldsymbol{a}_{33}}\left(e^{\boldsymbol{a}_{33}\,(\boldsymbol{t}_{33}-\boldsymbol{r}_{33})}-1\right)+\frac{\boldsymbol{\gamma}_{33}}{\boldsymbol{b}_{33}}\left(e^{\boldsymbol{b}_{33}\,(\boldsymbol{r}_{33}-\boldsymbol{t}_{33})}-1\right)\right\} \tag{6.5}$$

$$s.t. \quad 0.25 \le \mu_{V_f} \le 0.75;\ 0.006 \le t_i \le 0.6 \text{ in};$$

$$-90° \leq \theta_i \leq 90°;\ \ 0.1 \leq h_c \leq 5.0 \text{ in}$$

where

$$f_{22} = \left\{w_1\left[\left(\frac{W_{fs}-W_{fs}^{min}}{W_{fs}^{max}-W_{fs}^{min}}\right)\right] + \left[w_2\left(\frac{E_{em}^{T}-E_{em}^{min}}{E_{em}^{max}-E_{em}^{min}}\right) + w_3 V_f\right]\right\}$$

$$\boldsymbol{t}_{22} = \left(\boldsymbol{\mu}_{\boldsymbol{A}}^{\boldsymbol{T}}, \boldsymbol{\mu}_{\boldsymbol{B}}^{\boldsymbol{T}}, \boldsymbol{\mu}_{\boldsymbol{D}}^{\boldsymbol{T}}, \boldsymbol{\sigma}_{\boldsymbol{A}}^{\boldsymbol{T}}, \boldsymbol{\sigma}_{\boldsymbol{B}}^{\boldsymbol{T}}, \boldsymbol{\sigma}_{\boldsymbol{D}}^{\boldsymbol{T}}, t_f^T, h_c^T\right);\ \boldsymbol{r}_{22} = \left(\boldsymbol{\mu}_{\boldsymbol{A}}^{\boldsymbol{R}}, \boldsymbol{\mu}_{\boldsymbol{B}}^{\boldsymbol{R}}, \boldsymbol{\mu}_{\boldsymbol{D}}^{\boldsymbol{R}}, \boldsymbol{\sigma}_{\boldsymbol{A}}^{\boldsymbol{R}}, \boldsymbol{\sigma}_{\boldsymbol{B}}^{\boldsymbol{R}}, \boldsymbol{\sigma}_{\boldsymbol{D}}^{\boldsymbol{R}}, t_f^R, h_c^R\right)$$

$$\boldsymbol{A} = f_A(\boldsymbol{x}_{22}); \boldsymbol{B} = f_B(\boldsymbol{x}_{22}); \boldsymbol{D} = f_D(\boldsymbol{x}_{22}); t_f = 4\sum t_i$$

$$\boldsymbol{t}_{33} = \left(\mu_{E_{em}}^T, \sigma_{E_{em}}^T, \mu_{\nu_{em}}^T, \sigma_{\nu_{em}}^T\right); \boldsymbol{r}_{33} = \left(\mu_{E_{em}}^R, \sigma_{E_{em}}^R, \mu_{\nu_{em}}^R, \sigma_{\nu_{em}}^R\right)$$

$$\boldsymbol{x}_{22} = \left(\mu_{V_f}, t_i, \theta_i\right); \overline{\boldsymbol{x}}_{22} = (h_c^R, \boldsymbol{t}_{33}, \boldsymbol{x}_{22})$$

Assuming normal distribution for V_f, E_{em}, ν_{em} and the corresponding responses with $\sigma_{V_f} = 0.003$ along with following the chain rule estimation of standard deviation gives

$$\mu_{\boldsymbol{A}} = f_A(\boldsymbol{x}_{22}), \mu_{\boldsymbol{B}} = f_B(\boldsymbol{x}_{22}), \mu_{\boldsymbol{D}} = f_D(\boldsymbol{x}_{22}) \tag{6.6}$$

$$\sigma_{\boldsymbol{A}} = \sqrt{\left(\frac{\partial A}{\partial V_f}\sigma_{V_f}\right)^2 + \left(\frac{\partial A}{\partial E_{em}}\sigma_{E_{em}}\right)^2 + \left(\frac{\partial A}{\partial \nu_{em}}\sigma_{\nu_{em}}\right)^2} \tag{6.7}$$

$$\sigma_{\boldsymbol{B}} = \sqrt{\left(\frac{\partial B}{\partial V_f}\sigma_{V_f}\right)^2 + \left(\frac{\partial B}{\partial E_{em}}\sigma_{E_{em}}\right)^2 + \left(\frac{\partial B}{\partial \nu_{em}}\sigma_{\nu_{em}}\right)^2} \tag{6.8}$$

$$\sigma_{\boldsymbol{D}} = \sqrt{\left(\frac{\partial D}{\partial V_f}\sigma_{V_f}\right)^2 + \left(\frac{\partial D}{\partial E_{em}}\sigma_{E_{em}}\right)^2 + \left(\frac{\partial D}{\partial \nu_{em}}\sigma_{\nu_{em}}\right)^2} \tag{6.9}$$

Element 11

$$\min_{\bar{x}_{11}} \quad f_{11} + \left\{ \frac{\boldsymbol{\lambda}_{22}}{\boldsymbol{a}_{22}} \left(e^{\boldsymbol{a}_{22}\,(\boldsymbol{t}_{22} - \boldsymbol{r}_{22})} - 1 \right) + \frac{\boldsymbol{\gamma}_{22}}{\boldsymbol{b}_{22}} \left(e^{\boldsymbol{b}_{22}\,(\boldsymbol{r}_{22} - \boldsymbol{t}_{22})} - 1 \right) \right\} \tag{6.10}$$

$$s.t. \quad Pr(g_{cr} \geq 0) \geq \Phi(\beta);\ Pr(g_{sc} \geq 0) \geq \Phi(\beta);$$

$$Pr(g_{ib} \geq 0) \geq \Phi(\beta); Pr(g_w \geq 0) \geq \Phi(\beta);$$

$$0.0625 \leq S \leq 2.0 \text{ in};\ 0.0007 \leq t_c \leq 0.01 \text{ in}$$

where,

$$f_{11} = W_{SP}$$

$$\boldsymbol{t}_{22} = \left(\boldsymbol{\mu_A^T}, \boldsymbol{\mu_B^T}, \boldsymbol{\mu_D^T}, \boldsymbol{\sigma_A^T}, \boldsymbol{\sigma_B^T}, \boldsymbol{\sigma_D^T}, t_f^T, h_c^T, t_f^T, h_c^T \right); \boldsymbol{r}_{22} = \left(\boldsymbol{\mu_A^R}, \boldsymbol{\mu_B^R}, \boldsymbol{\mu_D^R}, \boldsymbol{\sigma_A^R}, \boldsymbol{\sigma_B^R}, \boldsymbol{\sigma_D^R}, t_f^R, h_c^R \right)$$

$$\boldsymbol{x}_{11} = (S, t_c);\ \bar{\boldsymbol{x}}_{11} = (\boldsymbol{t}_{22}, \boldsymbol{x}_{11})$$

The target reliability index used in this problem is β= 3.0 corresponding to reliability of 0.99865.

Table 6.1 gives the optimum design for a square sandwich plate under axial compression in the x direction with the weight factors being $w_1 = 1000, w_2 = w_3 = 100$. With focus on the uncertainty associated with the CNF and the continuous fiber volume fractions, the difference between the results in Table 6.1 and those in Table 5.6 is fairly modest. Although the computational design tool developed can accommodate a much larger set of uncertain variables, for the demonstration purposes, the number was kept low to reduce the computational cost. While a deterministic multilevel material-product design optimization problem takes approximately 6 CPU hours to solve, the non-deterministic counterpart considered here takes approximately 10 CPU hours on the same computer.

The results in Table 6.2 are for the square sandwich plate under axial compression in the y direction. As was seen in the deterministic case, the overall plate weight increases compared to the axial compression in the x direction. A similar trend is also seen in Table 6.3 for the pure shear loading case.

The results in Table 6.4 through 6.6 repeat those in Tables 6.1 through 6.3 for a rectangular plate. A similar trend as in the case of deterministic designs is observed with the heaviest plate being the one under axial compression in the y direction.

The results in Table 6.7 are for a bi-axial compression with the weight factors being different from those of the other cases. These results are the non-deterministic counterpart of those shown in Table 5.3. Again, a limited difference is found due to the modest effect of uncertainty in the volume fractions of the CNF and the continuous carbon fibers.

Table 6.1 Non-deterministic optimum designs for $a/b = 1$ and N_x

Design Variables	Lower Bound	Initial Design	Upper Bound	Optimum Design	CV 10%
$\mu_{V_{CNF}}$	0.0	0.01	0.03	0.0001	0.0001
μ_{V_f}	0.25	0.25	0.75	0.25	0.25
t_1, in	0.006	0.1515	0.6	0.0060	0.0145
t_2, in	0.006	0.1515	0.6	0.0070	0.0122
t_3, in	0.006	0.1515	0.6	0.0086	0.0067
t_4, in	0.006	0.1515	0.6	0.0082	0.0095
t_5, in	0.006	0.1515	0.6	0.0163	0.0076
t_6, in	0.006	0.1515	0.6	0.0060	0.0072
t_7, in	0.006	0.1515	0.6	0.0075	0.0067
t_7, in	0.006	0.1515	0.6	0.0060	0.0065
$\theta_1{}^\circ$	-90	0.0	90	-1.4140	-0.0700
$\theta_2{}^\circ$	-90	45.0	90	89.0443	89.4384
$\theta_3{}^\circ$	-90	-45.0	90	-90.0000	-88.8750
$\theta_4{}^\circ$	-90	90.0	90	-0.0654	-0.0806
$\theta_5{}^\circ$	-90	90.0	90	-0.0162	-0.0806
$\theta_6{}^\circ$	-90	-45.0	90	-90.0000	-88.8750
$\theta_7{}^\circ$	-90	45.0	90	89.0443	89.4384
$\theta_8{}^\circ$	-90	0.0	90	-2.1974	-1.5999
h_c, in	0.1	1.275	5.0	1.0564	1.0547
S, in	0.0625	1.265	2.5	0.0625	0.0625
t_c, in	0.0007	0.00535	0.01	0.0092	0.0094
Weight, lb	2.024	50.5	200.2	4.4440	4.7110
f_{22}	0.25	244.89	1000.85	37.2547	38.6067

Note: CNF-enhanced carbon-vinyl ester sandwich plate with $a = b = 12\ in$ and $N_x = -1.8 \times 10^6\ lb$, $f_{22} = \left\{1000\left[\left(\frac{W_{fs}-W_{fs}^{min}}{W_{fs}^{max}-W_{fs}^{min}}\right)\right] + \left[100\left(\frac{E_{em}^{T}-E_{em}^{min}}{E_{em}^{max}-E_{em}^{min}}\right) + 100\ V_f\right]\right\}$

Table 6.2 Non-deterministic optimum designs for $a/b = 1$ and N_y

Design Variables	Lower Bound	Initial Design	Upper Bound	Optimum Design	Optimum Simplified
$\mu_{V_{CNF}}$	0.0	0.01	0.03	0.0001	0.0001
μ_{V_f}	0.25	0.25	0.75	0.25	0.25
t_1, in	0.006	0.1515	0.6	0.0140	0.0150
t_2, in	0.006	0.1515	0.6	0.0075	0.0075
t_3, in	0.006	0.1515	0.6	0.0147	0.0150
t_4, in	0.006	0.1515	0.6	0.0068	0.0075
t_5, in	0.006	0.1515	0.6	0.0065	0.0075
t_6, in	0.006	0.1515	0.6	0.0075	0.0075
t_7, in	0.006	0.1515	0.6	0.0071	0.0075
t_7, in	0.006	0.1515	0.6	0.0074	0.0075
$\theta_1{}^\circ$	-90	0.0	90	-0.5475	0.0
$\theta_2{}^\circ$	-90	45.0	90	87.5392	0.0
$\theta_3{}^\circ$	-90	-45.0	90	-88.4731	90.0
$\theta_4{}^\circ$	-90	90.0	90	0.0121	0.0
$\theta_5{}^\circ$	-90	90.0	90	1.4716	0.0
$\theta_6{}^\circ$	-90	-45.0	90	-88.4731	90.0
$\theta_7{}^\circ$	-90	45.0	90	87.5392	0.0
$\theta_8{}^\circ$	-90	0.0	90	-0.4596	0.0
h_c, in	0.1	1.275	5.0	1.5988	1.60
S, in	0.0625	1.265	2.5	0.0625	0.06
t_c, in	0.0007	0.00535	0.01	0.01	0.01
Weight, lb	2.024	50.5	200.2	5.82	5.96
f_{22}	0.25	244.89	1000.85	44.20	45.19

Note: CNF-enhanced carbon-vinyl ester sandwich plate with $a = b = 12\ in$ and $N_y = -1.8 \times 10^6\ lb$, $f_{22} = \left\{1000\left[\left(\frac{W_{fs}-W_{fs}^{min}}{W_{fs}^{max}-W_{fs}^{min}}\right)\right] + \left[100\left(\frac{E_{em}^{T}-E_{em}^{min}}{E_{em}^{max}-E_{em}^{min}}\right) + 100\ V_f\right]\right\}$

Table 6.3 Non-deterministic optimum designs for $a/b = 1$ and N_{xy}

Design Variables	Lower Bound	Initial Design	Upper Bound	Optimum Design	Optimum Simplified
$\mu_{V_{CNF}}$	0.0	0.01	0.03	0.0001	0.0001
μ_{V_f}	0.25	0.25	0.75	0.25	0.25
t_1, in	0.006	0.1515	0.6	0.0061	0.0075
t_2, in	0.006	0.1515	0.6	0.0102	0.0150
t_3, in	0.006	0.1515	0.6	0.0060	0.0075
t_4, in	0.006	0.1515	0.6	0.0129	0.0150
t_5, in	0.006	0.1515	0.6	0.0060	0.0075
t_6, in	0.006	0.1515	0.6	0.0060	0.0075
t_7, in	0.006	0.1515	0.6	0.0091	0.0150
t_7, in	0.006	0.1515	0.6	0.0060	0.0075
$\theta_1{}^\circ$	-90	0.0	90	-0.1142	0.0
$\theta_2{}^\circ$	-90	45.0	90	90.0	90
$\theta_3{}^\circ$	-90	-45.0	90	-90.0	90
$\theta_4{}^\circ$	-90	90.0	90	0.1066	0.0
$\theta_5{}^\circ$	-90	90.0	90	2.0325	0.0
$\theta_6{}^\circ$	-90	-45.0	90	-90.0	90
$\theta_7{}^\circ$	-90	45.0	90	90.0	90
$\theta_8{}^\circ$	-90	0.0	90	-0.056	0.0
h_c, in	0.1	1.275	5.0	1.0538	1.00
S, in	0.0625	1.265	2.5	0.0625	0.06
t_c, in	0.0007	0.00535	0.01	0.01	0.01
Weight, lb	2.024	50.5	200.2	4.46	5.2
f_{22}	0.25	244.89	1000.85	37.34	41.36

Note: CNF-enhanced carbon-vinyl ester sandwich plate with $a = b = 12\ in$ and $N_{xy} = 1.8 \times 10^6\ lb$, $f_{22} = \left\{1000\left[\left(\frac{W_{fs}-W_{fs}^{min}}{W_{fs}^{max}-W_{fs}^{min}}\right)\right] + \left[100\left(\frac{E_{em}^{T}-E_{em}^{min}}{E_{em}^{max}-E_{em}^{min}}\right) + 100\ V_f\right]\right\}$

Table 6.4 Non-deterministic optimum designs for $a/b = 2$ and N_x

Design Variables	Lower Bound	Initial Design	Upper Bound	Optimum Design	Optimum Simplified
$\mu_{V_{CNF}}$	0.0	0.01	0.03	0.0001	0.0001
μ_{V_f}	0.25	0.25	0.75	0.25	0.25
t_1, in	0.006	0.1515	0.6	0.0060	0.0075
t_2, in	0.006	0.1515	0.6	0.0060	0.0075
t_3, in	0.006	0.1515	0.6	0.0121	0.0150
t_4, in	0.006	0.1515	0.6	0.0060	0.0075
t_5, in	0.006	0.1515	0.6	0.0060	0.0075
t_6, in	0.006	0.1515	0.6	0.0064	0.0075
t_7, in	0.006	0.1515	0.6	0.0060	0.0075
t_7, in	0.006	0.1515	0.6	0.0060	0.0075
$\theta_1{}^\circ$	-90	0.0	90	-1.3544	0.0
$\theta_2{}^\circ$	-90	45.0	90	-1.4278	0.0
$\theta_3{}^\circ$	-90	-45.0	90	-0.4092	0.0
$\theta_4{}^\circ$	-90	90.0	90	-0.6561	0.0
$\theta_5{}^\circ$	-90	90.0	90	-1.1547	0.0
$\theta_6{}^\circ$	-90	-45.0	90	-0.6169	0.0
$\theta_7{}^\circ$	-90	45.0	90	-1.1547	0.0
$\theta_8{}^\circ$	-90	0.0	90	-1.3077	0.0
h_c, in	0.1	1.275	5.0	1.0256	1.00
S, in	0.0625	1.265	2.5	0.0625	0.06
t_c, in	0.0007	0.00535	0.01	0.0065	0.007
Weight, lb	4.048	101	400.4	6.91	8.09
f_{22}	25	302.99	1175	32.55	35.54

Note: CNF-enhanced carbon-vinyl ester sandwich plate with $a = 12\ in$, $b = 24\ in$, and $N_x = -1.8 \times 10^6\ lb$, $f_{22} = \left\{1000\left[\left(\frac{W_{fs}-W_{fs}^{min}}{W_{fs}^{max}-W_{fs}^{min}}\right)\right] + \left[100\left(\frac{E_{em}^{T}-E_{em}^{min}}{E_{em}^{max}-E_{em}^{min}}\right) + 100\ V_f\right]\right\}$

Table 6.5 Non-deterministic optimum designs for $a/b = 2$ and N_y

Design Variables	Lower Bound	Initial Design	Upper Bound	Optimum Design	Optimum Simplified
$\mu_{V_{CNF}}$	0.0	0.01	0.03	0.0001	0.0001
μ_{V_f}	0.25	0.25	0.75	0.25	0.25
t_1, in	0.006	0.1515	0.6	0.0060	0.0075
t_2, in	0.006	0.1515	0.6	0.0078	0.0075
t_3, in	0.006	0.1515	0.6	0.0063	0.0075
t_4, in	0.006	0.1515	0.6	0.0135	0.0150
t_5, in	0.006	0.1515	0.6	0.0087	0.0150
t_6, in	0.006	0.1515	0.6	0.0060	0.0075
t_7, in	0.006	0.1515	0.6	0.0143	0.0150
t_7, in	0.006	0.1515	0.6	0.0060	0.0075
θ_1°	-90	0.0	90	-1.6680	0.0
θ_2°	-90	45.0	90	88.0587	90
θ_3°	-90	-45.0	90	-89.5392	90
θ_4°	-90	90.0	90	-0.2292	0.0
θ_5°	-90	90.0	90	-0.2795	0.0
θ_6°	-90	-45.0	90	-89.5392	90
θ_7°	-90	45.0	90	89.0587	90
θ_8°	-90	0.0	90	-1.1178	0.0
h_c, in	0.1	1.275	5.0	1.3681	1.40
S, in	0.0625	1.265	2.5	0.0625	0.06
t_c, in	0.0007	0.00535	0.01	0.0097	0.01
Weight, lb	4.048	101	400.4	10.4	11.83
f_{22}	25	302.99	1175	41.36	44.97

Note: CNF-enhanced carbon-vinyl ester sandwich plate with $a = 12\ in$, $b = 24\ in$, and $N_y = -1.8 \times 10^6\ lb$, $f_{22} = \left\{1000\left[\left(\frac{W_{fs}-W_{fs}^{min}}{W_{fs}^{max}-W_{fs}^{min}}\right)\right] + \left[100\left(\frac{E_{em}^{T}-E_{em}^{min}}{E_{em}^{max}-E_{em}^{min}}\right) + 100\ V_f\right]\right\}$

Table 6.6 Non-deterministic optimum designs for $a/b = 2$ and N_{xy}

Design Variables	Lower Bound	Initial Design	Upper Bound	Optimum Design	Optimum Simplified
$\mu_{V_{CNF}}$	0.0	0.01	0.03	0.0001	0.0001
μ_{V_f}	0.25	0.25	0.75	0.25	0.25
t_1, in	0.006	0.1515	0.6	0.0070	0.0075
t_2, in	0.006	0.1515	0.6	0.0060	0.0075
t_3, in	0.006	0.1515	0.6	0.0112	0.0150
t_4, in	0.006	0.1515	0.6	0.0076	0.0075
t_5, in	0.006	0.1515	0.6	0.0070	0.0075
t_6, in	0.006	0.1515	0.6	0.0073	0.0075
t_7, in	0.006	0.1515	0.6	0.0088	0.0150
t_7, in	0.006	0.1515	0.6	0.0061	0.0075
$\theta_1{}^\circ$	-90	0.0	90	-0.7329	0.0
$\theta_2{}^\circ$	-90	45.0	90	-0.8923	0.0
$\theta_3{}^\circ$	-90	-45.0	90	-88.5675	90
$\theta_4{}^\circ$	-90	90.0	90	-0.3229	0.0
$\theta_5{}^\circ$	-90	90.0	90	-0.4969	0.0
$\theta_6{}^\circ$	-90	-45.0	90	-88.5675	90
$\theta_7{}^\circ$	-90	45.0	90	87.1595	90
$\theta_8{}^\circ$	-90	0.0	90	-0.8353	0.0
h_c, in	0.1	1.275	5.0	0.9904	1.00
S, in	0.0625	1.265	2.5	0.0625	0.06
t_c, in	0.0007	0.00535	0.01	0.01	0.01
Weight, lb	4.048	101	400.4	8.59	9.78
f_{22}	25	302.99	1175	36.79	39.80

Note: CNF-enhanced carbon-vinyl ester sandwich plate with $a = 12\ in$, $b = 24\ in$, and $N_{xy} = 1.8 \times 10^6\ lb$, $f_{22} = \left\{1000\left[\left(\frac{W_{fs}-W_{fs}^{min}}{W_{fs}^{max}-W_{fs}^{min}}\right)\right] + \left[100\left(\frac{E_{em}^{T}-E_{em}^{min}}{E_{em}^{max}-E_{em}^{min}}\right) + 100\ V_f\right]\right\}$

Table 6.7 Comparison of initial and non-deterministic optimum designs

Design Variables	Lower Bound	Initial Design	Upper Bound	Optimum Design	Optimum Simplified
$\mu_{V_{CNF}}$	0.0	0.01	0.03	0.0032	0.0032
μ_{V_f}	0.25	0.25	0.75	0.6661	0.70
t_1, in	0.006	0.1515	0.6	0.0115	0.0150
t_2, in	0.006	0.1515	0.6	0.0109	0.0150
t_3, in	0.006	0.1515	0.6	0.0313	0.0300
t_4, in	0.006	0.1515	0.6	0.0061	0.0075
t_5, in	0.006	0.1515	0.6	0.0061	0.0075
t_6, in	0.006	0.1515	0.6	0.0188	0.0225
t_7, in	0.006	0.1515	0.6	0.0111	0.0150
t_7, in	0.006	0.1515	0.6	0.0063	0.0075
$\theta_1{}^\circ$	-90	0.0	90	-0.0739	0.0
$\theta_2{}^\circ$	-90	45.0	90	0.4929	0.0
$\theta_3{}^\circ$	-90	-45.0	90	-90.0	90.0
$\theta_4{}^\circ$	-90	90.0	90	-0.0968	0.0
$\theta_5{}^\circ$	-90	90.0	90	4.1343	0.0
$\theta_6{}^\circ$	-90	-45.0	90	-90.0	90.0
$\theta_7{}^\circ$	-90	45.0	90	0.0828	0.0
$\theta_8{}^\circ$	-90	0.0	90	-0.1199	0.0
h_c, in	0.1	1.275	5.0	3.8863	3.90
S, in	0.0625	1.265	2.5	0.0625	0.06
t_c, in	0.0007	0.00535	0.01	0.01	0.01
Weight, lb	2.024	50.5	200.2	11.16	11.92
f_{22}	0.25	244.89	1000.85	46.94	50.65

Note: CNF-enhanced carbon-vinyl ester sandwich plate with $a = b = 12\ in.$ and $N_x = N_y = -3.1 \times 10^6\ lb$, $f_{22} = \left\{1000\left[\left(\frac{W_{fs}-W_{fs}^{min}}{W_{fs}^{max}-W_{fs}^{min}}\right)\right] + \left[0.1\left(\frac{E_{em}^{T}-E_{em}^{min}}{E_{em}^{max}-E_{em}^{min}}\right) + V_f\right]\right\}$

CHAPTER VII

COMPUTATIONAL FRAMEWORK

A computational framework has been developed to implement the analytical target cascading approach with multiple computer codes working together. The mechanical modeling of nano-enhanced composite materials, failure analysis of composite sandwich plates under in-plane loading conditions, uncertainty propagation, deterministic and nondeterministic design optimization are embedded into the computational framework. The computational framework was used to obtain the results presented in the previous chapters.

All-at-once design optimization strategy

The all-at-once design optimization for product-material system relies on coupled simulations. Since the responses of a simulation analysis serve as input for another simulation, the simulations should be executed in sequence to obtain the final responses that represent the objective and constraints values. Therefore, a set of design variables is provided by the optimization tool as input to the computational framework, and objective and constraints values are determined as output set. Figure 7.1 illustrates the overview of the computational tool.

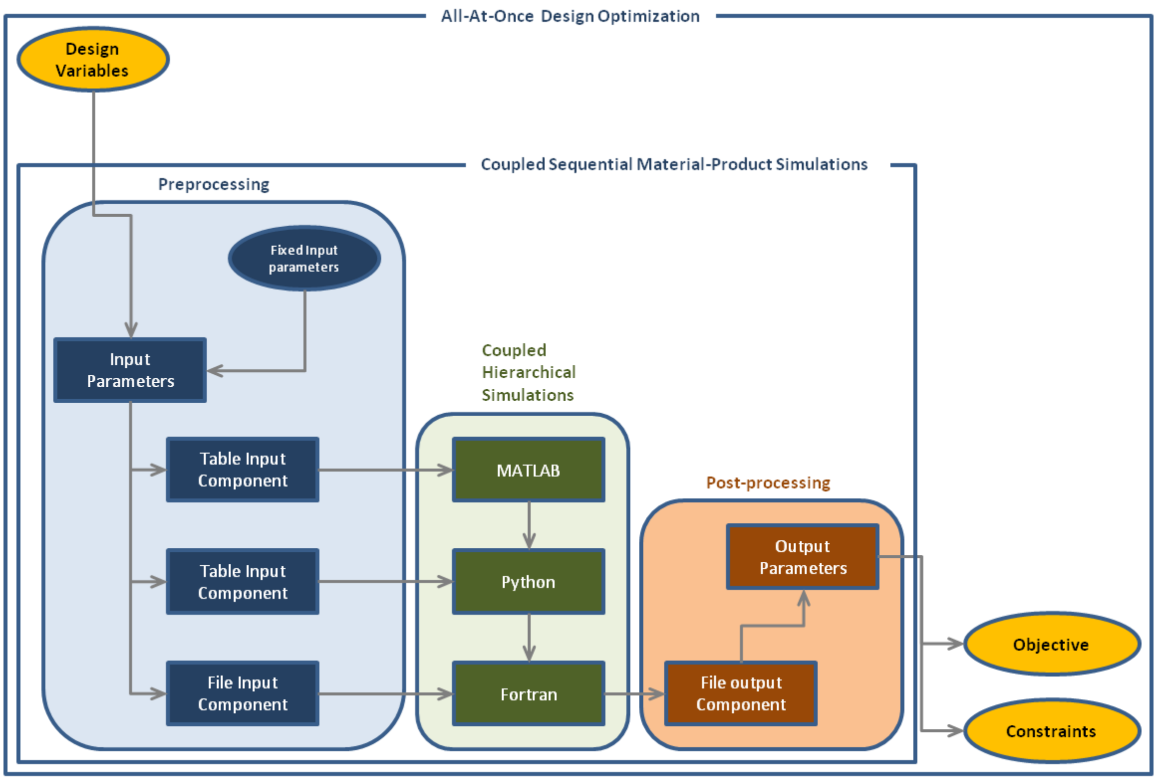

Figure 7.1 Overview of computational design framework for AAO approach

The computational framework is decomposed into three major segments:, preprocessing, simulation, and post-processing. In preprocessing, the input models for each simulation are created using file/table input component. Simulations are based on MATLAB, Python, and Fortran codes that are executed in hierarchical order, and post-processing provides the values of objective and constraint functions for the optimization tool.

Preprocessing

The set of design variables generated by the optimization tool is used to prepare the input models for the simulation and analysis codes. A set of design variables contains twenty-one elements $\{V_{CNF}, V_f, t_i, \theta_i, h_c, S, t_c\}$. V_{CNF} and V_f are the input parameters to MATLAB and Python codes which feed into the corresponding simulations using table input component. $t_i, \theta_i, h_c, S, t_c$ are the design variables related to sandwich plate analysis code written in Fortran. The file input component modifies the comp1.txt, which is one of the input .txt format files for Fortran code based on the input values.

Coupled hierarchical simulations

Once the input models are created, the coupled simulation is executed by starting the Mori-Tanaka method simulation written in MATLAB (Rouhi, 2011). To calculate the elastic properties of the nanofiber-reinforced matrix, the material modeling code is used. The MATLAB code (Mori-Tanaka.m) is developed for the model that does not include an interphase. The properties of the constituent materials such as the neat polymer matrix properties (E_m, ν_m), CNF properties (E_{CNF}, ν_{CNF}), as well as the geometric properties of the nanofiber such as geometric parameters of an ellipsoid representing a CNF (a_1, a_2, a_3), the wavelength of the wavy nanofibers (W_λ), the amplitude of the wavy nanofibers (W_a), the interphase thickness ratio (ITR), and the degradation factor (*n*) (Rouhi et al., 2010, Rouhi 2011), are input parameters to the code to determine Young's modulus (E_{em}) and Poisson's ratio (ν_{em}) of the nano-enhanced matrix as outputs.

After the micro-level material analysis, rule of mixtures analysis model written in Python is performed to find the Young's modulus in the fiber direction, transverse to the fibers, Poisson's ratio, and the transverse Young's modulus. The main purpose of the micro-level material and rule of mixture analysis is to determine the mechanical properties of the nano-enhanced orthotropic ply ($E_1, E_2, G_{12}, \nu_{12}$).

The structural analysis of sandwich plate has two input files in .txt format (material.txt and comp1.txt). Once the material properties are found, the file input component alters the material.txt accordingly. In analysis of composite sandwich plates, numerical techniques are used to determine the dominant modes of instability associated with sandwich plates under in-plane loading. The Classical Lamination Theory (CLT) is used to analyze the anisotropic composite face sheets and the resulting effective properties are used in the calculation of the modes of instability of the sandwich plate. The global buckling instability is calculated using the Rayleigh-Ritz energy method, and the remaining plate instabilities, wrinkling, shear crimping, and intracell buckling, are calculated using closed-form equations. The analysis of composite sandwich plates is applied by a code written in Fortran called structural analysis of sandwich plate code, which uses two input files; the file called "comp1.txt" stores information about the geometry of the sandwich plate including the number of layers, thickness of each layer, orientation of each ply, and core geometries. The second file called "material.txt" contains face sheet and core material properties, boundary conditions, and panel dimension.

Post-processing

In general, extracting the results is performed using VisualScript in post-processing section. The objective and constraint function values are the output required by the optimization tool at each function call.

Analytical Target Cascading Framework

All the individual computer tools used for each element-level analysis were modified to fit the description of the material-product design problem in figure 7.2. The functionality of each tool based on the individual input parameters was tested and verified through solution of a set of example problems. The multilevel computational framework for the sandwich plate design problem was set up and implemented using VisualDOC, a design, optimization, and process integration software. The flow diagram in figure 7.2 provides a general overview of the computational design tool.

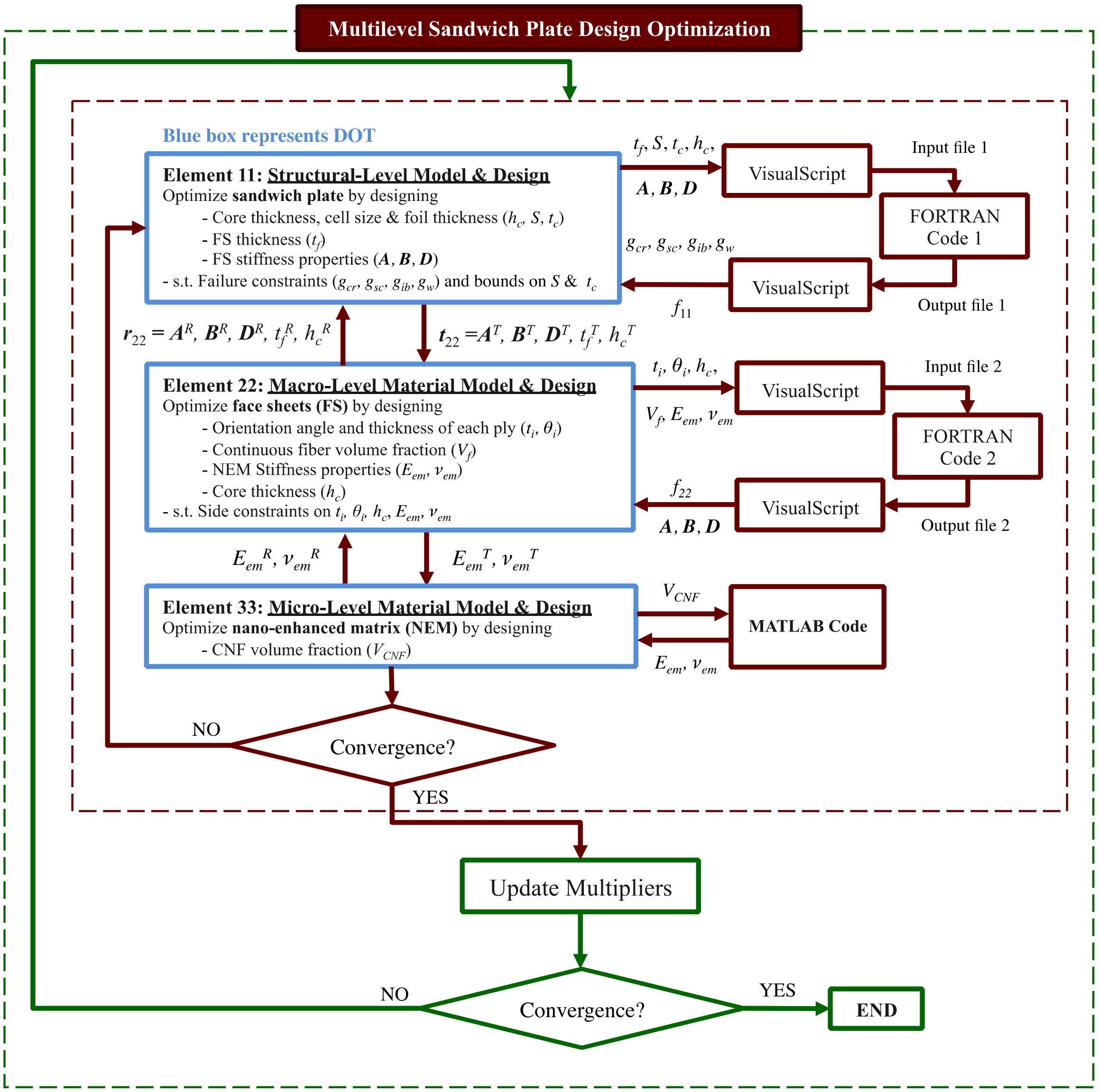

Figure 7.2 Flow diagram for integration of computer programs for multilevel product-material design.

Using the DOT design optimization library inside VisualDOC, we chose the modified method of feasible directions (MMFD) for solution of element 11 and sequential linear programming (SLP) for solution of elements 22 and 33. The optimization solver parameters were kept at their default values. Since the exponential terms in the augmented Lagrangian function can be very large due to the order of some design variable values, the optimization solver can fail. To alleviate this problem, the values of response/target variables are normalized before implementing the EPF formulation.

We chose the double-loop strategy (EPF I) in this study. The two possible coordination strategies for the three-level hierarchy are shown in Figure 3. In scheme I, the number of ATC iterations for all three elements are identical, which is not desirable as the computational cost is considerably different among the three elements. The optimization problem in element 11 is very computationally expensive. The scheme II is preferable to avoid extraneous solutions of element 11 due to discrepancies between target/responses of elements 22 and 33. In this scheme, convergence between levels two and three is obtained first before communicating with element 11. The inner loop convergence is reached when reduction in the objective function of the relaxed problem between two consecutive inner loop iterations is less than the termination tolerance $\tau_{inner} = 0.01$. The outer loop convergence criterion is defined based on reduction of the inconsistencies in two successive solutions with tolerance of $\tau_{outer} = 0.1$.

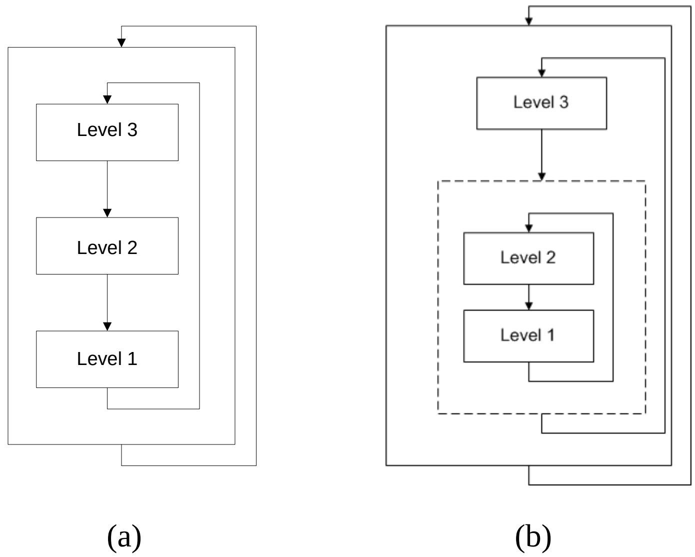

Figure 7.3 Multilevel coordination scheme (a) I and (b) II.

Bottom level element

The input parameters to this optimization problem are target values for nano-enhanced matrix material properties. Beside this input parameters, which is the part of ATC method, the preprocessing section discussed in previous is applicable here. This level optimization problem is designed similar to what is described about the nano-enhanced matrix properties in micro-level material model and design. Based on equation (5.8), the only design variable is volume fraction of CNF (V_{CNF}). The constituent material properties are held fixed as well as the geometric properties of the nanofiber. In this optimization problem, the objective function is minimization of the inconsistency between Young's modulus (E_{em}) and Poisson's ratio (ν_{em}) of the nano-enhanced matrix and its targets from the upper level element (E_{em}^T, ν_{em}^T). The E_{em}, ν_{em} corresponding to optimum design variables are extracted and sent to the top level element.

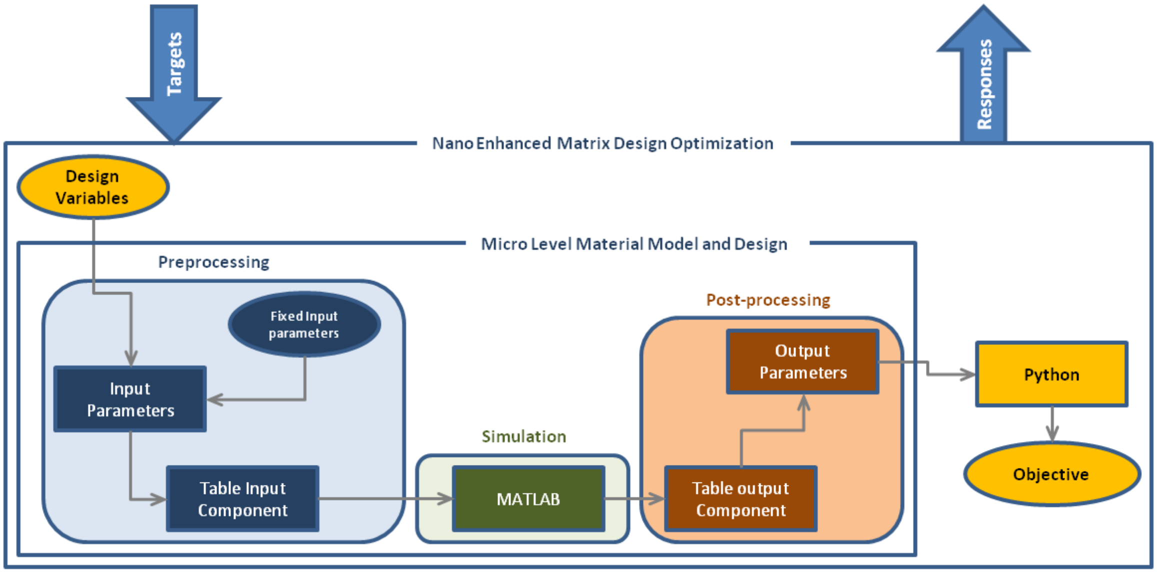

Figure 7.4 Micro-level material model and design computational element

Middle level element

In this element, the responses E_{em}^{R}, ν_{em}^{R} come from the lower level element, which is part of the ATC approach. The design variables of this optimization problem are as follows: $\{V_f, t_i, \theta_i, h_c, E_{em}, \nu_{em}\}$. The rule of mixtures, and the orthotropic ply, face sheet laminate, and sandwich plate stiffness properties calculations are performed sequentially. The conventional fiber properties represent the Young's modulus and Poisson's ratio (E_f, ν_f).

Conventional fiber properties +

$$(E_{em}, \nu_{em}) \Rightarrow [\text{Rule} - \text{of} - \text{Mixtures}] \Rightarrow (E_1, E_2, G_{12}, \nu_{12})$$

Number of layers in each face sheet + $(t_i, \theta_i, E_1, E_2, G_{12}, \nu_{12}, h_c) \Rightarrow [FORTRAN] \Rightarrow$

$$(f_{22}, \boldsymbol{A}, \boldsymbol{B}, \boldsymbol{D}).$$

The optimum values for $\sum t_i, h_c$ are send up to the top level element with the corresponding values for $\boldsymbol{A}, \boldsymbol{B}, \boldsymbol{D}$ extracted from the output of structural sandwich plate simulation. Also, optimum values for E_{em}, ν_{em} are provided to the lower level element as target values.

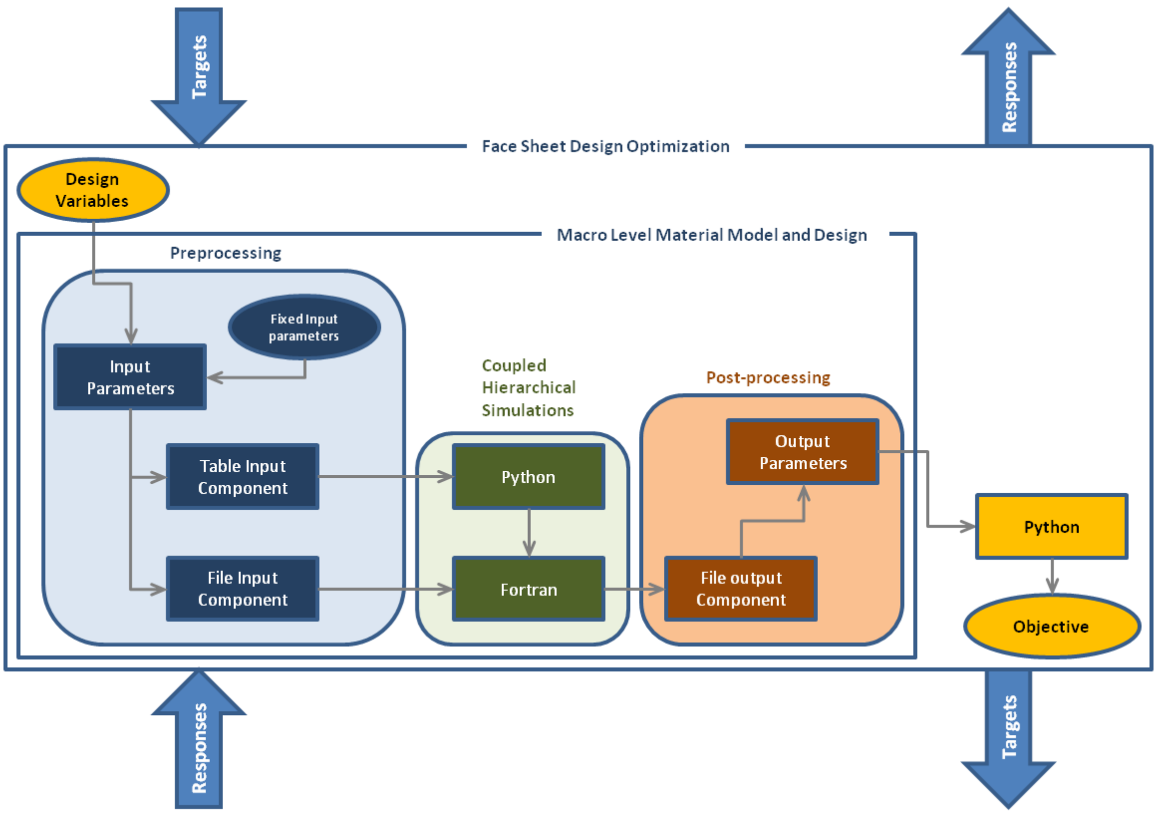

Figure 7.5 Macro-level material model and design computational element

Top level element

At the structural-level model and design, the overall dimensions of the sandwich plate and the boundary conditions, the applied in-plane loads (N_x, N_y, N_{xy}) along with the core material properties (E_c, G_c, ν_c) are fixed input parameters to the analysis code. The design variables $t_f, h_c, S, t_w, \boldsymbol{A}, \boldsymbol{B}, \boldsymbol{D}$ are the input values for the analysis in this section. The information flow at this level is given as:

$$\left(t_f, h_c, S, t_w, \boldsymbol{A}, \boldsymbol{B}, \boldsymbol{D}\right) \Rightarrow [FORTRAN] \Rightarrow (f_{11}, g_{cr}, g_{sc}, g_{ib}, g_w).$$

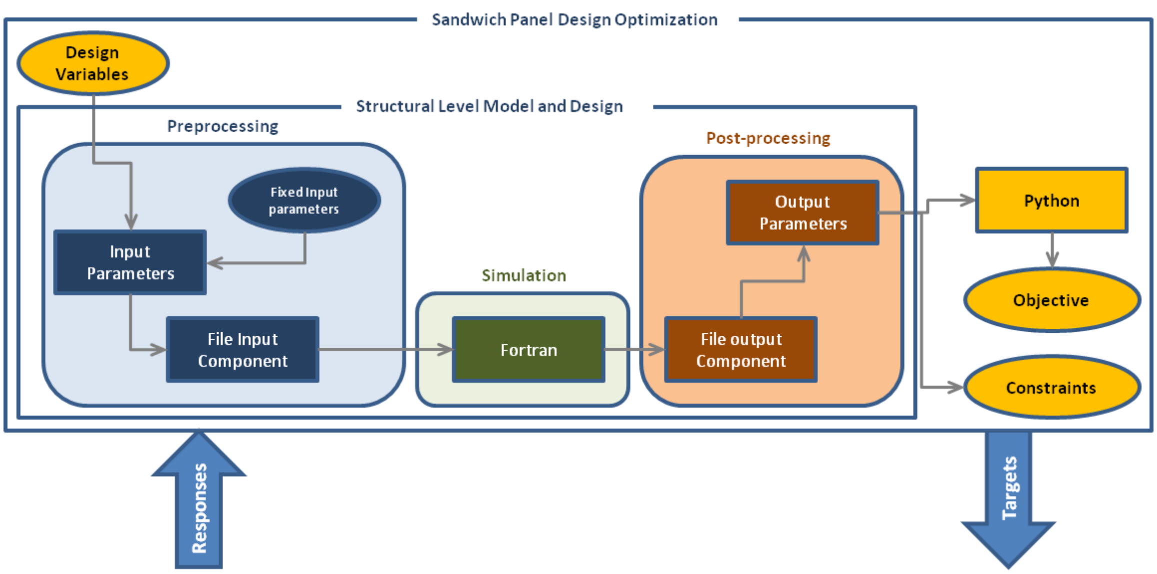

Figure 7.6 Structural level model and design computational element

The flowchart presented in Figure 7.2, is for deterministic problems. To consider the uncertainty in ATC framework, we alter each deterministic problem which converts the non-deterministic problem in a way that our deterministic framework faces minimum changes. In figure 7.7, the non-deterministic version of the top optimization problem presented in figure 7.6 is shown.

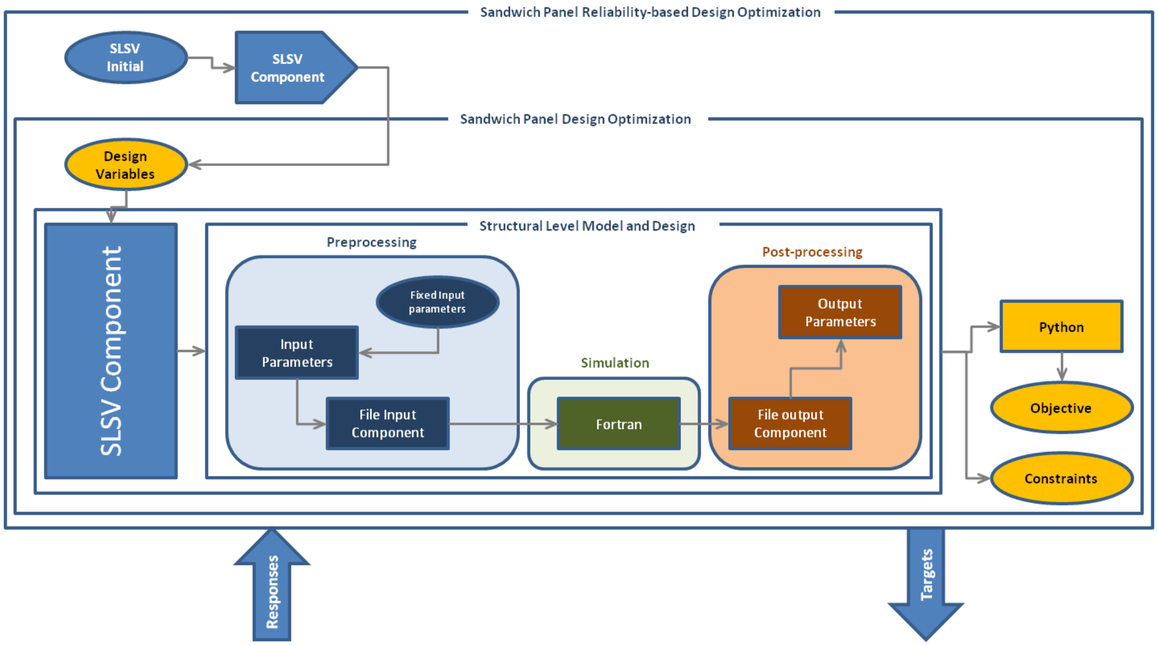

Figure 7.7 Non-deterministic structural level model and design computational element

CHAPTER VIII

SUMMARY AND FUTURE WORK

The augmented Lagrangian penalty formulation and four different coordination strategies were used to examine the numerical behavior of Analytical Target Cascading (ATC) for multilevel optimization of hierarchical systems. The coordination strategies considered include augmented Lagrangian using the method of multipliers and alternating direction method of multipliers, diagonal quadratic approximation, and truncated diagonal quadratic approximation. Properties examined include computational cost and solution accuracy based on the selected values for the different parameters that appear in each formulation. The different strategies were implemented using two- and three-level decomposed example problems. While the results showed the interaction between the selected ATC formulation and the values of associated parameters, they clearly highlighted the impact they could have on both the solution accuracy and computational cost.

The Single Loop Single Vector (SLSV) approach for reliability-based design optimization (RBDO) was integrated with Augmented Lagrangian (AL) formulation of analytical target cascading for solution of hierarchical multilevel optimization problems under uncertainty. In the proposed SLSV+AL approach, the uncertainties were propagated by matching the required moments of connecting responses/targets and linking variables present in the decomposed system. The accuracy and computational efficiency of SLSV+AL were demonstrated through the solution of four benchmark problems and comparison of results with those from other optimization methods reported in the literature.

An exponential penalty function (EPF) formulation based on method of multipliers was presented for solving multilevel optimization problems within the framework of analytical target cascading. The original all-at-once constrained optimization problem was decomposed into a hierarchical system with consistency constraints enforcing the target-response coupling in the connected elements. The objective function was combined with the consistency constraints in each element to formulate an augmented Lagrangian with EPF. The EPF formulation was implemented using double-loop (EPF I) and single-loop (EPF II) coordination strategies and two penalty-parameter-updating schemes. Four benchmark problems representing nonlinear convex and non-convex optimization problems with different number of design variables and design constraints were used to evaluate the computational characteristics of the proposed approaches. The same problems were also solved using four other approaches suggested in the literature, and the overall computational efficiency characteristics were compared and discussed.

Through micromechanical modeling of a carbon nanofiber (CNF) enhanced thermoset polymer material and macromechanical modeling of laminated plates, a hierarchical analysis framework was developed and used in design optimization of hybrid multiscale composite sandwich plates. Both CNF waviness and CNF-matrix interphase properties were included in the model. By decomposing the sandwich plate, structural and material designs were combined and treated as a multilevel optimization problem.

The application problem considered the minimum-weight design of an in-plane loaded sandwich plate with a honeycomb core and laminated composite face sheets that were reinforced by both conventional continuous fibers and CNF-enhanced polymer matrix. Besides global buckling, shear crimping, intracell buckling, and face sheet wrinkling were also treated as design constraints. The results of the multilevel sandwich plate optimization problem were presented and discussed.

Several topics can be considered for further investigation as part of future work. For example, convergence of the method is demonstrated by example, but it would strengthen the proposed approach to include mathematically rigorous discussion of convergence properties. Also, the feasibility of implementing the exponential method of multipliers in non-hierarchical system can be studied. In this study, aleatory uncertainty was considered and just the first two moments of each target/response distribution were matched. In future work, the possibility of matching more distribution characteristics with comparable computational cost can be investigated. The probabilistic ATC can be extended to reliability-based design optimization under epistemic uncertainty.

REFERENCES

Agarwal H, Mozumder CK, Renaud JE, Watson LT (2007) An inverse-measure-based unilevel architecture for reliability-based design optimization. Struct Multidiscip Optim 33:217–227. doi: 10.1007/s00158-006-0057-3

Bertsekas DP (1999) Nonlinear Programming. Athena Scientific, Belmont, MA.

Blouin V, Lassiter J, Wiecek M, Fadel G (2005) Augmented Lagrangian coordination for decomposed design problems. Proc. 6th world Congr. Struct. Multidiscip. Optim.

Bruhn E (1973) Analysis and Design of Flight Vehicle Structures. Jacobs publishing, Indianapolis, IN

Chan K (2008) A sequential linearization technique for analytical target cascading. Proc. ASME Des. Eng. Tech. Conf. Brooklyn, NY, pp 895–905

Chapra SC, Canale RP (1985) Numerical methods for engineers. McGraw-Hill, New York, NY

Chen X, Hasselman T, Neill D (1997) Reliability based structural design optimization for practical applications. Proc. 38th Struct. Struct. Dyn. Mater. Conf.

Chisholm N, Mahfuz H, Rangari VK, et al. (2005) Fabrication and mechanical characterization of carbon/SiC-epoxy nanocomposites. Compos Struct 67:115–124. doi: 10.1016/j.compstruct.2004.01.010

Cho TM, Lee BC (2011) Reliability-based design optimization using convex linearization and sequential optimization and reliability assessment method. Struct Saf 33:42–50. doi: 10.1016/j.strusafe.2010.05.003

Choi KK, Tu J, Park YH (2001) Extensions of design potential concept for reliability-based design optimization to nonsmooth and extreme cases. Struct Multidiscip Optim 22:335–350. doi: 10.1007/s00158-001-0154-2

Clements T, Rais-Rohani M (2000) Design optimization of a composite tilt-rotor wing with stability approximations. Proc. AIAA/ASME/ASCE/AHS/ASC Struct. Struct. Dyn. Mater. Conf. Washington DC, pp 829–838

Clements TM (1997) GLOBAL-LOCAL ANALYSIS AND DESIGN OPTIMIZATION OF A COMPOSITE TILT-ROTOR WING BOX STRUCTURE. 213.

Daniel I, Ishai O (1994) Engineering Mechanics of Composite Materials. Oxford University Press, New York, NY

DorMohammadi S, Rais-Rohani M (2012) Comparison of Alternative Strategies for Multilevel Optimization of Hierarchical Systems. Appl Math 03:1448–1462. doi: 10.4236/am.2012.330204

DorMohammadi S, Rais-Rohani M (2013) Exponential penalty function formulation for multilevel optimization using the analytical target cascading framework. Struct Multidiscip Optim 47:599–612. doi: 10.1007/s00158-012-0861-x

Du X, Chen W (2002) Sequential optimization and reliability assessment method for efficient probabilistic design. Proc. ASME Des. Eng. Tech. Conf. Montreal, QC, pp 871–880

Du X, Chen W (2004) Sequential Optimization and Reliability Assessment Method for Efficient Probabilistic Design. J Mech Des 126:225. doi: 10.1115/1.1649968

Enevoldsen I, Sørensen J (1994) Reliability-based optimization in structural engineering. Struct Saf 15:169–196. doi: http://dx.doi.org/10.1016/0167-4730(94)90039-6

Fisher F (2002) Nanomechanics and Viscoelastic Behavior of Carbon Nanotube Reinforced Polymers. Northwestern University

Garg M, Abdi F, McHugh S (2008) Analyzing interlaminar shear strength of multi-scale composites via combined finite element and progressive failure analysis approach. Proc. Int. SAMPE Tech. Conf.

Gojny FH, Wichmann MHG, Fiedler B, et al. (2005) Influence of nano-modification on the mechanical and electrical properties of conventional fibre-reinforced composites. Compos Part A Appl Sci Manuf 36:1525–1535. doi: 10.1016/j.compositesa.2005.02.007

Grandhi R V, Wang L (1998) Reliability-based structural optimization using improved two-point adaptive nonlinear approximations. Finite Elem Anal Des 29:35–48. doi: 10.1016/S0168-874X(98)00007-9

Haftka RT (1984) An Improved Computational Approach for Multilevel Optimum Design. J Struct Mech 12:245–261.

Han J (2008) Sequential Linear Programming Coordination Strategy for Deterministic and Probabilistic Analytical Target Cascading. 146.

Han J, Papalambros PY (2010) A Sequential Linear Programming Coordination Algorithm for Analytical Target Cascading. J Mech Des 132:021003 (8). doi: 10.1115/1.4000758

Harris RH (1995) Analysis and Design Optimization of Simply-Supported Rectangular Composite Sandwich Plates under Axial and Biaxial Loading. 131.

Hasofer A, Lind N (1974) An exact and invariant first-order reliability format. J Eng Mech 100:111–121.

Kharmanda G, Mohamed a., Lemaire M (2002) Efficient reliability-based design optimization using a hybrid space with application to finite element analysis. Struct Multidiscip Optim 24:233–245. doi: 10.1007/s00158-002-0233-z

Kharmanda G, Olhoff N (2007) Extension of optimum safety factor method to nonlinear reliability-based design optimization. Struct Multidiscip Optim 34:367–380. doi: 10.1007/s00158-007-0107-5

Kharmanda G, Olhoff N, El-Hami A (2004) Optimum values of structural safety factors for a predefined reliability level with extension to multiple limit states. Struct Multidiscip Optim 27:421–434. doi: 10.1007/s00158-004-0405-0

Kim H, Chen W, Wiecek M (2006) Lagrangian coordination for enhancing the convergence of analytical target cascading. AIAA J 44:2197–2207. doi: 10.2514/1.15326

Kim H, Geoff Rideout D, Papalambros P, Stein J (2001) Analytical target cascading in automotive vehicle design. Proc. ASME Des. Eng. Tech. Conf. Pittsburgh, PA, pp 661–670

Kim H, Kokkolaras M, Louca L, et al. (2002) Target cascading in vehicle redesign: a class VI truck study. Int J Veh Des 29:199–225. doi: 10.1504/IJVD.2002.002010

Kim H, Michelena N, Papalambros P, Jiang T (2000) Target Cascading in Optimal System Design. Proc. ASME Des. Eng. Tech. Conf. Baltimore, MD, pp 293–302

Kim H, Michelena N, Papalambros P, Jiang T (2003) Target cascading in optimal system design. J Mech Des Trans ASME 125:474–480. doi: 10.1115/1.1582501

Kim HM (2001) TARGET CASCADING IN OPTIMAL SYSTEM DESIGN. 154.

Kirjner-Neto C, Polak E, Kiureghian A Der (1998) An outer approximations approach to reliability-based optimal design of structures. J Optim Theory Appl 98:1–16. doi: 10.1023/A:1022647728419

Kirsch U (1975) Multilevel Approach to Optimum Structural Design. ASCE J Struct Div 101:957–974.

Koch PN, Kodiyalam S (1999) Variable complexity structural reliability analysis for efficient reliability-based design optimization. Proc. 1999 AIAA/ASME/ASCE/AHS/ASC Structrures, Struct. Dyn. Mater. Conf. Exhib. St. Louis, MO, pp 68–77

Kokkolaras M, Mourelatos ZP, Papalambros PY (2006) Design Optimization of Hierarchically Decomposed Multilevel Systems Under Uncertainty. J Mech Des 128:503–508. doi: 10.1115/1.2168470

Kort B, Bertsekas D (1972) A new penalty function method for constrained minimization. Decis Control 11:162–166. doi: 10.1109/CDC.1972.268971

Kuschel N, Rackwitz R (2000) A new approach for structural optimization of series systems. Appl Stat Probab 2:987–994.

Lassiter JB, Wiecek MM, Andrighetti KR (2005) Lagrangian Coordination and Analytical Target Cascading□: Solving ATC-Decomposed Problems with Lagrangian Duality. Optim Eng 6:361–381. doi: 10.1007/s11081-005-1744-4

Lee J, Kwak B (1995) Reliability-based structural optimal design using the Neumann expansion technique. Comput Struct 55:287–296.

Li Y, Lu Z, Michalek J (2008) Diagonal quadratic approximation for parallelization of analytical target cascading. J Mech Des 130:051402 (11). doi: 10.1115/1.2838334

Li Y, Lu Z, Michalek J (2007) Diagonal quadratic approximation for parallelization of Analytical Target Cascading. Proc. ASME Int. Des. Eng. Tech. Conf. Comput. Inf. Eng. Conf. Las Vegas, NV, pp 749–760

Libove C, Batdorf S (1948) A General Small-Deflection Theory for Flat Sandwich Plates. 24.

Liu H, Chen W, Kokkolaras M, et al. (2006) Probabilistic Analytical Target Cascading: A Moment Matching Formulation for Multilevel Optimization Under Uncertainty. J Mech Des 128:991. doi: 10.1115/1.2205870

Melchers R (1989) Importance sampling in structural systems. Struct Saf 6:3–10.

Mezura-Montes E, Coello C (2005) A simple multimembered evolution strategy to solve constrained optimization problems. IEEE Trans Evol Comput 9:1–17.

Michalek J, Papalambros P (2005a) An efficient weighting update method to achieve acceptable consistency deviation in analytical target cascading. J Mech Des 127:206–214. doi: 10.1115/1.1830046

Michalek J, Papalambros P (2005b) Weights, norms, and notation in analytical target cascading. J Mech Des 127:499–501. doi: 10.1115/1.1862674

Michelena N, Kim HM, Papalambros P (1999) A system partitioning and optimization approach to target cascading. Proc. 12th Int. Conf. Eng. Des. Munich, Germany, pp 24–26

Michelena N, Park H, Papalambros P (2003) Convergence properties of analytical target cascading. AIAA J 41:897–905. doi: 10.2514/2.2025

Mohsine A, Kharmanda G, El-Hami A (2006) Improved hybrid method as a robust tool for reliability-based design optimization. Struct Multidiscip Optim 32:203–213. doi: 10.1007/s00158-006-0013-2

Nemat-Nasser S, Hori M (1993) Micromechanics: Overall Properties of Heterogeneous Solids. Amsterdam

Nikolaidis E, Burdisso R (1988) Reliability based optimization: A safety index approach. Comput Struct 28:781–788.

Nowak A, Collins KR (2000) Reliability of structures. 338.

Papadrakakis M, Lagaros ND (2002) Reliability-based structural optimization using neural networks and Monte Carlo simulation. Comput Methods Appl Mech Eng 191:3491–3507. doi: 10.1016/S0045-7825(02)00287-6

Rais-Rohani M, Marcellier P (1999) Buckling and vibration analysis of composite sandwich plates with elastic rotational edge restraints. AIAA J 37:579–587.

Rao KM (1985) BUCKLING ANALYSIS OF ANISOTROPIC SANDWICH PLATES FACED WITH FIBER-REINFORCED PLASTICS. AIAA J 23:1247–1253.

Renaud J, Gabriele G (1989) Using the Generalized Reduced Gradient Method to Handle Equality Constraints Directly in a Multilevel Optimization. Proc. Adv. Des. Autom. American Society of Mechanical Engineers, Design Engineering Division (Publication) DE, Montreal, QC, pp 7–14

Rouhi M (2011) MODELING AND OPTIMIZATION OF NANO-ENHANCED POLYMER COMPOSITE STRUCTURES UNDER UNCERTAINTY. 139.

Rouhi M, Rais-Rohani M (2013) Effect of Nano-inclusions on Probabilistic Design of Components Made of Hybrid Composite Materials. Proc. 9th AIAA Multidiscip. Des. Optim. Spec. Conf.

Rouhi M, Rais-Rohani M, Lacy T, et al. (2010) Mechanical characterization of a nanofiber enhanced polymer with application to composite crush tubes. Proc. AIAA/ASME/ASCE/AHS/ASC Struct. Struct. Dyn. Mater. Conf.

Rubinstein R (1981) Simulation and the Monte Carlo Method. 278.

Sobieszczanski-Sobieski J (1974) Sizing of Complex Structures by the Integration of Several Different Optimal Design Algorithms. AGARD Lect Ser No 70 Struct Optim 4.1–4.19.

Sobieszczanski-Sobieski J (1982) A Linear Decomposition Method for Large Optimization Problems—Blueprint for Development. NASA TM 83248

Sobieszczanski-Sobieski J, James B, Dovi A (1985) Structural optimization by multilevel decomposition. AIAA J 23:1775–1782. doi: 10.2514/3.9165

Sobieszczanski-Sobieski J, James BB, Riley MF (1987) Structural sizing by generalized, multilevel optimization. AIAA J 25:139–145.

Thareja R, Haftka RT (1986) Numerical Difficulties Associated with Using Equality Constraints to Achieve Multi-level Decomposition in Structural Optimization. Proc. AIAA/ASME/ASCE/AH 27h Struct. Struct. Dyn. Mater. Conf. San Antonio, TX, pp 21–28

Thostenson E, Li W, Wang D, et al. (2002) Carbon nanotube/carbon fiber hybrid multiscale composites. J Appl Phys 91:6034–6037. doi: 10.1063/1.1466880

Tosserams S (2004) Analytical target cascading: convergence improvement by sub-problem post-optimality sensitivities. 214.

Tosserams S, Etman L, Papalambros P, Rooda J (2006) An augmented Lagrangian relaxation for analytical target cascading using the alternating direction method of multipliers. Struct Multidiscip Optim 31:176–189. doi: 10.1007/s00158-005-0579-0

Tosserams S, Etman L, Rooda J (2007a) An augmented Lagrangian coordination method for distributed optimal design in MDO□: Part I formulation and algorithms. 26.

Tosserams S, Etman L, Rooda J (2007b) An augmented Lagrangian coordination method for distributed optimal design in MDO□: Part II examples. 27.

Tosserams S, Etman L, Rooda J (2008) Augmented Lagrangian coordination for distributed optimal design in MDO. Int J Numer Methods Eng 73:1885–1910. doi: 10.1002/nme

Tosserams S, Etman LFP, Rooda JE (2009) Block-separable linking constraints in augmented Lagrangian coordination. Struct Multidiscip Optim 37:521–527. doi: 10.1007/s00158-008-0244-5

Tosserams S, Etman LFP, Rooda JE (2010a) Multi-modality in augmented Lagrangian coordination for distributed optimal design. Struct Multidiscip Optim 40:329–352. doi: 10.1007/s00158-009-0371-7

Tosserams S, Kokkolaras M, Etman LFP, Rooda JE (2010b) A Nonhierarchical Formulation of Analytical Target Cascading. J Mech Des 132:051002 (13). doi: 10.1115/1.4001346

Tseng P, Bertsekas DP (1993) On the convergence of the exponential multiplier method for convex programming. Math Program 60:1–19. doi: 10.1007/BF01580598

Tu J, Choi K, Park Y (1999) A new study on reliability-based design optimization. J Mech Des 121:557–564. doi: 10.1115/1.2829499

Tzevelekos N, Kokkolaras M, Papalambros P, et al. (2003) An empirical local convergence study of alternative coordination schemes in analytical target cascading. Proc. 5th world Congr. Struct. Multidiscip. Optim.

Vanderplaats G, Yang Y, Kim D (1990) Sequential Linearization Method for Multilevel Optimum. AIAA J 28:290–295.

Vinson JR, Sierakowski R (1986) The behavior of structures composed of composite materials. M. Nijhoff, Boston, MA

Wang L, Kodiyalam S (2002) An efficient method for probabilistic and robust design with non-normal distributions. Proc. 43rd AIAA/ASME/ASCE/AHS/ASC Struct. Struct. Dyn. Mater. Conf. Denver, CO, pp 1–13

Wang W, Wiecek MM, Blouin VY, et al. (2010) A CUTTING PLANE METHOD FOR ANALYTICAL TARGET CASCADING WITH AUGMENTED LAGRANGIAN COORDINATION. Proc. ASME 2010 Int. Des. Eng. Tech. Conf. Comput. Inf. Eng. Conf. IDETC/CIE 2010. Montreal, QC, pp 791–800

Wu Y (1994) Computational methods for efficient structural reliability and reliability sensitivity analysis. AIAA J 32:1717–1723. doi: 10.2514/3.12164

Wu Y, Burnside O (1988) Efficient probabilistic structural analysis using an advanced mean value method. Proc. 5th ASCE Spec. Conf.

Wu Y, Millwater H, Cruse T (1990) Advanced probabilistic structural analysis method for implicit performance functions. AIAA J 28:1663–1669. doi: 10.2514/3.25266

Wu Y, Shin Y, Sues R, Cesare M (2001) Safety-factor based approach for probability-based design optimization. Proc. 42nd AIAA/ASME/ASCE/AHS/ASC Struct. Struct. Dyn. Mater. Conf. Seattle, WA, pp 1–9

Wu Y, Wang W (1998) Efficient probabilistic design by converting reliability constraints to approximately equivalent deterministic constraints. J Integr Des Process Sci 2:13–21.

Yang RJ, Gu L (2004) Experience with approximate reliability-based optimization methods. Struct Multidiscip Optim 26:152–159. doi: 10.1007/s00158-003-0319-2

Yi P, Cheng G (2008) Further study on efficiency of sequential approximate programming for probabilistic structural design optimization. Struct Multidiscip Optim 35:509–522. doi: 10.1007/s00158-007-0120-8

Youn B, Choi K (2004a) Selecting probabilistic approaches for reliability-based design optimization. AIAA J 42:1–8.

Youn BD, Choi KK (2004b) A new response surface methodology for reliability-based design optimization. Comput Struct 82:241–256. doi: 10.1016/j.compstruc.2003.09.002

Yu X, Choi KK, Chang K-H (1997) A mixed design approach for probabilistic structural durability. Struct Optim 14:81–90. doi: 10.1007/BF01812509

Zhou Y, Pervin F, Jeelani S, Mallick P (2008) Improvement in mechanical properties of carbon fabric–epoxy composite using carbon nanofibers. J Mater Process Technol 198:445–453. doi: 10.1016/j.jmatprotec.2007.07.028

Zou T, Mahadevan S (2006) A direct decoupling approach for efficient reliability-based design optimization. Struct Multidiscip Optim 31:190–200. doi: 10.1007/s00158-005-0572-7

APPENDIX A

DIFFERENT PARAMETER UPDATING APPROACHES

Alternative approaches for choosing the penalty parameters are considered, where $a_{\mathrm{ij}}^{\mathrm{k}} = a_0$ and $b_{\mathrm{ij}}^{\mathrm{k}} = b_0\ \forall$ k or $a_{\mathrm{ij}}^{\mathrm{k+1}} = \beta a_{\mathrm{ij}}^{\mathrm{k}} > a_{\mathrm{ij}}^{\mathrm{k}}$ and $b_{\mathrm{ij}}^{\mathrm{k+1}} = \beta b_{\mathrm{ij}}^{\mathrm{k}} > b_{\mathrm{ij}}^{\mathrm{k}}$ $\forall$k with no dependence on values of the multipliers. For this case, $a_{\mathrm{ij}} = b_{\mathrm{ij}} = 1$ or $a_{\mathrm{ij}}^{\mathrm{k+1}} = \beta a_{\mathrm{ij}}^{\mathrm{k}}$ and $b_{\mathrm{ij}}^{\mathrm{k+1}} = \beta b_{\mathrm{ij}}^{\mathrm{k}}$ with $\beta = 2$. For the updating approach with dependence on values of the multipliers, $\boldsymbol{\omega}_{ij}^{k} = \boldsymbol{\omega}_0 = 1\ \ \forall k$ and $\boldsymbol{\nu}_{ij}^{k} = \boldsymbol{\nu}_0 = 1$ as well as $\boldsymbol{\omega}_{ij}^{k+1} = \beta \boldsymbol{\omega}_{ij}^{k}$ and $\boldsymbol{\nu}_{ij}^{k+1} = \beta \boldsymbol{\nu}_{ij}^{k}$ with $\beta = 2$. These approaches were applied in the solution to Problem 2 of Chapter IV according to EPF I approach. Same initial design point $\boldsymbol{x}^{(0)} = [3,3,3,3,3,3,3]$ was selected for all approaches with $\mu^{(0)} = 1$ and $\gamma^{(0)} = 1$.

Table A.1 Comparison of results in Problem 2 of Chapter 4 with different parameter updating approaches

		No. of Func. Evals	e	CPU Time, s	τ
Without Dependency	Fixed a, b	3830	0.00622	2.12	0.01
		5745	0.00042	3.02	0.001
		7462	0.00005	3.81	0.0001
		10101	0.00002	5.03	0.00001
	Updating a, b	3939	0.00048	2.17	0.01
		5317	0.00006	2.84	0.001
		7257	0.00001	3.84	0.0001
		9047	0.00002	4.72	0.00001
With Dependency	Fixed ω, ν	4881	0.03387	2.56	0.01
		8853	0.00318	4.35	0.001
		13119	0.00028	6.32	0.0001
		17189	0.00002	8.17	0.00001
	Updating ω, ν	4235	0.00100	2.26	0.01
		5909	0.00009	3.07	0.001
		8180	0.00002	4.15	0.0001
		10053	0.00002	5.05	0.00001

Results in Table A.1 show that for the same level of accuracy, the number of function evaluations and CPU time are generally reduced when the penalty parameters are kept independent of the multipliers. Also, by allowing the penalty parameters to be updated during the optimization process, solution efficiency improves.

APPENDIX B

EFFECT OF DECOMPOSITION

Problem 3 of Chapter IV is solved using three different decompositions. Decomposition 1, as shown in figure B.1(a), consists of two elements, element 1 at the top level and element 2 at the bottom. The target/response variables are x_3 and x_6, $\{x_1, x_2, x_4, x_5, x_7\}$ are the local variables for element 1 and $\{x_8, x_9, x_{10}, x_{11}, x_{12}, x_{13}, x_{14}\}$ are the local variables for elements 2. The objective function is assigned to element 1. The constraints g_1, g_2, h_1, h_2 are allocated to elements 1 and the others to element 2. Decomposition 2 shown in figure B.1(b) also consists of two elements as in the previous case, but the target/response variables are x_5 and x_{11}, $\{x_1, x_3, x_4, x_8, x_9, x_{10}\}$ are the local variables for element 1 and $\{x_2, x_6, x_7, x_{12}, x_{13}, x_{14}\}$ are the local variables for elements 2. The objective function is decomposed into two parts, x_1^2 assigned to element 1 and x_2^2 to element 2. The constraints g_1, g_3, g_4, h_1, h_3 are allocated to elements 1 and the others to element 2. Decomposition 3 is the three-level hierarchy presented in figure (4.9).

Figure B.2 displays the number of function evaluations and the CPU time versus the absolute solution error e for termination tolerances τ = 10^{-2}, 10^{-3}, 10^{-4}, 10^{-5}. The initial values for the penalty parameters in EPF I and EPF II are set to $\mu^{(0)} = 1$ and $\gamma^{(0)} = 1$. The starting point for all decompositions is $\boldsymbol{x}^{(0)} = [5.0, 5.0, 2.76, 0.25, 1.26, 4.64, 1.39, 0.67, 0.76, 1.7, 2.26, 1.41, 2.71, 2.66]$.

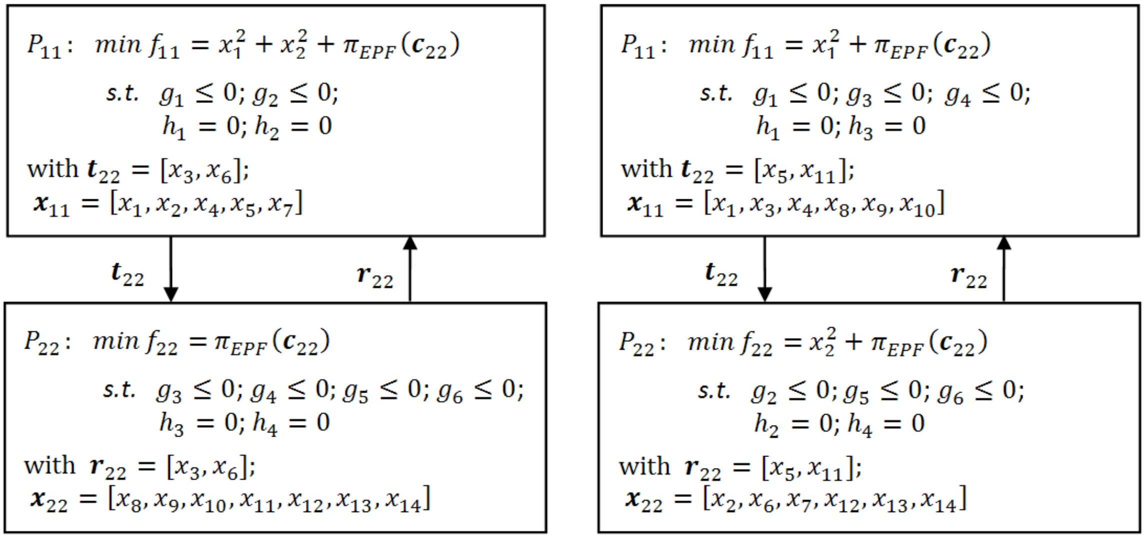

$$\pi_{EPF}(\boldsymbol{c}_{22}) = \left\{\boldsymbol{\mu}_{22}\left(e^{\,(\boldsymbol{t}_{22}-\boldsymbol{r}_{22})} - 1\right) + \boldsymbol{\gamma}_{22}\left(e^{\,(\boldsymbol{r}_{22}-\boldsymbol{t}_{22})} - 1\right)\right\}$$

Figure B.1 Hierarchical decompositions 1 and 2 of Problem 3 of Chapter IV

The results show that the form of decomposition affects computational efficiency. For all the cases considered, decomposition 1 is more efficient than the other two. Moreover, EPF II (single-loop) is more computationally efficient than EPF I regardless of the decomposition used. In particular, EPF II for decomposition 1 requires the least number of function evaluations and CPU time whereas EPF I for decomposition 3 requires the most. Comparing the two-level decompositions 1 and 2, it appears that EPF I_1 requires 61% less function evaluations than EPF I_2, whereas EPF II_1 requires 32% less function evaluations than EPF II_2. In terms of CPU time, EPF I_1 is 78% faster than EPF I_2, whereas EPF II_1 is 16% faster than EPF II_2.

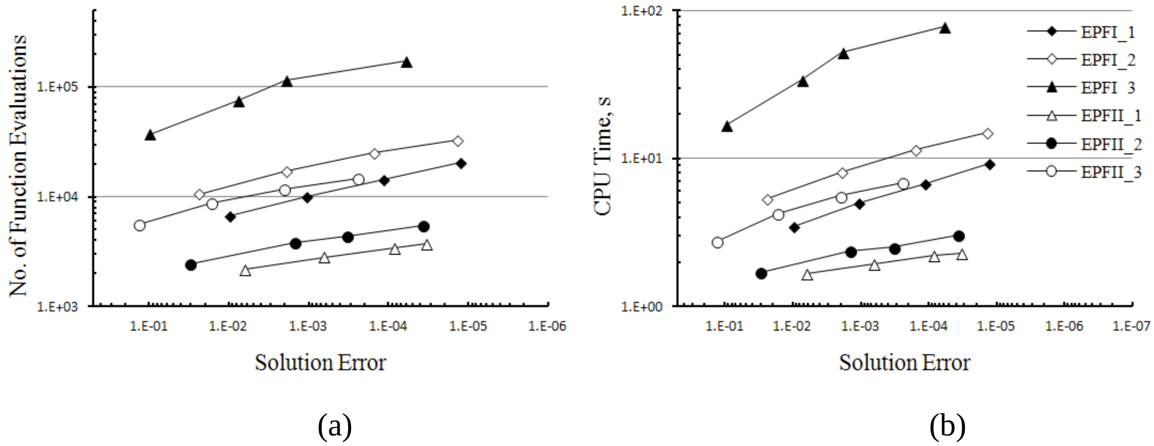

Figure B.2 Function evaluations (a) and CPU time (b) versus solution error in Problem 3 of Chapter 4 for decompositions 1, 2, and 3